



**Calhoun: The NPS Institutional Archive**  
**DSpace Repository**

---

Theses and Dissertations

1. Thesis and Dissertation Collection, all items

---

2023-09

# OPTIMIZED TRAJECTORIES FOR SATELLITE FORMATION FLYING USING DIFFERENTIAL DRAG MANEUVERS

Demoss, Andrew G.

Monterey, CA; Naval Postgraduate School

---

<https://hdl.handle.net/10945/72344>

---

This publication is a work of the U.S. Government as defined in Title 17, United States Code, Section 101. Copyright protection is not available for this work in the United States.

*Downloaded from NPS Archive: Calhoun*



Calhoun is the Naval Postgraduate School's public access digital repository for research materials and institutional publications created by the NPS community. Calhoun is named for Professor of Mathematics Guy K. Calhoun, NPS's first appointed -- and published -- scholarly author.

**Dudley Knox Library / Naval Postgraduate School**  
**411 Dyer Road / 1 University Circle**  
**Monterey, California USA 93943**

<http://www.nps.edu/library>



**NAVAL  
POSTGRADUATE  
SCHOOL**

**MONTEREY, CALIFORNIA**

**THESIS**

**OPTIMIZED TRAJECTORIES FOR SATELLITE  
FORMATION FLYING USING DIFFERENTIAL  
DRAG MANEUVERS**

by

Andrew G. DeMoss

September 2023

Thesis Advisor:  
Co-Advisor:

Giovanni Minelli  
Mark Karpenko

**Approved for public release. Distribution is unlimited.**

THIS PAGE INTENTIONALLY LEFT BLANK

<b>REPORT DOCUMENTATION PAGE</b>			<i>Form Approved OMB No. 0704-0188</i>
Public reporting burden for this collection of information is estimated to average 1 hour per response, including the time for reviewing instruction, searching existing data sources, gathering and maintaining the data needed, and completing and reviewing the collection of information. Send comments regarding this burden estimate or any other aspect of this collection of information, including suggestions for reducing this burden, to Washington headquarters Services, Directorate for Information Operations and Reports, 1215 Jefferson Davis Highway, Suite 1204, Arlington, VA 22202-4302, and to the Office of Management and Budget, Paperwork Reduction Project (0704-0188) Washington, DC, 20503.			
<b>1. AGENCY USE ONLY (Leave blank)</b>	<b>2. REPORT DATE</b> September 2023	<b>3. REPORT TYPE AND DATES COVERED</b> Master's thesis	
<b>4. TITLE AND SUBTITLE</b> OPTIMIZED TRAJECTORIES FOR SATELLITE FORMATION FLYING USING DIFFERENTIAL DRAG MANEUVERS		<b>5. FUNDING NUMBERS</b>	
<b>6. AUTHOR(S)</b> Andrew G. DeMoss			
<b>7. PERFORMING ORGANIZATION NAME(S) AND ADDRESS(ES)</b> Naval Postgraduate School Monterey, CA 93943-5000		<b>8. PERFORMING ORGANIZATION REPORT NUMBER</b>	
<b>9. SPONSORING / MONITORING AGENCY NAME(S) AND ADDRESS(ES)</b> N/A		<b>10. SPONSORING / MONITORING AGENCY REPORT NUMBER</b>	
<b>11. SUPPLEMENTARY NOTES</b> The views expressed in this thesis are those of the author and do not reflect the official policy or position of the Department of Defense or the U.S. Government.			
<b>12a. DISTRIBUTION / AVAILABILITY STATEMENT</b> Approved for public release. Distribution is unlimited.		<b>12b. DISTRIBUTION CODE</b> A	
<b>13. ABSTRACT (maximum 200 words)</b>  The demand for space capabilities is growing rapidly, and one promising approach to increase the availability of space assets quickly and cost-effectively is by deploying large numbers of small satellites that can collaborate and combine their capabilities. CubeSats, whether operating as a distributed constellation or in close swarms, have the potential to unlock new possibilities for the United States. Leveraging differential drag techniques to manage satellite formations offers several advantages, including lower production and launch costs and the utilization of readily available technologies. Implementing differential drag maneuvers presents challenges as they require a delicate balance between formation management and satellite operations. Both aspects necessitate precise attitude determination and control, which can potentially conflict with one another. Optimization techniques, such as Pontryagin's Principle, can be employed to develop trajectories for satellites and automate constellation management which could enable new applications and enhance space capabilities and capacity. This thesis demonstrates that by optimizing orbit transfer and formation flying trajectories, the duration of differential drag maneuvers can be reduced while accommodating mission requirements. It also develops tools to generate commands for satellites that would allow them to achieve the desired formation. As a result, the overall efficiency and effectiveness of CubeSats can be enhanced.			
<b>14. SUBJECT TERMS</b> trajectory optimization, CubeSat, formation flying, differential drag, Pontryagin's Principle		<b>15. NUMBER OF PAGES</b> 129	
		<b>16. PRICE CODE</b>	
<b>17. SECURITY CLASSIFICATION OF REPORT</b> Unclassified	<b>18. SECURITY CLASSIFICATION OF THIS PAGE</b> Unclassified	<b>19. SECURITY CLASSIFICATION OF ABSTRACT</b> Unclassified	<b>20. LIMITATION OF ABSTRACT</b> UU

NSN 7540-01-280-5500

Standard Form 298 (Rev. 2-89)  
Prescribed by ANSI Std. Z39-18

THIS PAGE INTENTIONALLY LEFT BLANK

**Approved for public release. Distribution is unlimited.**

**OPTIMIZED TRAJECTORIES FOR SATELLITE FORMATION FLYING  
USING DIFFERENTIAL DRAG MANEUVERS**

Andrew G. DeMoss  
Major, United States Army  
BS, United States Military Academy, 2011

Submitted in partial fulfillment of the  
requirements for the degrees of

**MASTER OF SCIENCE IN ASTRONAUTICAL ENGINEERING**

and

**MASTER OF SCIENCE IN SPACE SYSTEMS OPERATIONS**

from the

**NAVAL POSTGRADUATE SCHOOL  
September 2023**

Approved by: Giovanni Minelli  
Advisor

Mark Karpenko  
Co-Advisor

Brian S. Bingham  
Chair, Department of Mechanical and Aerospace Engineering

James H. Newman  
Chair, Space Systems Academic Group

THIS PAGE INTENTIONALLY LEFT BLANK

## ABSTRACT

The demand for space capabilities is growing rapidly, and one promising approach to increase the availability of space assets quickly and cost-effectively is by deploying large numbers of small satellites that can collaborate and combine their capabilities. CubeSats, whether operating as a distributed constellation or in close swarms, have the potential to unlock new possibilities for the United States. Leveraging differential drag techniques to manage satellite formations offers several advantages, including lower production and launch costs and the utilization of readily available technologies. Implementing differential drag maneuvers presents challenges as they require a delicate balance between formation management and satellite operations. Both aspects necessitate precise attitude determination and control, which can potentially conflict with one another. Optimization techniques, such as Pontryagin's Principle, can be employed to develop trajectories for satellites and automate constellation management which could enable new applications and enhance space capabilities and capacity. This thesis demonstrates that by optimizing orbit transfer and formation flying trajectories, the duration of differential drag maneuvers can be reduced while accommodating mission requirements. It also develops tools to generate commands for satellites that would allow them to achieve the desired formation. As a result, the overall efficiency and effectiveness of CubeSats can be enhanced.



THIS PAGE INTENTIONALLY LEFT BLANK

# TABLE OF CONTENTS

<b>I.</b>	<b>INTRODUCTION .....</b>	<b>1</b>
<b>A.</b>	<b>NEED FOR SPACE-BASED INTELLIGENCE, SURVEILLANCE, AND RECONNAISSANCE (ISR) .....</b>	<b>1</b>
<b>B.</b>	<b>PROBLEMS WITH LEGACY SYSTEMS .....</b>	<b>3</b>
<b>C.</b>	<b>ADVANTAGES/DISADVANTAGES OF CUBESATS / SMALLSATS .....</b>	<b>3</b>
<b>D.</b>	<b>RESEARCH QUESTION .....</b>	<b>6</b>
<b>II.</b>	<b>BACKGROUND AND PROBLEM FRAMING .....</b>	<b>9</b>
<b>A.</b>	<b>WHAT IS FORMATION FLYING AND DIFFERENTIAL DRAG? .....</b>	<b>9</b>
<b>B.</b>	<b>HOW FORMATION FLYING CAN BE USED FOR CUBESAT MISSIONS .....</b>	<b>10</b>
<b>C.</b>	<b>CURRENT METHODS FOR USING DIFFERENTIAL DRAG TO FORMATION FLY .....</b>	<b>15</b>
<b>D.</b>	<b>OPTIMAL TRAJECTORY AS PART OF A SYSTEM .....</b>	<b>20</b>
<b>III.</b>	<b>PROBLEM FORMULATION AND MODEL VERIFICATION .....</b>	<b>23</b>
<b>A.</b>	<b>DYNAMIC MODEL .....</b>	<b>23</b>
<b>1.</b>	<b>Orbital Dynamics for Differential Drag Operations .....</b>	<b>23</b>
<b>2.</b>	<b>Modeling the Atmosphere .....</b>	<b>26</b>
<b>3.</b>	<b>Modeling Spacecraft Attitude and Drag Area .....</b>	<b>34</b>
<b>B.</b>	<b>TESTS TO VALIDATE AND VERIFY MODEL .....</b>	<b>37</b>
<b>1.</b>	<b>ISS Orbit Propagation .....</b>	<b>37</b>
<b>2.</b>	<b>Orbital Lifetime Comparison .....</b>	<b>39</b>
<b>3.</b>	<b>Conservation of Energy .....</b>	<b>41</b>
<b>4.</b>	<b>Quaternion Norm Condition .....</b>	<b>42</b>
<b>5.</b>	<b>Drag Area Calculations .....</b>	<b>44</b>
<b>IV.</b>	<b>TRAJECTORY OPTIMIZATION PROBLEM .....</b>	<b>47</b>
<b>A.</b>	<b>SOLVING A SIMPLIFIED DIFFERENTIAL DRAG MANEUVER .....</b>	<b>47</b>
<b>1.</b>	<b>Problem Description .....</b>	<b>47</b>
<b>2.</b>	<b>Simplified Problem Formulation .....</b>	<b>48</b>
<b>3.</b>	<b>Scaling and Balancing .....</b>	<b>50</b>
<b>B.</b>	<b>APPLYING PONTRYAGIN'S PRINCIPLE AND FINDING CONDITIONS FOR OPTIMALITY .....</b>	<b>51</b>

1.	Lagrangian of the Hamiltonian .....	51
2.	Conditions for Optimality .....	52
C.	USING DIDO TO SOLVE OPTIMIZATION PROBLEM.....	53
D.	FEASIBILITY AND OPTIMALITY OF SOLUTION .....	55
1.	Feasibility Assessment .....	55
2.	Optimality Assessment .....	56
V.	GENERAL SOLUTION FOR DIFFERENTIAL DRAG MANEUVERS FOR FORMATION FLYING.....	61
A.	COMPLETE PROBLEM FORMULATION .....	61
B.	DIFFERENTIAL DRAG MANEUVER PLANNING TOOL .....	64
1.	User Inputs for Maneuver Planning Tool.....	66
2.	Defining Initial Conditions.....	67
3.	Orbit Propagation.....	70
4.	Solar Power Production Calculations .....	73
VI.	RESULTS OF MANEUVER PLANNING TOOL .....	77
A.	IMPACT OF ORBIT SELECTION ON MANEUVERS.....	84
1.	Altitude Effects.....	84
2.	Inclination Effects .....	85
B.	IMPACT OF SPACECRAFT DESIGN ON MANEUVERS.....	90
1.	High vs. Low Drag Configuration Ratio.....	90
2.	Size and Mass .....	91
3.	Solar Power Considerations.....	91
C.	MANEUVER SPEED .....	95
VII.	CONCLUSIONS AND FUTURE RESEARCH.....	99
A.	KEY TAKEAWAYS.....	99
B.	FUTURE RESEARCH.....	100
1.	Improvements and Potential Additional Capabilities for the Maneuver Planning Tool .....	100
2.	Using the Maneuver Planning Tool for Satellite Operations, Architecture Design, and Mission Development .....	101
3.	Applications Beyond Formation Flying.....	102
C.	FINAL CONCLUSIONS.....	103
	LIST OF REFERENCES .....	105
	INITIAL DISTRIBUTION LIST .....	109

## LIST OF FIGURES

Figure 1.	Geolocation simulation using CubeSats in formation .....	13
Figure 2.	Geolocation simulation using an aircraft .....	13
Figure 3.	Concept of a differential drag maneuver .....	16
Figure 4.	Planet’s Dove 3U CubeSat in different orientations; a) low drag orientation; b) high drag orientation; c) intermediate orientation. Source: [12].....	17
Figure 5.	Planet control algorithm to create the constellation. Source: [12].....	18
Figure 6.	Block diagram of a formation using optimized differential drag. Optimal trajectory is generated at stage highlighted in red. ....	20
Figure 7.	Models for the Earth’s atmosphere in space. Source: [21] .....	27
Figure 8.	Specifications of hypothetical 6U Cube used for the modeling .....	28
Figure 9.	Effect of solar flux versus orbital lifetime of a standard 6U CubeSat .....	30
Figure 10.	Logarithmic plot of average air density for over entire orbit versus altitude at different inclinations from 300 km to 500 km altitudes.....	31
Figure 11.	Air density versus spacecraft elevation angle for a spacecraft orbiting at 500km and 90° inclination.....	32
Figure 12.	Spacecraft orientation of reference frames. Source: [24] .....	34
Figure 13.	Spacecraft model for drag area calculations .....	35
Figure 14.	Solar flux for 2006–2018. Source: [26] .....	38
Figure 15.	Propagation of the International Space Station for one month.....	39
Figure 16.	Comparison of orbital and atmosphere models .....	40
Figure 17.	Quaternions over time of the rotational dynamics simulation .....	42
Figure 18.	3D plot of the tracks of each body frame axis with respect to orbital frame during orbits and 90° rotation .....	43
Figure 19.	Norm of quaternions over time .....	43
Figure 20.	Spacecraft model for drag area calculations .....	44

Figure 21.	Graph of states from DIDO solution: a.) Periods of each satellite; b.) Difference between the distances travelled by each satellite.....	54
Figure 22.	Satellite’s drag areas from DIDO solution.....	54
Figure 23.	Trajectories of satellites during maneuver from DIDO solution .....	55
Figure 24.	Propagation test for feasibility of DIDO solution.....	56
Figure 25.	Stationary condition plots demonstrating the control optimality.....	57
Figure 26.	a) Control histories which are bounded due to the values $\mu_1$ and $\mu_2$ b) Values $\mu_1$ and $\mu_2$ .....	57
Figure 27.	Hamiltonian value over time.....	59
Figure 28.	Depiction of the earth’s orbit with longitude of the ecliptic represented by $\lambda_{\odot}$ . Source: [30].....	68
Figure 29.	Earth, Sun, Spacecraft Geometry. Source: [31].....	75
Figure 30.	Geometry of the spacecraft relative to the Earth’s umbra. Source: [31].....	76
Figure 31.	Example maneuver’s relative orbital motion.....	79
Figure 32.	Drag areas of each satellite in the example maneuver .....	80
Figure 33.	Depiction of the spacecraft orientations .....	81
Figure 34.	Top-down view of the rotation .....	82
Figure 35.	Simulation quaternions for Satellite 1.....	82
Figure 36.	RAAN adjusted quaternions for Satellite 1 .....	83
Figure 37.	Left: Original quaternions; Right: RAAN adjusted quaternions .....	83
Figure 38.	Graph of power production of each satellite during the maneuver.....	84
Figure 39.	Maneuver at 90 degrees inclination .....	86
Figure 40.	Maneuver at 0 degrees inclination .....	87
Figure 41.	Atmospheric density experienced by spacecraft during maneuver.....	88
Figure 42.	Impact of high inclination on solar power production.....	89

Figure 43.	Impact of low inclination on solar power production.....	89
Figure 44.	6U CubeSat with deployable solar panel. Source: [33].....	92
Figure 45.	Solar power evaluation spacecraft power levels.....	93
Figure 46.	Baseline spacecraft power levels .....	94
Figure 47.	Power production for baseline maneuver performed in March .....	95
Figure 48.	Maneuver performed at Speed 1 .....	96
Figure 49.	Maneuver performed at Speed 2.....	96
Figure 50.	Maneuver performed at Speed 3 .....	97

THIS PAGE INTENTIONALLY LEFT BLANK

## LIST OF TABLES

Table 1.	Small satellite launch prices for rideshare by Spaceflight. Source: [8] .....	5
Table 2.	In-track atmospheric speeds on a spacecraft orbiting at 400km .....	33
Table 3.	Comparison of different atmosphere models .....	40
Table 4.	Drag areas calculated from quaternion rotations .....	44
Table 5.	User inputs for maneuver planning tool.....	67
Table 6.	Example maneuver inputs.....	78
Table 7.	Figures of merit for differential drag maneuvers performed at different altitudes .....	85
Table 8.	Figures of merit for maneuver performed at different inclinations .....	86
Table 9.	Effect of high to low drag ratios on maneuvers .....	90
Table 10.	Effect of spacecraft mass with fixed 6U volume on maneuver .....	91
Table 11.	Solar power evaluation space craft parameters.....	92
Table 12.	Average power produced at different times of year.....	94



THIS PAGE INTENTIONALLY LEFT BLANK

## LIST OF ACRONYMS AND ABBREVIATIONS

ADCS	Attitude Determination and Control System
DOD	Department of Defense
ECI	Earth Centered Inertial Reference Frame
EOIR	Electro-Optical and Infra-Red
FDOA	Frequency Difference of Arrival
GPS	Global Positioning System
HDM	High Drag Maneuver
ISR	Intelligence, Surveillance, and Reconnaissance
LEO	Low Earth Orbit
LQR	Linear Quadratic Regulator
MEO	Medium Earth Orbit
NASA	National Aeronautics and Space Administration
NOAA	National Oceanic and Atmospheric Administration
NRO	National Reconnaissance Office
PID	Proportional, Integral, and Derivative Controller
RAAN	Right Ascension of the Ascending Node
RPO	Rendezvous and Proximity Operations
SAR	Synthetic Aperture Radar
STK	Systems Tool Kit
TDOA	Time Difference of Arrival
TT&C	Tracking, Telemetry, and Control
UAV	Unmanned Aerial Vehicle

THIS PAGE INTENTIONALLY LEFT BLANK

## ACKNOWLEDGMENTS

I would like to thank my family for their endless support and patience during my time in graduate school. Also, to my friends and colleagues who helped and aided me along the way. Finally, thank you to my advisors and the faculty who taught and guided me throughout my journey at the Naval Postgraduate School.

THIS PAGE INTENTIONALLY LEFT BLANK

# I. INTRODUCTION

Rapid advances in technology, a changing geopolitical landscape, and new developments and innovations in the implementation of technology are defining the modern era. Space capabilities are at the forefront of these changes, and any nation that can find a way to pull ahead in the race for new capabilities can gain a significant advantage over their competitors. This thesis seeks to provide a step towards that aim for the United States by investigating the use of differential drag techniques to employ small satellites as formations, and thus increasing the effectiveness of low-cost space assets.

## A. NEED FOR SPACE-BASED INTELLIGENCE, SURVEILLANCE, AND RECONNAISSANCE (ISR)

The United States Department of Defense (DOD) has an ever-growing need for greater situational awareness to maintain its competitive advantage in the global environment. The warfighting domain of space offers tremendous possibilities on this front, but in recent decades space has become increasingly contested. This means that in order to exploit the possibilities offered by space, while also managing the risks, we will need to find creative and innovative solutions and systems that will be able to operate in this ever-changing battlefield. Any new systems will have to be robust, resilient, and responsive in addition to being able to provide tremendous capabilities to warfighters and to do so in a rapidly changing environment with many new threats. Many space-based Intelligence, Surveillance, and Reconnaissance (ISR) platforms have been in use for years and have already proven their worth in numerous recent conflicts, but emerging technologies offer even more capabilities and ways to exploit the high ground above the Kármán Line which separates the terrestrial domains from space.

The space domain offers unique advantages to warfighters that new technologies are making possible. First, space is very difficult to access and therefore spacecraft are inherently protected from harm as compared to aircraft or ground-based systems. Very few countries can detect, track, target, and effectively engage a spacecraft with kinetic, non-kinetic, electronic, or cyber means [1]. Also, these anti-satellite weapons are very costly

and therefore, by moving capabilities into space, the DOD would impose a higher price on its adversaries by potentially reducing their capabilities in other areas. Next, space offers global access on a continuous basis, and thus offers a high level of responsiveness. There is no need to reposition assets such as Unmanned Aerial Vehicles (UAVs), manned systems, or ground sensors to politically sensitive areas while risking the loss of lives or material as spacecraft can be deployed to observe anywhere on Earth in a matter of minutes to hours. For these reasons and more, the national intelligence and military communities are constantly developing new space-based systems and have been for decades [2].

In recent years the explosion of new space technologies, decreasing launch costs, and miniaturization has led to far more interest in proliferating space with new ISR systems for both the government and commercial users. The National Reconnaissance Office (NRO) and the Space Force have recently begun a collaboration to create new capabilities [3], and the commercial sector has already developed systems of this nature and is already operating them. Space-based imaging and observation from companies such as Maxar, Black Sky, Cappella, and Planet have proven that proliferated systems are very useful as ISR platforms. The NRO and DOD are investing heavily in these partners, and the demand for these capabilities is only increasing [4].

This new effort is focused on providing space capabilities to tactical users as opposed to strategic collection for national requirements. This would be an enormous benefit to warfighters; it would give them access to timely intelligence that they could dynamically re-task as needed, and this could be done in a clandestine manner without the enemy being aware it had occurred at all. Space based ISR at the tactical level, coupled with new long-range weapon systems, will provide the U.S. military with potentially revolutionary capabilities. The ongoing Russo-Ukrainian war has been an excellent example of how space systems can affect the battlefield. The commercial images and data gave the world warning of the war as Russian troops massed on the border, and now these images provide critical targeting information to the Ukrainian Armed Forces [5]. From this, it is clear that space based ISR is a critical capability for the DOD. Faster, cheaper, more

agile, and responsive systems are needed to ensure that the United States has the advantages it needs in an increasingly dangerous world.

## **B. PROBLEMS WITH LEGACY SYSTEMS**

Many legacy satellites tend to be highly capable, expensive, and offer obvious targets for adversaries in the event of a conflict. In the past, launching assets into orbit was very difficult and expensive, and satellites were often built as unique platforms. As a result, they had significant capabilities and hosted many different payloads that could perform multiple missions all from the same bus. These attributes mean that a relatively small number of highly capable assets provided services to many different customers, and thus were routinely in very high demand. This made them difficult to access for anyone except priority customers paying a high price for satellite services, or the entity which owns the satellites themselves. This can exclude many users, particularly military personnel operating at the tactical edge.

Additionally, legacy satellites have been priority targets for adversaries due to their large number of capabilities, difficulty to replace quickly, and high cost. Adding defenses on these satellites can increase complexity and challenges significantly [1]. Defenses could include things such as nulling antennas to protect from jamming, electromagnetic shielding, dedicated space situational awareness assets, and increased maneuverability which all add complexity, costs, weight, loss of mission lifetime, and operating challenges [1].

## **C. ADVANTAGES/DISADVANTAGES OF CUBESATS / SMALLSATS**

Large, capable, and unique space assets may have made sense in the past, but now many factors are changing the calculus. The advent of a thriving commercial launch industry has enabled ride sharing and smaller satellites to be a far cheaper option. Also, miniaturization and rapid advancements in digital technologies mean that more and more capability can be employed on smaller and smaller platforms and at cheaper prices. CubeSats offer standardized sizes and components that can further drive down costs, and this opens the doors to many use cases for CubeSats that are just now being explored.



The advantages offered by small satellites have been widely recognized and thus their use has grown significantly. The strategic consulting firm Euroconsult predicts that one ton of small satellites could be launched per day on average over the next 10 years [6]. These small satellites can perform many missions such as communications, Earth observation, data transfer and processing, technology demonstrators, and national security applications including ISR, science, and space logistics [6]. Many of these small satellites will be bespoke CubeSats developed by the DOD, while others will include systems such as the SpaceX Starlink network, OneWeb, and commercial ISR/observation companies such as Planet, Capella, and Maxar. In another interesting point, the Euroconsult report asserts that the number of these satellites operating as a constellation will increase from 75% of all CubeSats currently to approximately 81% in the next 10 years, and this brings with it many opportunities and challenges. These constellations will require considerable maintenance and station keeping activities to ensure they are able to perform the required tasks [6].

The cost to launch these satellites is far more affordable than it used to be. First, launch prices have dropped considerably recently; for example, the Russian Soyuz rocket, which was once a major workhorse of the industry, costs roughly \$225 million but the new most common launcher, the Falcon 9, is \$67 million per launch [7]. There are even options for smaller launchers such as the Rocket Lab Electron that will fly for as low as \$5 million [7]. Next, many small satellites and almost all CubeSats can ride to space as a secondary payload and thus not incur the full cost of the launch. As of August 2022, rideshare provider Spaceflight offers the prices shown in Table 1.

Table 1. Small satellite launch prices for rideshare by Spaceflight. Source: [8]

DETAIL	CONTAINERIZED			SATELLITE CLASS				
	PAYLOAD TYPE	3U	6U	12U	50kg	100Kg	150kg	200kg
LENGTH (CM)	34.05	34.05	34.05	80	100	100	100	125
HEIGHT/DIA (CM)	10	10	22.63	40	50	60	80	100
WIDTH (CM)	10	22.63	22.63	40	50	60	80	100
MASS (KG)	5	10	20	50	100	150	200	300
PRICE- LEO	\$145k	\$295k	\$595k	\$895k	\$975k	\$1,350k	\$1,350k	\$1,850k
PRICE- GTO	\$915k	\$1,400k	\$2,750k	\$4,600k	\$8,500k	\$9,800k	\$11,200k	\$14,000k

Pricing in USD

\*Prices may vary by launch provider, orbit and/or spacecraft technical requirements.

The cost of building CubeSats has dropped considerably due to standardized parts, buses, and payloads as well as other innovations. Many sources claim CubeSats are anywhere from \$1,000 to \$500,000 to build depending on size, payloads, and complexity [9]. This means that a 10 kg 6U CubeSat could cost an estimated \$300,000 to build and \$295,000 to launch. For larger constellations this price could be even lower if mass production is possible. Also, as new launch vehicles are developed the price could drop even lower in the near future. This combination of low prices and wide-ranging mission sets makes CubeSats an important platform for space operations. However, notable downsides to using CubeSats include their limited or lack of propulsion and small size which can limit certain payloads and their ability to carry redundant systems to improve the reliability of any individual spacecraft.

#### **D. RESEARCH QUESTION**

Given the high demand for space-based ISR capability, is it possible to use CubeSats in a way to exploit their advantages, while mitigating their challenges? CubeSats offer a low-cost solution to many different problem sets. However, by their very nature they are a less capable platform with limitations that can impact several important missions. One potential way to overcome CubeSat form-factor's limitations is by using many CubeSats working together, via formation flying, to achieve some goal. Currently, this is a challenge as it is a labor-intensive task and not easily accomplished. The purpose of this thesis is to investigate optimized formation flying of CubeSats using differential drag techniques.

Optimization techniques are ideally suited to create trajectories for satellites using differential drag to maneuver, as there are many challenges when doing these maneuvers for formation flying or constellation management. First, optimization could reduce the uncertainty for the maneuvers, especially for close swarm formations. For example, Planet uses  $2^\circ$  slots for each satellite as a margin of error, which is a separation of 200–250 km depending on the altitude [12]. Also, formation-keeping maneuvers are often postponed for operational purposes, since changing and maintaining orientations for longer durations can disrupt other pointing requirements for imaging or data transmission. Other concerns such as power consumption, and effective area of the solar panels pointing at the sun for power generation, mean that the satellites may not be able to maintain the orientations needed for formation flying. Finally, this is a very labor-intensive process, and it requires a human in the loop at all times to balance station-keeping operations and other concerns. Using optimization as a technique for automation would allow these impacts to be taken into account so that the satellites are able to maintain both their operational requirements and conduct formation flying maneuvers in the shortest possible time.

Both the DOD and the scientific community in general will benefit from this thesis, as it will provide an option for using low cost CubeSats for more sophisticated missions than they have in the past. By using an autonomous process to maintain precise constellations and formations of satellites, important figures of merit such as target area

revisit times, coverage time, spatial resolution of remote sensing, and others could be greatly improved. Also, by making the system autonomous it will greatly reduce cost of the total system architecture by reducing the manpower requirements and simplifying the ground segment. This will impact not just DOD ISR missions but also scientific Earth observation research, commercial interests, and space situational awareness and research as well. Additionally, using differential drag to perform constellation or formation station keeping could be used on larger spacecraft to preserve fuel and extend mission lifetimes of more expensive and capable systems.

This thesis uses optimization techniques to identify the fastest method to conduct differential drag formation flying maneuvers, and then create a maneuver planning tool which can rapidly generate commands which could be uploaded to a spacecraft to perform the maneuver. Chapter II frames the problem and discuss how such maneuvers could be employed. Chapter III discusses the development and validation of the models and dynamics required to calculate the maneuvers. Chapter IV uses optimization to determine the trajectories of the satellites. Chapters V and VI describe the maneuver planning tool and how it can be used to plan operations and conduct the maneuvers.

THIS PAGE INTENTIONALLY LEFT BLANK

## II. BACKGROUND AND PROBLEM FRAMING

Differential drag maneuvers and controlling the relative motion of spacecraft are challenging problems. Fundamentally, it involves using the rotational motion of a spacecraft to achieve a desired translational motion, but doing so with two or more spacecraft simultaneously so that their final relative positions meet some operational goal.

### A. WHAT IS FORMATION FLYING AND DIFFERENTIAL DRAG?

Formation flying is a relevant and important part of modern space flight and is being used by many organizations to achieve their goals. As stated by NASA:

- The focus of formation flying is to maintain a targeted orbit configuration of various spacecraft. Having multiple satellites fly in a specific geometry avoids the technical and financial challenge of building one satellite of equivalent size.
- NASA Ames has taken a close interest in formation flying missions. Formation flying consists of the maintenance of a desired relative separation and orientation between multiple spacecraft. There are various types of formation flying missions, such as constellations (a collection of spacecrafts that make up the space element of a distributed space mission), and swarms (a collection of spacecrafts operating in close proximity as a single entity). [10]

There are many advantages to using this method. Formation flying allows for consistent and reliable performance of the constellation in terms of revisit times, coverage over an area of interest, maintenance of satellite cross links, and the employment of multiple satellites simultaneously. Examples include the dozens of constellations currently in orbit such as Starlink, Iridium, and many more.

Over time, orbital perturbations cause the orbits of satellites to shift and change. This results in irregularities in the shape and structure of formations [11]. Maneuvers must be conducted to correct for these errors and conduct general station keeping operations. Again, this can be challenging for CubeSats since they do not typically employ propulsion systems and must maneuver using differential drag. This method uses the atmosphere and the properties of the CubeSat to maneuver, which could be analogous to sky divers

changing their body positions to fly in formation as opposed to traditional aircraft with engines. Based on the size, shape, and weight of a CubeSat, it can fly in different attitudes relative to the direction of travel and this will change the drag force on the satellite [12]. In practical terms, these maneuvers should be conducted at less than 600 km of altitude and can only be done to drop the altitude of the satellite thus changing relative velocity between the spacecraft. This presents a downside of differential drag maneuvers; they will always reduce the overall mission lifetime as they lower the spacecraft's altitude by some amount depending on the duration of the maneuver, orbit, the spacecraft, and other factors.

## **B. HOW FORMATION FLYING CAN BE USED FOR CUBESAT MISSIONS**

There are many potential uses for flying CubeSats in constellations or swarms, especially as they apply to national defense, ISR, and scientific applications. As a result, this is an area of very active research for many commercial, government, and academic applications. The strength of formations is shown by the company Planet which operates hundreds of 3U CubeSats called Doves which carry no propellant and were extremely cheap to manufacture and simple to operate when compared to larger satellites. For example, Planet deployed 105 Dove satellites on one rocket into a sun-synchronous orbit, and they then used differential drag to evenly distribute themselves around the Earth in a single orbital plane and then maintain even spacing for the life of those satellites [12]. Using this method, Planet is able to photograph the entire Earth at least once per day with 3–5 meter spatial resolution. This would not be possible without using differential drag maneuvers [12].

Flying in formations offers a form of passive defense for the satellites against an adversary seeking to disrupt the constellation or swarm [1]. First, formations can allow for a disaggregation of capabilities onto multiple satellites, as opposed to a single large legacy system, and thus decrease the impact of a kinetic, non-kinetic, or cyber strike against a single spacecraft [1]. Next, it distributes the capabilities so that the loss of a single system does not degrade the overall effectiveness of the entire network. This is the case for the GPS constellation, which would still operate near full capacity even without several of its satellites [1]. Distributing capabilities also reduces the risk of launch and could lower the

burden of expensive and time-consuming testing on the ground by allowing satellite designers to use statistical methods based on operational data to estimate the failure rate of satellites. CubeSats can also be used in proliferated constellations, which use very large numbers of the same CubeSat that can work together to provide a complete capability [1]. Finally, diversified architectures make it possible for formations with different orbital regimes to be used together, such as Low Earth Orbits (LEO) and Medium Earth Orbits (MEO). This takes advantage of the benefits of both geometries and preserve greater capacity if attacked [1]. Diversified architectures can be used in concert with other tactics, such as the disaggregation of capabilities. For example, a smaller number of more capable data transport satellites in a higher orbit could provide data processing or even Telemetry, Tracking, and Command (TT&C) services for a large, proliferated formation of CubeSat sensors in a lower orbit. The CubeSats could send the raw data up where it would be processed by data transport satellites and then sent directly to users on the ground.

Another important aspect of using CubeSats in formation is that they offer a high degree of rapid deployment and reconstitution if necessary [1]. Nearly every launch today can ferry small dispersible CubeSats to orbit, and even though the orbits may not be perfectly ideal in some cases, the sheer volume that can be deployed will allow for the mission's goals to be achieved. National security missions could easily be prioritized on upcoming launches if needed to get assets into space, and since CubeSat sizes are generally standardized, it is likely that the launch vehicle would be able to support them. In the event of a sudden crisis, it is easy to imagine the rapid deployment of hundreds of CubeSats into an ideal orbit to accomplish a desired task. If some of these are destroyed or damaged by an enemy the waiting period for more orbital assets would be relatively short since new stocks of CubeSats could be held in reserve on the ground.

A second option could be to have a CubeSat fleet in reserve already in orbit [13]. They could launch into a higher orbit at nearly 600 km and enter a low drag mode or use a deployable, and stowable, drag device similar to a parachute or sail. When needed, a specified number of them could adjust their attitude into a high drag configuration and rapidly descend to the target altitude and orbit. Using J2 perturbations, it would even be



possible to adjust the Right Ascension of the Ascending Node (RAAN) of the orbit by just changing the altitude. This occurs as the unevenness of the Earth's gravity, due to the planet's oblateness, precesses the orbit and adjusts its RAAN according to Equation 1.

$$\dot{\Omega} = -\frac{2}{3} \left( \frac{\sqrt{\mu} J_2 R^2}{(1-e^2)^2 a^3} \right) \cos(i) \quad (1)$$

In Equation 1,  $\Omega$  is the RAAN angle,  $J_2$  is a value specific to the oblateness of the Earth which equals  $1.0826 \times 10^{-3}$ ,  $R$  is the Earth's radius,  $e$  is the orbit's eccentricity,  $a$  is the semi-major axis, and  $i$  is the orbit's inclination. This reconfigurable constellation method would likely be the most responsive use of CubeSat formations and could provide the U.S. with a significant advantage [13].

The use of swarm formations could be very useful for remote sensing and ISR missions. Many formation-flying CubeSats could travel with a short separation of dozens of kilometers and combine their individual capabilities. One such application could be for the geolocation of radio frequency signals using Time Difference of Arrival (TDOA) or Frequency Difference of Arrival techniques (FDOA) [14]. By using both a consistent distance between CubeSats and their relatively high rate of travel over the ground they could give a highly accurate geolocation. How accurate is very dependent on a number of factors such as frequency, antenna gains, distance off nadir, and many others.

For an example, the following simulation was conducted to simulate a pair of satellites separated by 10 km at a 450 km orbit flying directly over an emitter. For comparison, an equivalent simulation using an aircraft flying at 600 km/hr at 10,000 m altitude was also conducted. The primary output is the size of the geolocation ellipse that shows the possible location of the ground emitter using TDOA and FDOA geolocation techniques. A smaller ellipse means that there is a higher degree of accuracy for the location of the emitter. As shown in Figures 1 and 2, the satellites are roughly 20 times more accurate than an aircraft despite being much further from the emitter, and they are also protected from threats due to their altitude and speed versus an aircraft. That said, aircraft could likely host more robust equipment than small CubeSats, but there is still a major advantage to operating from space for geolocation of radio emissions.

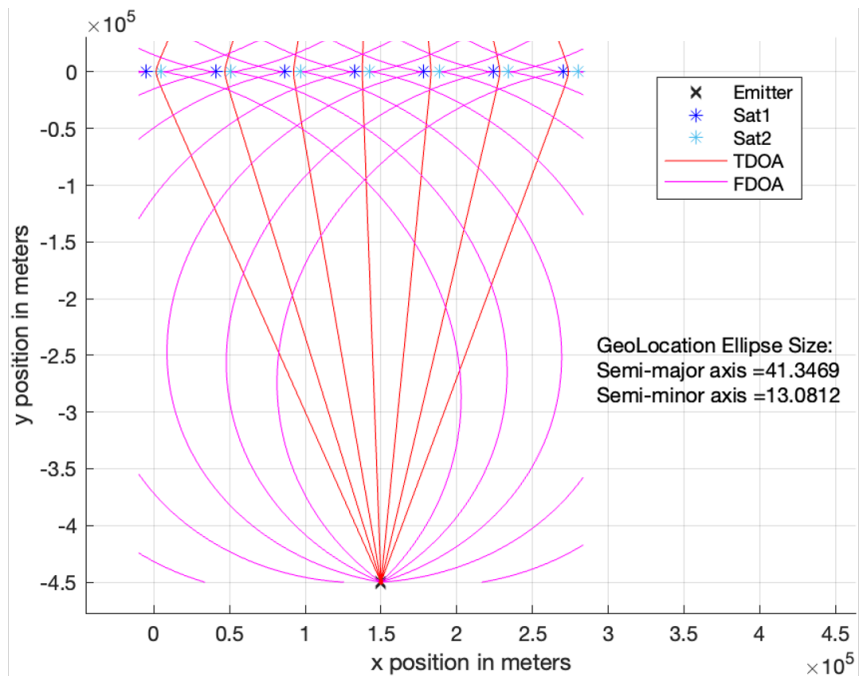


Figure 1. Geolocation simulation using CubeSats in formation

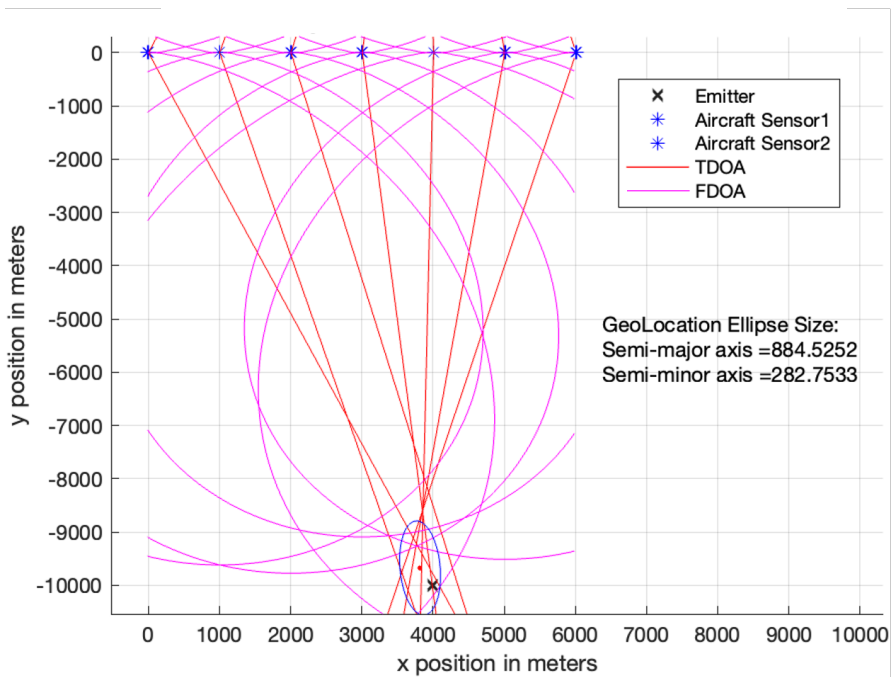


Figure 2. Geolocation simulation using an aircraft

From Figures 1 and 2 we can see that a very accurate location could be possible from satellites, and the geolocation is far more accurate than an aircraft using the same equipment. This is shown by the size of the location ellipses in each figure.

Another use for a swarm of small satellites could be for electrooptical sensors in either visible or infrared spectrums (EOIR). Currently, Planet is able to use its Dove CubeSats to take 3–5 meter resolution images, but this could be greatly improved using a swarm [12]. By employing a method known as stereo image super-resolution, two images taken from slightly different angles can be stitched together using machine learning to increase the spatial resolution [15]. This would be a data processing problem outside the scope of this thesis, but it certainly applies to using formations of CubeSats to deliver ISR capabilities to the warfighters on the ground. Finally, formations could be used to create bistatic synthetic aperture radar (SAR) images, which offer qualitative advantages over a single sensor [16].

All of these methods could be combined into a train of disaggregated satellites to fully investigate areas of interest using tipping and queuing. For example, the train could be led by radio frequency geolocation CubeSats that identify signals of interest to users. That information could be passed back to a pair of bistatic SAR satellites that cover a wide area around the signal to identify the emitter or other targets [17]. Finally, a CubeSat pair equipped with EOIR sensors could take detailed images of the targets. All of this could be coordinated using a data processing formation above them that would pass the useful information to a user on the ground. If this could all be done automatically, and in a secure way, it would greatly improve the responsiveness and situational awareness of the U.S. military operating worldwide, and without the need of extensive terrestrial resources or assets.

### **C. CURRENT METHODS FOR USING DIFFERENTIAL DRAG TO FORMATION FLY**

Conceptually, differential drag operations consist of three different phases that require precise timing and attitude control to achieve the desired separation between the spacecraft. This could be applied to just two spacecraft, or each could represent multiple satellites if a large constellation was being managed and a gap opened between two sections. The desired gap is arbitrary, and this could be used effectively regardless of the distance between the satellites. Figure 3 depicts the steps of the maneuver. The term High Drag Maneuver (HDM) references the periods when the satellites present the maximum drag area toward the direction of the velocity vector ( $\mathbf{V}_{BAR}$ ) as opposed to the direction away from the center of the Earth ( $\mathbf{R}_{BAR}$ ).

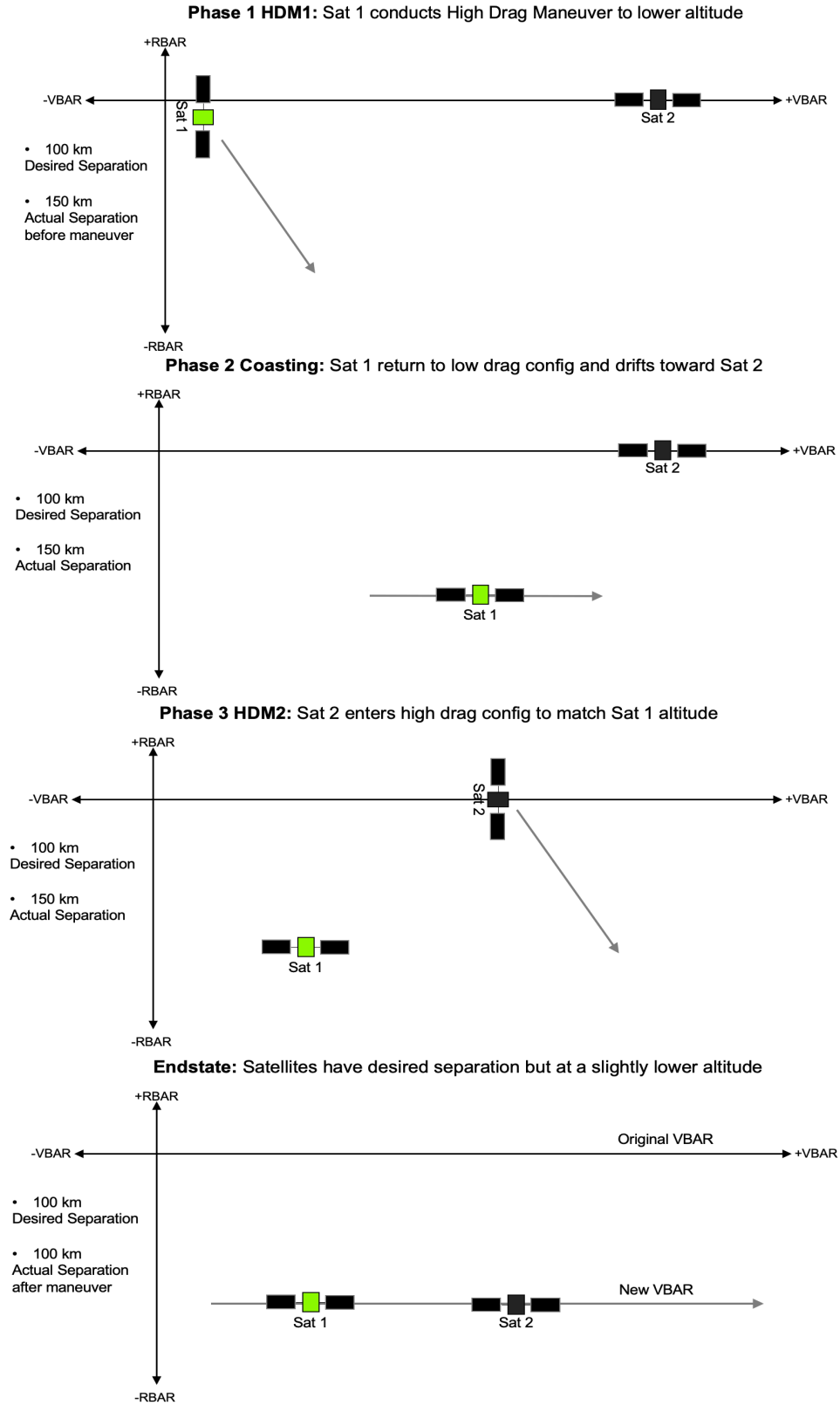


Figure 3. Concept of a differential drag maneuver

To gain a better understanding of how differential drag works in practice, it is valuable to examine how current satellite operators are using differential drag to manage formations and constellations. A good first example of the current state of technology for CubeSat formations is the Planet commercial imaging constellation. The design of their satellite is shown in Figure 4.

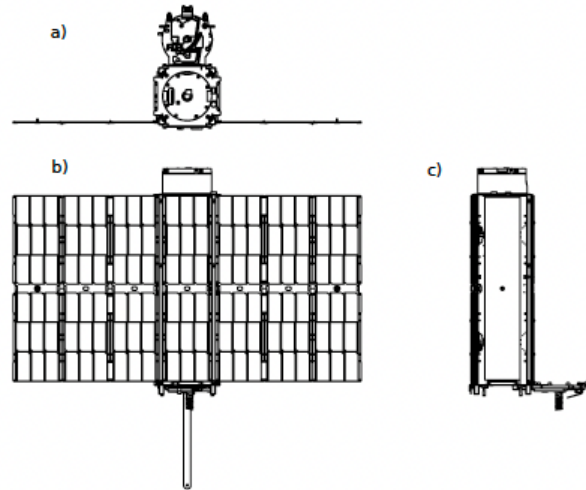


Figure 4. Planet’s Dove 3U CubeSat in different orientations; a) low drag orientation; b) high drag orientation; c) intermediate orientation. Source: [12]

Each orientation can thus create different “thrusts” by altering the drag forces based on the area facing into the wind along the direction of travel for the satellite.

Planet uses this concept to manage a very large formation for commercial purposes. They launch and deploy many satellites at once and allow for natural perturbation to slowly separate the CubeSats. Once there is enough separation to resolve individual spacecraft and determine their orbits, they are given commands one by one to enter the formation. Whichever satellite is at the front of the pack is commanded to enter a high drag attitude. This increases the drag force which causes the satellite to descend. At a lower altitude, the orbital velocity increases, and this creates a separation between the satellites. Planet then repeat this for each satellite with careful timing to create the desired distribution according to the algorithm shown in Figure 5:

---

**Algorithm 2** Differential Drag Control Algorithm

---

```
1: procedure CREATE HIGH-DRAG WINDOWS
2:   remove any previously issued high-drag windows
3:   compute  $\theta_i, \dot{\theta}_i$  of each satellite  $i$  relative to previous leader (mean, not osculating)
4:   compute  $\ddot{\theta}$  of a satellite in high-drag vs. low-drag mode
5:   assign leader to be satellite with greatest  $\dot{\theta}$  (i.e. lowest altitude)
6:   for each satellite  $i$  that is not the leader do
7:     offset  $\theta_i, \dot{\theta}_i$  to be relative to new leader:  $\theta_i = \theta_i - \theta_{leader}, \dot{\theta}_i = \dot{\theta}_i - \dot{\theta}_{leader}$ 
8:     get required high-drag duration to null relative speed with leader:  $\Delta t_{i,hd} = -\frac{\dot{\theta}_i}{\ddot{\theta}}$ 
9:     get angle travelled during desired high-drag window:  $\theta_{i,hd} = \frac{1}{2}\ddot{\theta}\Delta t_{i,hd}^2$ 
10:    get wait time to target desired slot:  $\Delta t_{i,wait} = \frac{\theta_{i,hd} - \theta_i}{\dot{\theta}_i}$ 
11:    create high-drag window for satellite  $i$  starting at  $t_{now} + \Delta t_{i,wait}$  for duration  $\Delta t_{i,hd}$ 
12:  end for
13: end procedure
```

---

Figure 5. Planet control algorithm to create the constellation. Source: [12]

Once their 105 Dove satellites were evenly distributed around the sun-synchronous orbit in a single plane then they needed to maintain the spacing. Each satellite operates independently and performs a number of tasks, including imaging and transmitting data to ground stations. These operations are mostly done from the nominal low drag configuration with the camera pointed nadir and the side panels facing into the wind, but over time even minor differences and changes add up and the spacing degrades demanding high drag maneuvers to maintain the desired relative positions. These high drag maneuvers were performed as needed using the algorithm in Figure 5 for groups of 10 satellites at a time. Planet found that the control authority depended greatly on altitude and atmospheric conditions which are greatly affected by the solar cycle [12]. This is a relatively simple algorithm that is an effective method of control, but it is monitored and managed with humans in the loop which increases cost and lowers overall efficiency.

A second method that is used is a classical Proportional Integral Derivative (PID) controller to manage the attitude of the spacecraft and maneuver them into a formation. This method is relatively simple as well and uses tried and true classical control methods to achieve the desired effect. One such system uses the following control law [18]:

$$\delta A = K_p \cdot \delta E + K_i \cdot \int \delta E dt + K_d \cdot \frac{d\delta E}{dt} \quad (2)$$

In Equation 2,  $A$  is the drag area,  $E$  represents the orbital energy,  $K_p$  is the proportional gain value,  $K_i$  is the integral gain, and  $K_d$  is the derivative gain. This method is effective and can reduce the gap between the satellites to within tens of meters of the intended separation [18]. However, this method alone is unable to account for additional constraints such as pointing requirements for sensors or solar panels and is limited in its ability to account for changing atmospheric conditions or achieve the minimum possible time and thus increase the impact to other satellite operations.

The third existing method of using differential drag for formation flying is using an adaptive method based on a Linear Quadratic Regulator (LQR). This controller is better able to account for unknown conditions such as those in the atmosphere and is more complex than the PID or algorithm-based control systems. This approach uses a chaser spacecraft that would have to start out in a higher orbit and then maneuver down to link up with a second spacecraft [19]. It would then use mechanical dynamic drag devices to change its shape according to inputs from the LQR. In this way the chase spacecraft could maneuver itself into the desired position in relation to the first. This method is also effective, but it requires additional complexity. The LQR controller can increase the need for on-board processing, and it requires additional mechanisms on the spacecraft [19].

An optimal control system would be able to improve on both of these methods by providing faster results and the flexibility of accounting for numerous dynamic constraints. It would allow for simple commands to be uploaded from ground stations to any pair of satellites and could use custom guidance inputs based on their specific size and dimensions. There is no need for the cost of added complexity from drag devices or on-board processing, and an optimal control trajectory can account for mission related constraints while maintaining the constellation's desired spacing.



#### D. OPTIMAL TRAJECTORY AS PART OF A SYSTEM

This optimal trajectory will be created as part of a larger system. The desired end state of this system is that it is fully autonomous and has as little human input as possible. The system operators could simply input the desired formation separations, mission requirements, and spacecraft parameters and then the optimizer would generate the spacecraft attitudes over time that would achieve the desired results.

The major pieces of the system would be the spacecraft themselves, the physical effects from the environment, the situational awareness systems for determining the orbit, and finally the spacecraft operators who manage the spacecraft and generate the commands for the optimized attitudes and trajectories. This flow of information is shown in Figure 6:

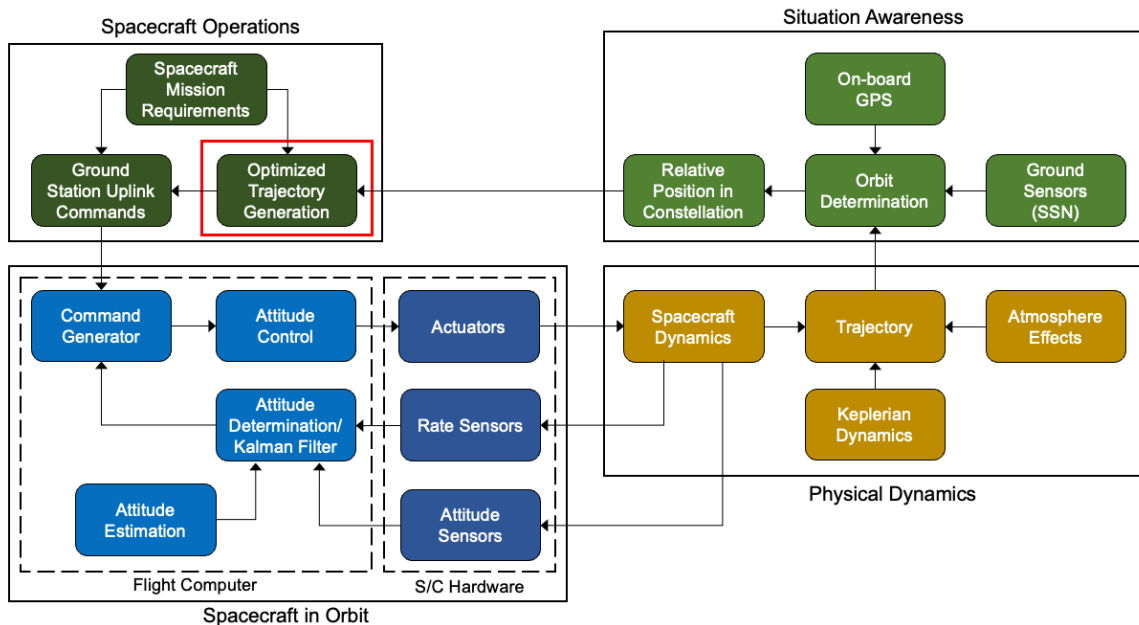


Figure 6. Block diagram of a formation using optimized differential drag. Optimal trajectory is generated at stage highlighted in red.

In this concept, higher level tasking comes from the spacecraft operators who make decisions about what the spacecrafts' mission requirements are. This can include targets for imaging, communications opportunities with ground site and users, power needs driving solar panel collect levels, or many other tasks depending on the payloads of the

spacecraft. These needs are fed into the trajectory planning program that uses the tasking as constraints in the optimizer software. The optimal trajectory planner then receives information from situational awareness systems to determine what adjustments are needed for the formation separations and calculates a new trajectory with the output of orientations, in quaternions, that can be sent to the spacecraft. This new trajectory is received via a TT&C link and the on-board command generator in the bus sends the guidance to the attitude determination and control system (ADCS) to begin adjusting the spacecraft's orientation. The ADCS then uses actuators such as momentum exchange devices, thrusters, or magnetorquers to reorient the spacecraft according to the guidance and control systems. This is a feedback loop which uses input from rate and attitude sensors, as well as Kalman filters employing dynamics modeling to ensure the spacecraft is performing the needed maneuvers. The physical spacecraft will dynamically interact with the environment according to the aero drag forces stemming from the relative motion of the spacecraft through the atmosphere and the Keplerian motion of the orbit. This will change its trajectory over time. The orbits of each spacecraft are then determined using on-board GPS units and from ground-based sensors. This updated orbit information is fed back into the ground stations where autonomous software and operators make adjustments to the trajectory and thus repeating the entire loop.

The information presented in this chapter serves as a conceptual framework for how and why differential drag maneuvers can be used to enable CubeSats to fly in formations as either large constellations or in swarms. This understanding is important when planning for or conducting the maneuvers required to build and maintain such formations. The following chapters will explore the specific calculations required to generate the commands needed for spacecraft which perform such maneuvers.

THIS PAGE INTENTIONALLY LEFT BLANK

### III. PROBLEM FORMULATION AND MODEL VERIFICATION

In order to actually model, simulate, and plan for a set of formation flying maneuvers, it is critical to understand the operating environment as well as the sets of equations which govern the rotational and translational motion of the spacecraft. Once the necessary dynamics equations and models are found, they must be verified against real-world data and systems to ensure that they are of sufficient fidelity, and thus able to predict and describe how the spacecraft will fly. This will provide a higher level of confidence to any maneuver planning tools that use these equations to generate commands for a formation flying spacecraft.

#### A. DYNAMIC MODEL

##### 1. Orbital Dynamics for Differential Drag Operations

The first major portion of the dynamic model is the development of the orbital dynamics that will dictate the trajectory of the spacecraft as it moves around the Earth. These equations are derived from Keplerian 2-body orbital motion and the aerodynamic drag forces on the spacecraft. The only major assumption used in developing these equations was that the orbits are circular, which is typically the case for CubeSats and small satellites in LEO as the drag forces will morph any slightly elliptical orbit into a nearly circular orbit over time [20]. The primary focus of these equations is to track the period, which is related to the semi-major axis or orbital altitude, and the true anomaly.

For a circular orbit, Equation 3 is used to calculate the period of an orbit as a function of the semi-major axis [20]:

$$P = \sqrt{\frac{4\pi^2 a^3}{\mu}} \quad (3)$$

In this equation,  $P$  is the orbital period,  $\mu$  is the Earth's standard gravitational parameter, and  $a$  is the semi-major axis. Next, we must find how the drag impacts the orbit. The drag force acts to remove energy from the satellite's orbit and slow down the instantaneous velocity of the satellite. When the energy of the orbit is reduced, the

satellite's altitude will decrease. Counter-intuitively, the reduction of altitude will cause the orbital velocity to increase. The higher velocity then increases the force of the drag and lowers the satellite into increasingly more dense layers of the atmosphere causing the exponential decay of the orbit as it descends in altitude. The drag force on the satellite is calculated using Equation 4 for aerodynamic drag:

$$D = \frac{1}{2} \rho v^2 A C_d \quad (4)$$

In Equation 4,  $D$  is the drag force,  $v$  is the velocity,  $A$  is the drag surface area,  $\rho$  is the atmospheric density, and  $C_d$  is the drag coefficient. By combining the equations for the length of the orbital period and the drag force it is possible to create a formula describing the rate of change of the orbital period due to the drag force for a circular orbit as a function of the radius represented by  $r$ . This was done by the Australian Space Weather Agency, and their results are shown in Equation 5 [20]. In this equation  $m$  is used to represent the spacecraft mass:

$$\frac{dP}{dt} = -3\pi r \rho \left( \frac{A C_d}{m} \right) \quad (5)$$

Equations 6 and 7 [20] were used to substitute the radius for a velocity term in circular orbits:

$$r v^2 = \frac{4\pi^2 r^3}{P^2} \quad (6)$$

$$r = \sqrt{\frac{v^2 P^2}{4\pi^2}} \quad (7)$$

Equations 8, 9, and 10 [20] were used to express the velocity term in terms of the orbital period for a circular orbit:

$$v_{circ} = \sqrt{\frac{\mu}{r}} \quad (8)$$

$$P_{circ} = \frac{2\pi}{\sqrt{\mu}} r^{\frac{3}{2}} \quad (9)$$

$$v = \frac{\sqrt[3]{2^3 \pi^3 \mu}}{\sqrt[3]{P_{circ}}} \quad (10)$$

Thus, the dynamics equations for the two different satellites' periods are the following:

$$\frac{dP_1}{dt} = \dot{P}_1 = -3\pi \sqrt{\frac{\left(\frac{\sqrt[3]{2^3 \pi^3 \mu}}{\sqrt[3]{P_1}}\right)^2 P_1^2}{4\pi^2}} \rho \frac{A_1 * Cd}{m} \quad (11)$$

$$\frac{dP_2}{dt} = \dot{P}_2 = -3\pi \sqrt{\frac{\left(\frac{\sqrt[3]{2^3 \pi^3 \mu}}{\sqrt[3]{P_2}}\right)^2 P_2^2}{4\pi^2}} \rho \frac{A_2 * Cd}{m} \quad (12)$$

Next, the dynamics for the position of the satellites within their orbits are determined. This will be represented by the number of orbits starting from the ascending node instead of the degrees from the ascending node. This value will be represented by  $X$  and it will be calculated using the angular rate of change for the satellite over an orbit. This is a function of the orbital velocity and the radius of the orbit, both of which are in terms of the orbital period as shown in the previous equations. This is captured in Equations 13 and 14 which are the rates of change for the number of orbits for each satellite.

$$\frac{dX_1}{dt} = \dot{X}_1 = \text{atan} \left( \frac{\left(\frac{\sqrt[3]{2^3 \pi^3 \mu}}{\sqrt[3]{P_1}}\right)^{\frac{2}{3}}}{\left(\frac{P_1 \sqrt{mu}}{2\pi}\right)^{\frac{2}{3}}} \right) / 2\pi \quad (13)$$

$$\frac{dX_2}{dt} = \dot{X}_2 = \text{atan} \left( \frac{\left(\frac{\sqrt[3]{2^3 \pi^3 \mu}}{\sqrt[3]{P_2}}\right)^{\frac{2}{3}}}{\left(\frac{P_2 \sqrt{mu}}{2\pi}\right)^{\frac{2}{3}}} \right) / 2\pi \quad (14)$$

## 2. Modeling the Atmosphere

The next important part of simulating formation flying using differential drag is the development of a reasonable model for the density and behavior of the upper atmosphere. Since differential drag operations do not make use of onboard propulsion, the small drag forces exerted by the atmosphere effectively act as the thrust for the spacecraft. For performing maneuver calculations, knowing the density and properties of the atmosphere is crucial. The atmosphere in space is notoriously difficult to predict as it is rarified and subject to many influences. There have been many models developed to do this, but all of them only represent an approximation of the atmosphere and are subject to a 10–15% error rate [20]. Generally, atmospheric models are based on one of three core principles. First, they could be based on empirical measurements of satellites in orbit and how they decay over time. Second, there are models which use data drawn from measurements taken from the ground based on the flow of charged particles and their interactions with the Earth's magnetic field. Lastly, they come from general circulation models that use fluid flow models to describe the upper atmosphere's behavior [21]. These models are shown in Figure 7. Few if any of these are analytical methods, instead they generally pull data from databases or look-up tables based on empirical data or models. This renders them mathematically challenging to manipulate. There is not even much consensus over which of these models are best, or how to evaluate the validity of one over the other, but nevertheless it is critical to have a reasonably accurate model of the upper atmosphere to optimize differential drag maneuvers.

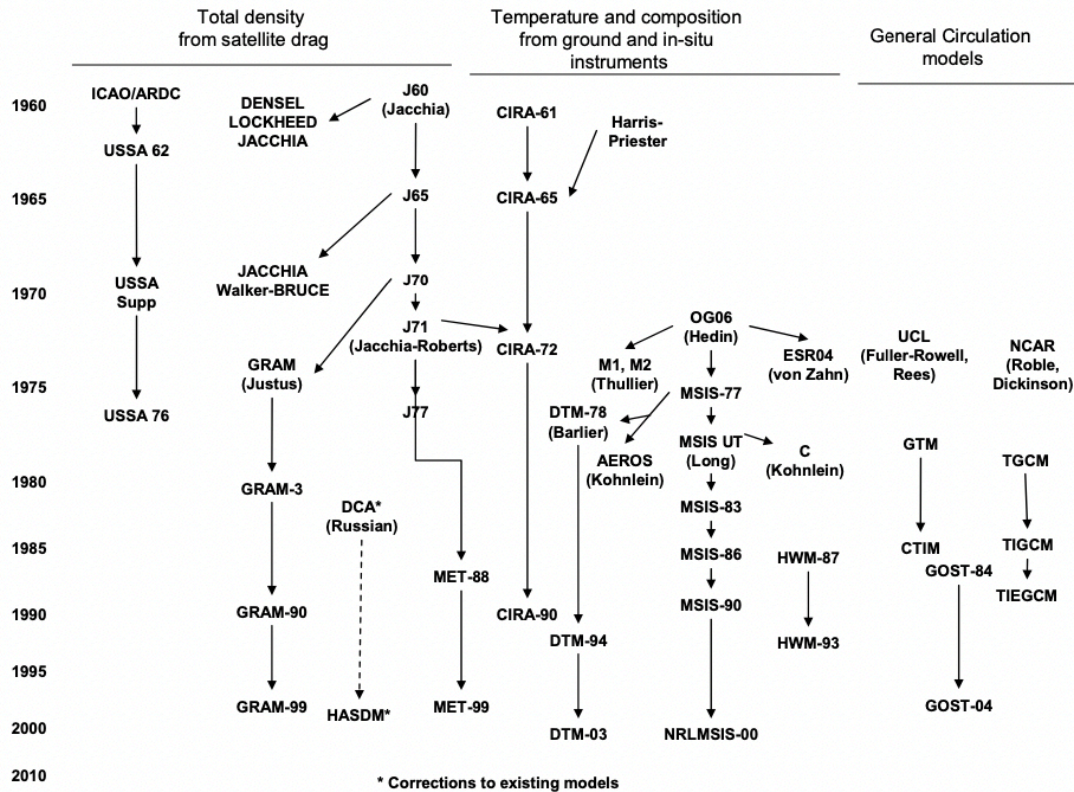



Figure 7. Models for the Earth’s atmosphere in space. Source: [21]

There are many factors that affect the upper atmosphere in the troposphere, the thermosphere where differential drag is effective, and out into the exosphere deeper in space. Generally, the region we are interested in is from 65 to 1000 km above the Earth’s surface. Below 65 km the reentry forces will destroy any spacecraft not designed for them, and above 1000 km the atmosphere density is so low it has a negligible effect on spacecraft operations on any meaningful timescale. For differential drag maneuvers to be effective or reliable they are typically done starting from 600 km down to around 250 km after which time the spacecraft will reenter in a matter of weeks or days depending on many factors. There are four major factors to consider when modeling this region: altitude, temperature, latitude, and the Earth’s rotation. To aid in understanding, the effects of these factors are modeled in a MATLAB simulation on a hypothetical 6U CubeSat such as the one shown in Figure 8.





Parameter	Value
Height	34.05 cm
Width	22.63 cm
Length	10 cm
Mass	12 kg
Cd	2.2
High Drag Area	0.07706 m <sup>2</sup>
Low Drag Area	0.02263 m <sup>2</sup>

Figure 8. Specifications of hypothetical 6U Cube used for the modeling

The first major factor to consider in drag effects is the altitude above the Earth. This has the most significant impact on the air density and decreases exponentially with altitude. This means that the lower in altitude a spacecraft descends, the faster the density will increase. In general, this means that very few satellites operate in altitudes below 300 km, since their orbits will decay very rapidly below that, and in general the atmosphere has very little impact on the spacecraft above approximately 1000 km in altitude. Equation 15 is used to calculate the density as a function of the altitude, solar activity, and the Earth's magnetism as discussed in the following section [20]. For these equations  $\rho_o$  is the density based on altitude (kg/m<sup>3</sup>),  $F_{10.7}$  is the Solar Flux Units (SFUs),  $A_p$  is the Geomagnetic Index (no units),  $h$  is the altitude of the spacecraft (km),  $H$  is the scale height (km),  $M$  is used to capture the altitude as part of the scale height (Kelvin/km), and  $T$  is the temperature (Kelvin) which is also factors into the scale height [20].

$$\rho_o = 6 \times 10^{-10} * e^{\left(\frac{h-175}{H}\right)} \quad (15)$$

$$h = a - \text{Earth Radius} \quad (16)$$

$$H = \frac{T}{M} \quad (17)$$

$$T = 900 + 2.5(F_{10.7} - 70) + 1.5A_p \quad (18)$$

$$M = 27 - 0.012(h - 200) \quad (19)$$

The second factor is the temperature of the upper atmosphere, and this is a function of the amount of solar activity at the current time. The sun experiences 11-year cycles during which its magnetic poles flip. When the sun's magnetic poles align with its

rotational poles, the sun is relatively stable and is considered in a low activity state. If it is a period while the magnetic poles are flipping there is intense heliomagnetic turbulence deep inside the sun's structures and this results in a large number of sunspots, solar flares, coronal mass ejections, and increase in solar wind output. This increases the amount of radiation, mostly X-rays and charged high speed particles, that wash over the Earth and interact with its magnetic field and upper atmosphere causing it to heat [20]. This heating causes an expansion of the troposphere and thermosphere which actually raises the denser layers higher into space thus increasing air density for a particular orbital regime. Solar activity is measured by the F10.7 solar radio flux scale. This is measured in Solar Flux Units which range from about 65 to over 300 and are measured in  $10^{-22}\text{W/m}^2/\text{Hz}$ ; this is an equivalence index of all the factors that heat the atmosphere. The geomagnetic index, known as  $Ap$ , must be taken into account as well, which describes the effect of solar storms on the Earth's magnetic field and ranges from 0 to 400 [20].

Using the density equation, it is possible to propagate the orbit of the 6U CubeSat from Figure 8 at different levels of solar activity from an orbit of 500 km until it re-enters and burns up in the thicker portions of the Earth's atmosphere below 100 km of altitude. This is shown in Figure 9, and it is clear that solar activity has a dramatic impact on the lifetime of the satellite. The exact solar flux at any given time is also notoriously variable and difficult to predict; it contributes to the large uncertainty in the atmosphere's behavior.

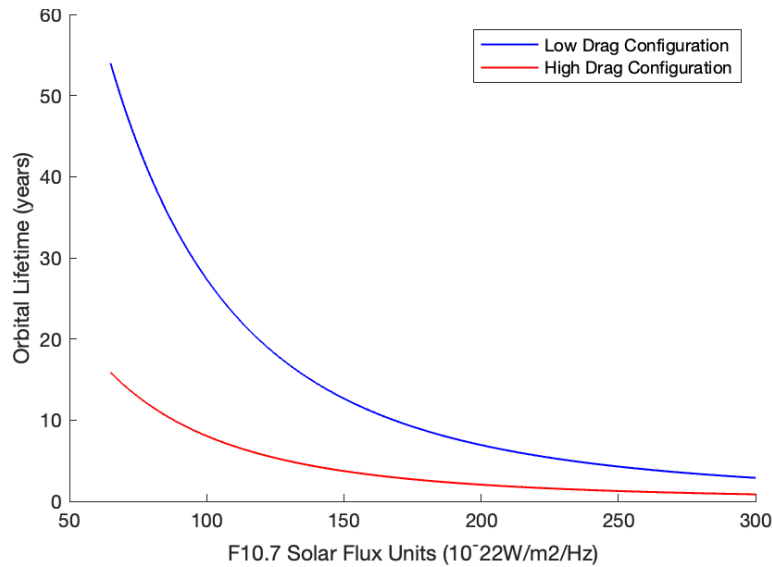


Figure 9. Effect of solar flux versus orbital lifetime of a standard 6U CubeSat

The effect of solar activity has a dramatic effect on the air density, and thus both the lifetime of the satellite and the control authority it has when performing maneuvers with differential drag.

The third major consideration of modeling the atmosphere is that its density is not uniformly distributed around the entire planet. The calculations described thus far provide an average density around the Earth, but this is not reflective of reality for all latitudes. The atmosphere is markedly thinner over the poles than it is around the equator, and this is a result of the oblateness of the Earth around the equator that affects the density in several ways [3]. First, the gravity is greater around the equator, and this pulls a larger amount of air mass to this region. Second, the Earth rotates faster at the equator and this increased velocity is imparted to the atmosphere which means the air extends deeper into space, thus increasing the density at higher altitudes. This effect is shown in Figure 10. At the higher latitudes the density decreases, and while it may appear at first to be minor, at a sample altitude of 400 km the average air density is roughly 30% less in a 90° inclination orbit as it is in a 0° orbit. Note that the values shown in Figure 10 are derived Equation 15 and are averages over the entire orbit and not representative of a particular point.

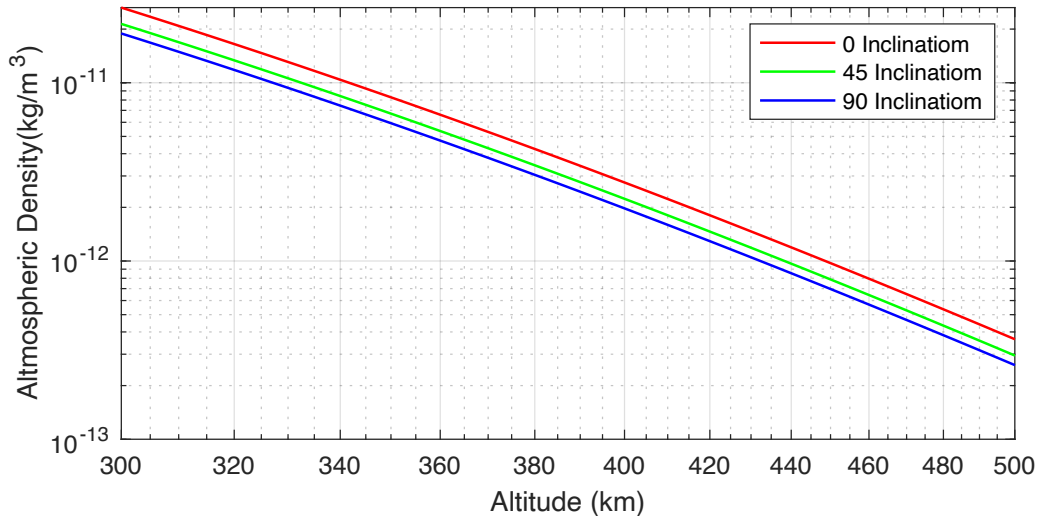


Figure 10. Logarithmic plot of average air density for over entire orbit versus altitude at different inclinations from 300 km to 500 km altitudes

To see how the inclination factor affects the spacecraft at a given altitude and inclination, Figure 11 shows the density changes as a function of spacecraft latitude, or how far above or below the spacecraft is from the equator. Given that all equations must be in terms of orbital period and orbits a new expression had to be formulated by the author for this thesis. This new expression was created manually via trial and error by adjusting values until the new model matched existing atmospheres as closely as possible. This process was necessary to create a concise, smooth, and continuously differentiable equation to describe the density at a particular latitude which allowed for the calculations of formation flying maneuvers. The validation for this model will be described in a later section, and the equation for calculating the density based on altitude and latitude, represented by  $\rho$ , is shown below:

$$\rho = \rho_o(1.1\cos(i|\sin(X2\pi)|) + 0.4) \quad (20)$$

Using Equation 20 to modify the  $\rho_o$  value from Equation 15, it is possible to plot the atmospheric density at any latitude and altitude for a spacecraft.

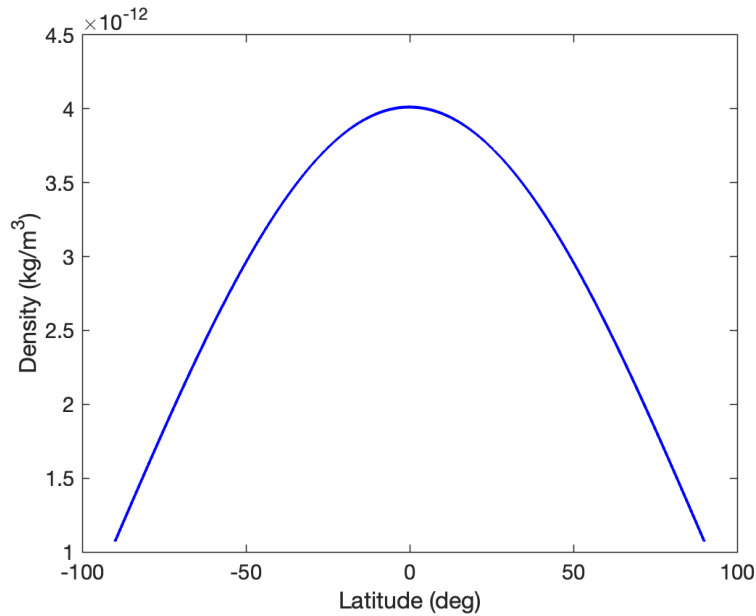


Figure 11. Air density versus spacecraft elevation angle for a spacecraft orbiting at 500km and 90° inclination

As shown in Figure 11, the air density at the equator is nearly four times the density above the poles, and this has a proportional impact on the drag force experienced by the spacecraft. Also, the densities described in Figure 11 are consistent with measurements of the thickness of the lower regions of the atmosphere as well. For example, the troposphere at the equator extends to an altitude of roughly 20 km and only to 6 km at the poles [22]. This ratio is consistent with the ratio of densities at the different latitudes in Figure 11.

The fourth factor for modeling a spacecraft in the Earth’s extreme upper atmosphere is that the air mass in which it flies is also rotating around the Earth at roughly the same speed the Earth is rotating [23]. Any motion of the atmosphere which is in-track with the motion of the spacecraft will either increase or decrease the air speed of the spacecraft while the effects of the cross-track air motion are negligible on the orbit of the spacecraft. This means that if a spacecraft is in a 0° inclination it experiences a “tailwind” effect. The spacecraft moves along through the air in the same direction that the air is moving, and its air speed will be reduced and thus there is a decrease in the amount of drag force. This effect will lessen as the inclination increases, and as the “tailwind” effect the spacecraft experiences at 0° becomes a “crosswind” at 90°. At this point the motion of the air is orthogonal to the motion of the spacecraft and therefore this cross-track effect does

not add to or detract from the in-track air speed, or drag force, experienced by the spacecraft. As the orbit goes past 90° and becomes retrograde the spacecraft will begin to encounter a “headwind” effect which will increase the overall drag force. This effect varies at each altitude and latitude because it is a function of how far the spacecraft is from the axis of rotation for the Earth. The air is not orbiting, is it effectively behaving as if it is part of the Earth so at the poles it moves very slowly and at the equator it the farthest from the Earth’s z-axis and thus is moving faster. The effect of this is described by the following equation and shown in Table 2:

$$\text{Length of Sidereal Day} = (23 * 60 * 60 + 56 * 60 + 4.0905) = 86,164 \text{ sec} \quad (21)$$

$$\text{Rotation Rate of Earth} = \omega = \left(\frac{360^\circ}{86164}\right) = 0.0042 \text{ deg/s} = 7.2921 \times 10^{-5} \text{ rad/s} \quad (22)$$

$$\text{In Track Atmospheric Speed} = \cos(\sin(X * 2\pi) * i) * \cos(i) * \left(\frac{P\sqrt{\mu}}{2\pi}\right)^{\frac{2}{3}} * \omega \quad (23)$$

Table 2. In-track atmospheric speeds on a spacecraft orbiting at 400km

		In-Track Atmospheric Speed (km/s)						
		Latitudes (deg)						
		0	15	30	45	60	75	90
Inclination (deg)	0	0.49						
	30	0.43	0.37	0.43				
	60	0.25	0.12	0.25	0.13	0.18		
	90	0	0	0	0	0	0	0
	120	-0.27	-0.12	-0.25	-0.13	-0.18		
	150	-0.43	-0.37	-0.43				
	180	-0.49						

As shown in Table 2, the spacecraft experiences nearly 500 m/s of wind speed in the direction of the Earth’s rotation at the equator and virtually none at the poles. This is a significant fraction of the 7.67 km/s orbital velocity for a spacecraft at 400 km in altitude, and thus will impact the overall drag force experienced by the spacecraft.

All of these factors combine to greatly affect the ability of a satellite operator to effectively plan and execute a differential drag maneuver to maintain a formation of flying CubeSats. Lower densities will result in maneuvers that take much longer to execute because the difference between the force of drag imposed on the spacecraft will be relatively smaller. At higher densities the spacecraft will lose more altitude each time it executes a maneuver. Also, these factors mean that the inclination of the spacecraft greatly impacts how it will behave, and this is an important consideration when mission planning.

### 3. Modeling Spacecraft Attitude and Drag Area

Finally, it is vital to accurately calculate the drag area of the spacecraft when performing differential drag maneuvers. The drag area will be a function of the size and shape of the spacecraft as well as the orientation of the spacecraft with respect to the direction of travel, which is analogous to the orbital reference frame. In this reference frame, the  $x$ -axis is defined as the direction of the spacecraft's velocity vector, the  $y$ -axis is in the cross-track direction, and the  $z$ -axis is radial from the center of the Earth through the spacecraft [24]. This is depicted in Figure 12.

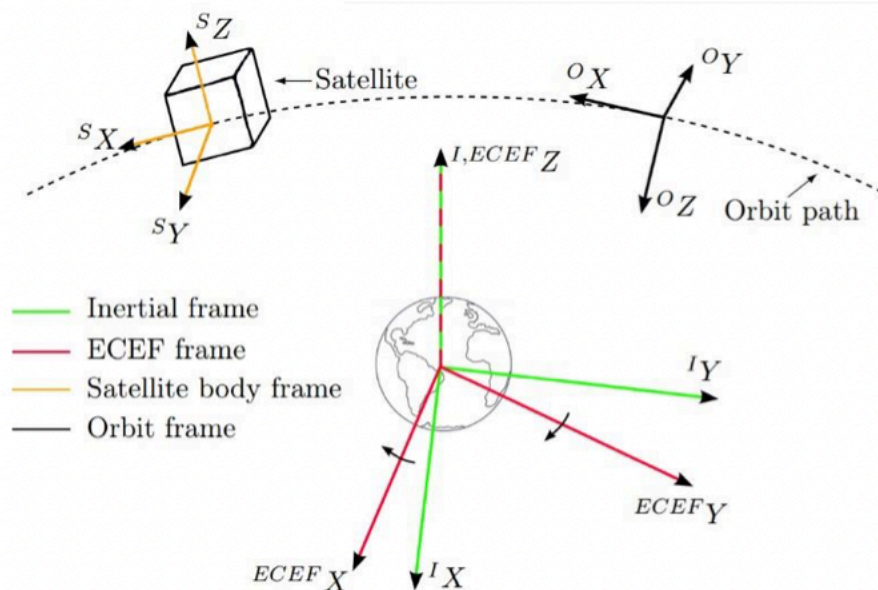


Figure 12. Spacecraft orientation of reference frames. Source: [24]

The spacecraft body reference frame can rotate with respect to the orbital frame throughout the orbit. The preferred orientation will depend on many factors such as the placement and objectives of the sensors and payloads on the spacecraft as well as the solar panels which will need to remain oriented towards the sun some minimum amount in order to produce enough power for the spacecraft. The manipulation of the orientation of the spacecraft with respect to the direction of travel is also how differential drag operations are able to adjust relative positions of spacecraft.

To model the spacecraft, a simple rectangular shape was chosen. This shape will allow for all six sides to be individually accounted for and allows for a more accurate modeling of the shape of most spacecraft and placement of components such as solar panels. The dimensions of the spacecraft are defined, and then the area of each face is calculated. This area is then applied as a scalar multiplier to the basis vectors of the spacecraft body reference frame. This model is depicted in Figure 13:

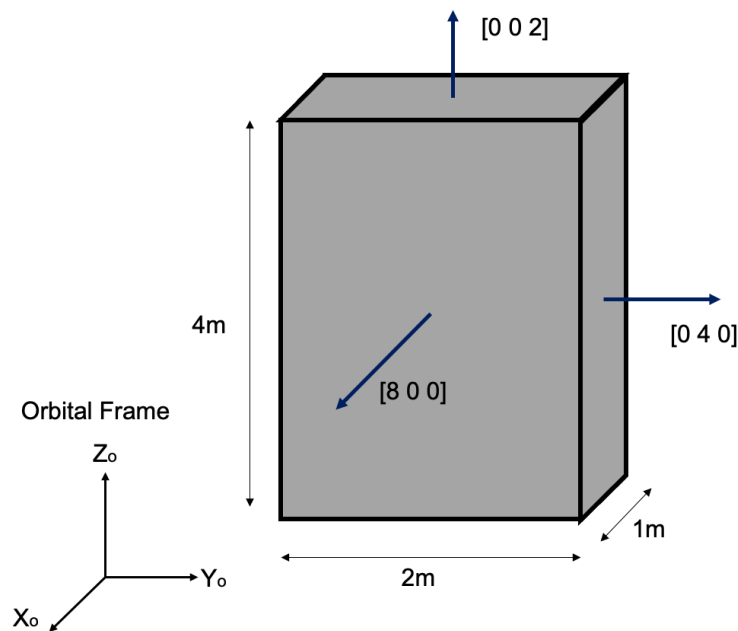


Figure 13. Spacecraft model for drag area calculations

The next step is to define the spacecraft orientation using quaternions. The quaternion of the orientation of the body frame with respect to the orbital frame is defined



by the Equations 24 through 27 where  $[e_1 e_2 e_3]$  is the eigenaxis of rotation and  $\alpha$  is the rotation about the eigenaxis:

$$q_0 = \cos\left(\frac{\alpha}{2}\right) \quad (24)$$

$$q_1 = e_1 * \sin\left(\frac{\alpha}{2}\right) \quad (25)$$

$$q_2 = e_2 * \sin\left(\frac{\alpha}{2}\right) \quad (26)$$

$$q_3 = e_3 * \sin\left(\frac{\alpha}{2}\right) \quad (27)$$

To use the quaternions to transform a vector they must be converted into a direction cosine matrix (DCM) using Equation 28:

$$C_{BO} = \begin{bmatrix} 1 - 2(q_2^2 + q_3^2) & 2(q_1q_2 + q_3q_0) & 2(q_1q_3 - q_2q_0) \\ 2(q_2q_1 - q_3q_0) & 1 - 2(q_1^2 + q_3^2) & 2(q_2q_3 + q_1q_0) \\ 2(q_3q_1 + q_2q_0) & 2(q_3q_2 - q_1q_0) & 1 - 2(q_1^2 + q_2^2) \end{bmatrix} \quad (28)$$

The six normal vectors for each face can then be transformed by the quaternion by using the DCM created from Equation 29 and multiplying it by each of the six vectors. These new rotated vectors will now represent the direction of each face of the spacecraft with respect to the orbital reference frame. Each of these six face vectors will still retain their original magnitude which denotes the surface area of each face.

To calculate the drag area, the component of each face vector which is projected on the orbital x-axis must be calculated and then summed together to find the area. However, since each of the six faces have a face that is their equal and opposite, only the rotated face vectors with positive values can be added together. This calculation can be performed using Equation 29 which is suitable for most computing applications. However, the use of absolute values can create problems when using optimization tools, which generally require continuous functions that have smooth derivatives. As a result, the absolute values can be replaced with sigmoid functions as shown in Equation 30. Both of these methods will be employed as part of this thesis.

$$Area = \left| [1 \ 0 \ 0] \left( C_{BO} \begin{bmatrix} 8 \\ 0 \\ 0 \end{bmatrix}_{face\ 1} \right) \right| + \left| [1 \ 0 \ 0] \left( C_{BO} \begin{bmatrix} 0 \\ 4 \\ 0 \end{bmatrix}_{face\ 2} \right) \right| + \left| [1 \ 0 \ 0] \left( C_{BO} \begin{bmatrix} 0 \\ 0 \\ 2 \end{bmatrix}_{face\ 3} \right) \right| \quad (29)$$

$$Area = \frac{1}{1 + e^{-200 * \frac{[1 \ 0 \ 0] * \left( C_{BO} \begin{bmatrix} 8 \\ 0 \\ 0 \end{bmatrix}_{face\ 1} \right)}{8}}} * \left( [1 \ 0 \ 0] \left( C_{BO} \begin{bmatrix} 8 \\ 0 \\ 0 \end{bmatrix}_{face\ 1} \right) \right) + Face2 + Face3 + \dots \quad (30)$$

Using these calculations, it is possible to determine the exact drag area for any orientation of the spacecraft based on its size and shape. This will be useful when constraining certain orientations of the spacecraft to allow for mission operations, while still allowing for maneuvers to occur. Equations 29 and 30 apply for any spacecraft which can be modeled based on the cuboid shape shown in Figure 13.

## B. TESTS TO VALIDATE AND VERIFY MODEL

To verify that the dynamics and models explored thus far are correct and accurately reflect established models and real-world data, it is vital to validate and verify that the equations reflect real world systems and are corroborated by other methods.

### 1. ISS Orbit Propagation

As a first step the dynamics were used to create a propagator based on MATLAB's ODE45 function, and this was used to simulate the orbit of the International Space Station (ISS) to compare it to real-world data for a current system. For this test the following values were used to model the ISS

- 459,023 kg for ISS mass [25]
- 1951 m<sup>2</sup> for ISS drag area [25]
- 2.0 for Coefficient of Drag [25]
- 400 km altitude [25]
- Solar Flux: 119 SFU for solar max year (2013), 60 for solar min year (2009) [8]

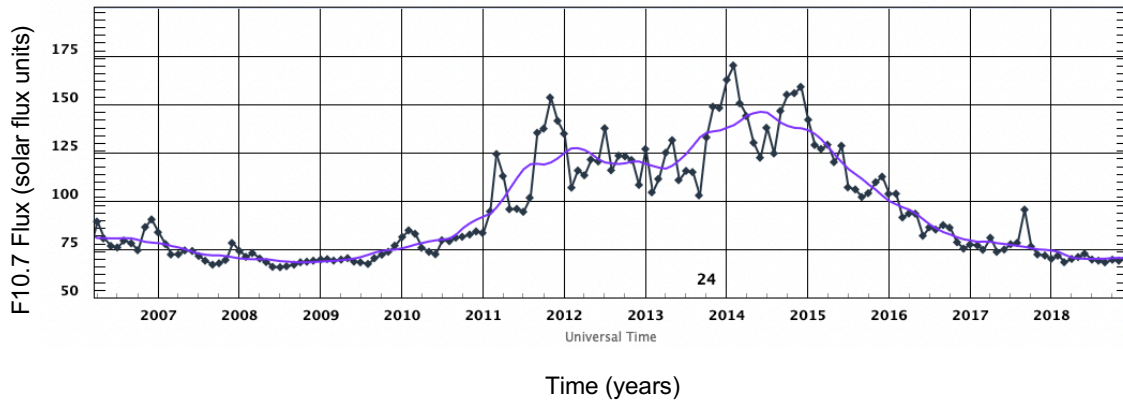


Figure 14. Solar flux for 2006–2018. Source: [26]

Based on these values Figure 15 was produced to show the ISS’s orbital decay over a year and calculate its expected altitude drop due to the drag force. From empirical data since it finished construction, the ISS should experience a  $38 \pm 14$  km of drop in a solar maximum year, and  $13 \pm 5$  km of drop in a solar minimum year [27]. However, this drop amount is not all consecutive because of the maintenance burns that the ISS periodically conducts. This means that the altitude typically varies between 410 km and 390 km at any given time. Therefore, the values of 38 km and 7 km of altitude loss are a summation of the total amount the orbit decays, and not a difference from the beginning of the year to the end. To replicate this, the orbit of the ISS is propagated for one month at a time and then multiplied by 12 to find the total amount of orbital decay over a year. This one-month decay is shown in Figure 15.

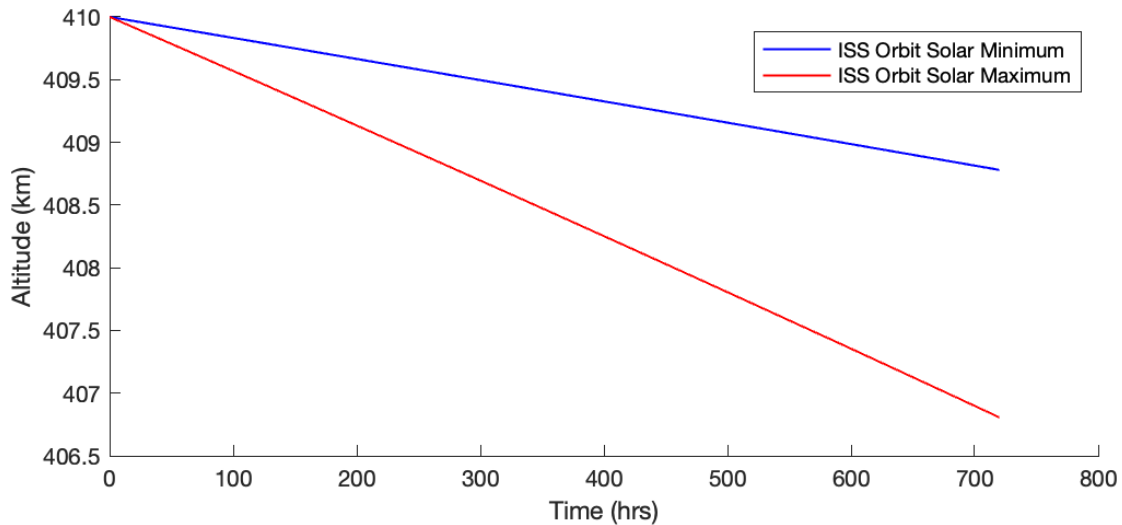


Figure 15. Propagation of the International Space Station for one month

As shown in Figure 15, the atmospheric model and orbital dynamics equations predict a drop of 14.6 kilometers over a one-year period during solar minimum, and 38.3 kilometers over a one-year period during a solar maximum. This is a useful figure of merit to validate the model and show that it is well within the 10–15% expected uncertainty of an upper atmosphere model.

## 2. Orbital Lifetime Comparison

The second test is to use the orbital propagator to test how long a small CubeSat would stay in orbit before its orbit decays and it is destroyed in the atmosphere. In this test the new atmosphere model (referred to as DeMoss 2022) is compared against simulations of other established models, and a 6U CubeSat, such as the one shown in Figure 8, in a 500 km orbit was used in the simulation. To establish a baseline for comparison AGI’s Systems Tool Kit (STK) was used to import the atmosphere models and propagate the satellite’s positions until it fully deorbits. The same satellite was then run through the DeMoss 2022 propagator for evaluation. To measure the effects of changing inclinations, and their effects on latitude/density and in-track atmospheric speeds, the orbital lifetime evaluation was conducted at a range of inclinations from 0° to 180°. Table 3 and Figure 16 show the results of this test.

Table 3. Comparison of different atmosphere models

Orbital Lifetime in years from 500km for Drag Area of 0.07706 m <sup>2</sup> , 12kg S/C, 119 SFUs						
Inclination	Model (Orbital Lifetime in years from 500km)					Error from Mean (%)
	Jacchia 70	NRLMSISE 2000	DTM 2012	Mean Value	DeMoss 2022	
0	4.2	4.1	4.0	4.1	4.2	2.44
30	4.7	4.6	4.4	4.6	4.4	3.65
60	5.9	5.8	5.3	5.7	5.0	11.76
90	6.7	6.7	6.1	6.5	6.5	0.00
120	4.9	4.8	4.6	4.8	4.8	0.70
150	3.7	3.7	3.6	3.7	3.9	6.36
180	3.4	3.4	3.3	3.4	3.7	9.90

From Table 3 it is clear that the new model and dynamics are not perfect at all inclinations, but it is generally within 5% of the other models on average and well within the expected 15% variation between models. The major advantage of the DeMoss 2022 atmosphere model is the relative simplicity, and ease of calculation and application for optimization problems. The model performs adequately for these needs.

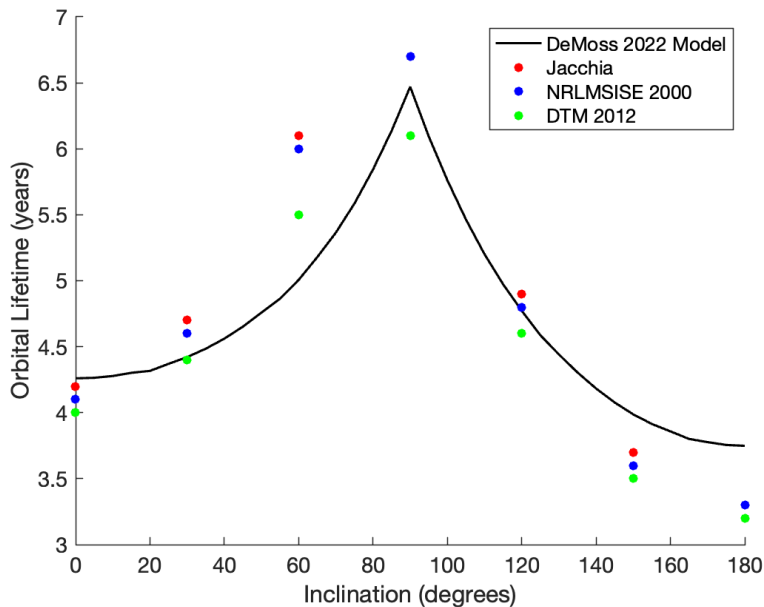


Figure 16. Comparison of orbital and atmosphere models

### 3. Conservation of Energy

The next test is to evaluate whether or not the model and dynamics conserve energy. The orbital energy of the spacecraft will be reduced by the aerodynamic drag forces and therefore, the energy lost from orbital energy and the energy lost to the drag force should be equivalent. The following equations can be used to describe this effect:

$$E = \frac{1}{2} * \frac{\mu}{\left(\frac{P\sqrt{\mu}}{2\pi}\right)^{\frac{2}{3}}} \quad (31)$$

$$E_{Loss} = E_{initial} - E_{final} \quad (32)$$

$$D = \frac{1}{2}(V - RelWind)^2 ACd 6x10^{-10} \rho \quad (33)$$

$$E_{Drag} = D * Distance \quad (34)$$

In Equations 31–34,  $E$  refers to the total orbital energy of the spacecraft (kJ),  $E_{Loss}$  is the difference between the orbital energies at the beginning and end of the simulation (kJ),  $D$  is the drag force (kN), and  $E_{Drag}$  is the energy lost to the force of drag (kJ). However, since the drag force changes as the satellite drops in altitude it is necessary to average the initial and final values of the force:

$$D = \frac{D_{initial} + D_{final}}{2} \quad (35)$$

The same must be done to calculate the distance, because as the orbit drops the distance around the orbit changes as well:

$$Distance = 2\pi * a * Number\ of\ Orbits \quad (36)$$

$$Distance = \frac{2\pi\left(\frac{P_{initial}\sqrt{\mu}}{2\pi}\right)^{\frac{2}{3}} + 2\pi\left(\frac{P_{final}\sqrt{\mu}}{2\pi}\right)^{\frac{2}{3}}}{2} * X \quad (37)$$

For Equation 37,  $P_{initial}$  is the orbital period at the beginning of the simulation and  $P_{final}$  is the orbital period at the end of the simulation.

These equations are then applied to the case of the ISS orbit decay over a single orbit. By doing so we find that the loss of orbital energy is 9,926 kJ and the total energy

lost to the drag force is 9,967 kJ, which are 0.4% of each other. For comparison, this means that the ISS loses approximately 2,757 Watt-hours of energy per orbit due to drag.

#### 4. Quaternion Norm Condition

An important property of quaternions is that the norm of all the elements of the quaternion must equal 1. This test will evaluate the outputs from a differential drag simulation using the rotational dynamics previously described. This simulation solves for the rotational maneuvers needed to conduct a minimum time differential drag maneuver. It controls the rotational velocities of each of the three-body frame axis to manipulate the quaternions. If the dynamics are correctly implemented, the norm over time should remain constant at 1. To conduct this test all the quaternion states from the simulation of maneuvering the spacecraft through many orientations as it orbits, and maneuvers will be normalized and then analyzed.

This test evaluated 10,000 quaternions produced by the simulation when moving through one full orbit, performing a 90° rotation about the  $y$ -axis, and then completing another orbit. This test produced the Figures 17, 18, and 19 that describe the rotation:

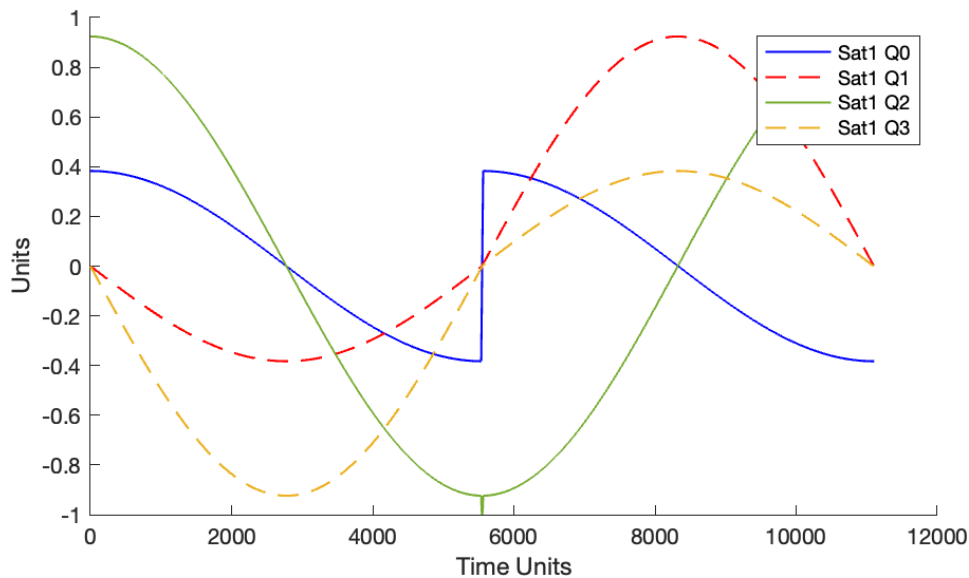


Figure 17. Quaternions over time of the rotational dynamics simulation

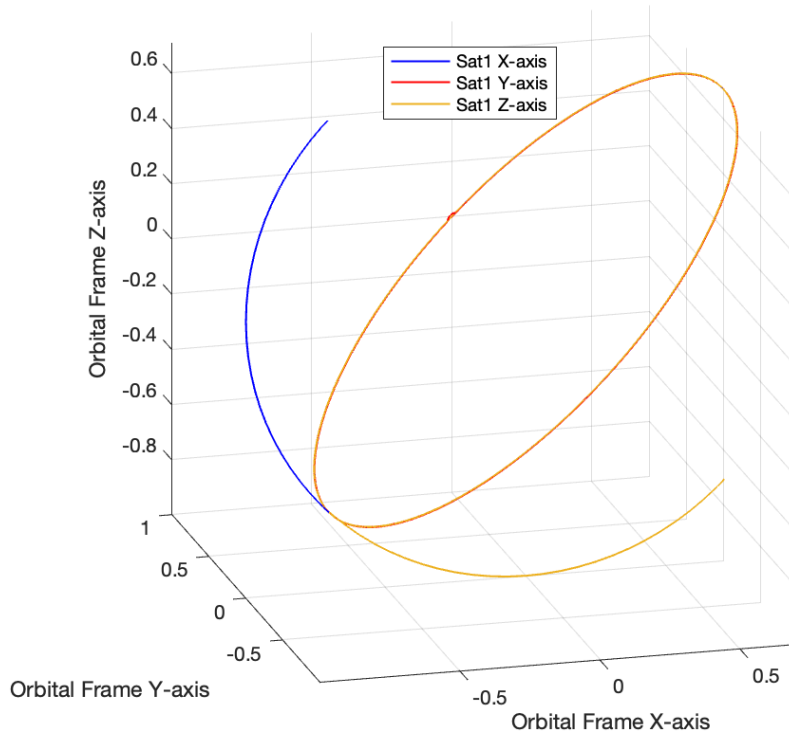


Figure 18. 3D plot of the tracks of each body frame axis with respect to orbital frame during orbits and 90° rotation

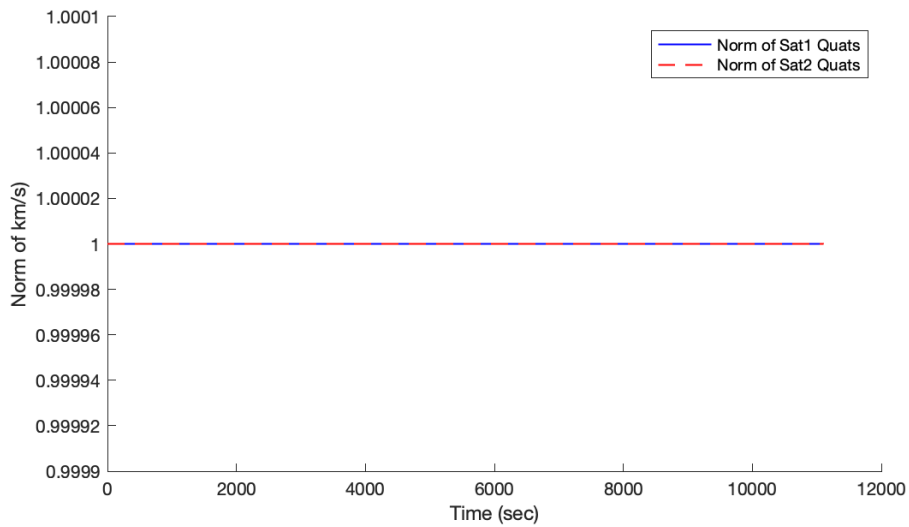


Figure 19. Norm of quaternions over time

The simulation produced 10,000 quaternions, one for each time step, and the norm of all 10,000 was equal to 1. This shows that the rotational dynamics are valid.



## 5. Drag Area Calculations

The final test was to evaluate the ability of the drag area calculation function to accurately find the area of the spacecraft which is facing in the direction of the velocity vector. For this test, the spacecraft model from Figure 13 was used:

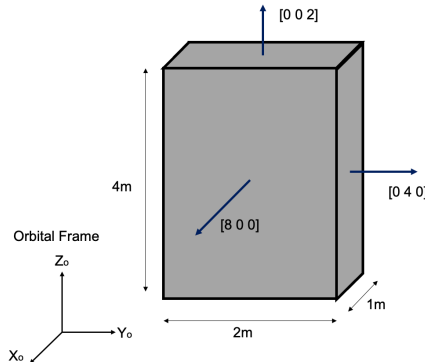


Figure 20. Spacecraft model for drag area calculations

Based on this test, some simple rotations were verified mathematically, and then compared to the area calculation function to verify it is performing the correct calculations.

Table 4. Drag areas calculated from quaternion rotations

Drag Area Calculation Test				
Rotation Axis	Rotation Angle (deg)	Expected Value	Area Calculator	Quaternion
X	90	same side faces $VBAR = 8$	8	[0.707, 0.707, 0, 0]
X	180	same side faces $VBAR = 8$	8	[0, 1, 0, 0]
X	45	same side faces $VBAR = 8$	8	[0.924, 0.383, 0, 0]
Y	90	$\cos(90)*8 + \sin(90)*2 = 2$	2	[0.707, 0, 0.707, 0]
Y	180	$\cos(180)*8 + \sin(180)*2 = 8$	8	[0, 0, 1, 0]
Y	45	$\cos(45)*8 + \sin(45)*2 = 7.07$	7.07	[0.924, 0, 0.383, 0]
Z	90	$\cos(90)*8 + \sin(90)*4 = 4$	4	[0.707, 0, 0, 0.707]
Z	180	$\cos(180)*8 + \sin(180)*4 = 8$	8	[0, 0, 0, 1]
Z	45	$\cos(45)*8 + \sin(45)*4 = 8.48$	8.48	[0.924, 0, 0, 0.383]

The results of this test show that the area calculation function is valid and will be able to produce the maximum and minimum possible areas for a spacecraft to use during

differential drag maneuvers while its orientation is constrained due to mission requirements.

Overall, the models and dynamics developed in this chapter accurately describe the motion of a spacecraft as it orbits through the thin upper atmosphere that exists in LEO. They are able to predict how the rotational motion of a spacecraft will impact its orbital trajectory due to the force of drag, and can do so in a manner consistent with both real-world spacecraft such as the ISS and other simulation environments like STK. These equations will serve as the foundation on which maneuvers can be calculated to produce a set of commands for spacecraft to perform to achieve the desired formation.

THIS PAGE INTENTIONALLY LEFT BLANK

## IV. TRAJECTORY OPTIMIZATION PROBLEM

Pontryagin's Principle will be used to solve the problem of how to conduct a minimum time formation flying maneuver using differential drag techniques. This is an optimization technique used to create a boundary value problem that if solved produces a solution to the optimization problem. Essentially, this technique uses the dynamics equations that govern the behavior of the system, a set of initial and final conditions, any constraints on the system, and a cost metric that must be minimized to generate the controls for the system to achieve the desired results [28]. Using an optimization technique will provide critical insights for how to construct and achieve a formation flying protocol for small propulsion-less spacecraft.

### A. SOLVING A SIMPLIFIED DIFFERENTIAL DRAG MANEUVER

#### 1. Problem Description

Solving a simplified differential drag maneuver to close the gap between two satellites without using the rotational dynamics equations is a necessary step in solving the formation flying problem. In this case, the drag areas of two spacecraft will be the control variables instead of the rates of rotation of the spacecraft. Many of the details of the atmospheric models and the rotational dynamics described in Chapter III were removed in order to simplify the problem. This was necessary in order to use Pontryagin's Principle to solve the underlying problem and find the optimal trajectories of maneuvering two satellites to adjust the distance between them.

To find the trajectories of spacecraft in a differential drag maneuver, a problem was formulated, and a MATLAB optimal control solver known as DIDO was used to create a solution and provide valuable insight on how to achieve a minimum time maneuver [29]. However, differential drag maneuvers, as with all low thrust maneuvers, are uniquely challenging problems to solve. This is because they involve long durations and involve rapidly changing conditions, like variable atmospheric conditions at different latitudes during an orbit, making the dynamics equations inherently stiff due to the multiple time scales involved. This means they become unstable if the sample rate is too low, and thus

they must be modified or simplified to be able to find a solution using a solver such as DIDO which is not designed to use potentially thousands of nodes [29]. Still, DIDO is a very valuable tool to solve short duration maneuvers using simplified models, and this method will conceptually demonstrate optimal trajectories which can be applied to a wider range of scenarios using a higher fidelity simulator. The inputs for the DIDO model will also require a satellite of unrealistic physical characteristics, much too lightweight and much too large, but again this is required to increase the effects of the drag forces and allow the solver to generate a useful solution while using fewer nodes over a shorter duration. Future work could involve finding methods of adding realistic fidelity while maintaining the requirement needed for DIDO to produce an extremal solution, or one which is feasible and meets the requirements established in the problem formulation.

## 2. Simplified Problem Formulation

$$\text{States: } \vec{X}^T = [P_1, X_1, P_2, X_2] \quad (38)$$

$$\text{Controls: } \vec{U}^T = [U_1, U_2] \quad (39)$$

The states in this problem are  $P_1$  and  $P_2$  which represent the orbital periods of satellites 1 and 2 as well as  $X_1$  and  $X_2$  which are the number of orbits completed by satellites 1 and 2 [29]. The controls for this problem will be the inverse of the ballistic coefficient where  $A$  is the area of the spacecraft that faces towards its direction of travel,  $Cd$  is the drag coefficient, and  $m$  is the mass of the spacecraft. Using Equations 40 and 41 to define the controls allows for a greater magnitude of the control term after the problem is properly scaled and balanced. This allows for the problem to be coded using DIDO which functions more efficiently when working with values closer in range to each other.

$$U_1 = (A_1 * Cd)/m \quad (40)$$

$$U_2 = (A_2 * Cd)/m \quad (41)$$

$$\text{Minimize } J[x(\cdot), u(\cdot), t_f] = t_f \quad (42)$$

Subject to

$$\dot{P}_1 = -3\pi \sqrt{\frac{\left(\frac{\sqrt[3]{2}\sqrt[3]{\pi}\sqrt[3]{\mu}}{\sqrt[3]{P_1}}\right)^2 P_1^2}{4\pi^2}} * \rho * U_1 \quad (43)$$

$$\dot{P}_2 = -3\pi \sqrt{\frac{\left(\frac{\sqrt[3]{2}\sqrt[3]{\pi}\sqrt[3]{\mu}}{\sqrt[3]{P_2}}\right)^2 P_2^2}{4\pi^2}} * \rho * U_2 \quad (44)$$

$$\dot{X}_1 = \text{atan}\left(\frac{\left(\frac{\sqrt[3]{2}\sqrt[3]{\pi}\sqrt[3]{\mu}}{\sqrt[3]{P_1}}\right)^{\frac{2}{3}}}{\left(\frac{P_1\sqrt{\mu}}{2\pi}\right)^{\frac{2}{3}}}\right) / 2\pi \quad (45)$$

$$\dot{X}_2 = \text{atan}\left(\frac{\left(\frac{\sqrt[3]{2}\sqrt[3]{\pi}\sqrt[3]{\mu}}{\sqrt[3]{P_2}}\right)^{\frac{2}{3}}}{\left(\frac{P_2\sqrt{\mu}}{2\pi}\right)^{\frac{2}{3}}}\right) / 2\pi \quad (46)$$

The following initial conditions and parameters were generated using the previously described atmosphere model and by using 119 Solar Flux Units and 0 for the geomagnetic index (these were the values on 1 December 2022) [26] and orbits at 400 km of altitude with an initial separation of 50 km which correspond to the values shown in Equations 47–50.

### Initial Conditions

$$P_1(t_0) = 5553.58 \text{ seconds} \quad (47)$$

$$P_2(t_0) = 5553.58 \text{ seconds} \quad (48)$$

$$X_1(t_0) = 0.00117 \text{ orbits} \quad (49)$$

$$X_2(t_0) = 0 \text{ orbits} \quad (50)$$

### Final Conditions

$$P_1(tf) - P_2(tf) = 0 \text{ seconds} \quad (51)$$

$$X_1(tf) - X_2(tf) = 0 \text{ orbits} \quad (52)$$

### Parameters

$$Re = 6378.1 \text{ km} \quad (53)$$

$$\mu = 3.986004418 \times 10^5 \text{ s}^2/\text{km}^3 \quad (54)$$

$$m = 70 \text{ kg} \quad (55)$$

$$Cd = 2.2 \quad (56)$$

$$\rho = 2.8921 \times 10^{-3} \frac{\text{kg}}{\text{km}^3} \quad (57)$$

### Constraints

$$4.714 \times 10^{-6} \leq U_1 \leq 1.886 \times 10^{-5} \text{ m}^2/\text{kg} \quad (58)$$

$$4.714 \times 10^{-6} \leq U_2 \leq 1.886 \times 10^{-5} \text{ m}^2/\text{kg} \quad (59)$$

The upper and lower values of  $U_1$  and  $U_2$  correspond to a maximum drag area of 0.060 km<sup>2</sup> and a minimum drag area of 0.015 km<sup>2</sup>. These are unrealistically large dimensions of a spacecraft, but they are used for demonstrating the concepts being applied in this problem formulation.

### **3. Scaling and Balancing**

To solve this problem, it is necessary to scale the input parameters in order to reduce the values of the states and controls to within a more manageable range. To do this the following values were chosen and applied to the parameter and boundary values:

- Distance Scale:

$$L = 100,000 \text{ km} \quad (60)$$

- Time Scale:

$$T = 100,000 \text{ sec} \quad (61)$$

- Mass Scale:

$$M = 100,000,000 \text{ kg} \quad (62)$$

- State Boundaries Scaled:

$$\frac{P(to)}{T}, \frac{P(tf)}{T} \quad (63)$$

- Parameters Scaled:

$$\frac{Re}{L}; \mu * \frac{T^2}{L^3}; \frac{Amax}{L^2}; \frac{Amin}{L^2}; \rho * \frac{L^3}{M}; \frac{m}{M} \quad (64)$$

## B. APPLYING PONTRYAGIN'S PRINCIPLE AND FINDING CONDITIONS FOR OPTIMALITY

Using the problem formulation and applying Pontryagin's Principle allows for the discovery of the necessary conditions of optimality. These conditions will serve as means to determine if the solution to the problem is indeed a minimum time orbit transfer using differential drag techniques. All values shown in the following sections will be scaled, but not marked as such. Unscaling back to engineering units will occur only after a solution is found.

### 1. Lagrangian of the Hamiltonian

$$\begin{aligned} \bar{H} = & -\lambda_{P_1} 3\pi \sqrt{\frac{\left(\frac{\sqrt[3]{2^3 \sqrt{\pi^3 \sqrt{\mu}}}}{\sqrt[3]{P_1}}\right)^2 P_1^2}{4\pi^2}} \rho U_1 + -\lambda_{P_2} 3\pi \sqrt{\frac{\left(\frac{\sqrt[3]{2^3 \sqrt{\pi^3 \sqrt{\mu}}}}{\sqrt[3]{P_2}}\right)^2 P_2^2}{4\pi^2}} \rho U_2 + \\ & \lambda_{X_1} \operatorname{atan} \frac{\left(\frac{\sqrt[3]{2^3 \sqrt{\pi^3 \sqrt{\mu}}}}{\sqrt[3]{P_1}}\right)^{\frac{2}{3}}}{\left(\frac{P_1 \sqrt{\mu}}{2\pi}\right)^{\frac{2}{3}}} / 2\pi + \lambda_{X_2} \operatorname{atan} \frac{\left(\frac{\sqrt[3]{2^3 \sqrt{\pi^3 \sqrt{\mu}}}}{\sqrt[3]{P_2}}\right)^{\frac{2}{3}}}{\left(\frac{P_2 \sqrt{\mu}}{2\pi}\right)^{\frac{2}{3}}} / 2\pi + \mu_1 U_1 + \mu_2 U_2 \end{aligned} \quad (65)$$



## 2. Conditions for Optimality

### a. Hamiltonian Minimization Condition

$$U_1^* = 0 = \lambda_{P_1} 3\pi \sqrt{\frac{\left(\frac{3\sqrt{2}^3 \sqrt{\pi}^3 \sqrt{\mu}}{3\sqrt{P_1}}\right)^2 P_1^2}{4\pi^2}} \rho + \mu_1 \quad (66)$$

$$U_2^* = 0 = \lambda_{P_2} 3\pi \sqrt{\frac{\left(\frac{3\sqrt{2}^3 \sqrt{\pi}^3 \sqrt{\mu}}{3\sqrt{P_2}}\right)^2 P_2^2}{4\pi^2}} \rho + \mu_2 \quad (67)$$

### b. Complementarity Condition

$$\mu_1 = \begin{cases} \leq 0 & \text{if } U_1 = 4.714x10^{-6} \\ = 0 & \text{if } 4.714x10^{-6} < U_1 < 1.886x10^{-5} \\ \geq 0 & \text{if } U_1 = 1.886x10^{-5} \end{cases} \quad (68)$$

$$\mu_2 = \begin{cases} \leq 0 & \text{if } U_2 = 4.714x10^{-6} \\ = 0 & \text{if } 4.714x10^{-6} < U_2 < 1.886x10^{-5} \\ \geq 0 & \text{if } U_2 = 1.886x10^{-5} \end{cases} \quad (69)$$

### c. Hamiltonian Value Condition

$$\bar{E} = t_f + v^T e \quad (70)$$

$$\bar{H}(t_f) = -\frac{\partial \bar{E}}{\partial t_f} = -1 \quad (71)$$

### d. Hamiltonian Evolution Condition

$$\frac{\partial \bar{H}}{\partial t} = 0 \quad (72)$$

These conditions will be used to verify and validate that the solution is feasible and optimal.

### C. USING DIDO TO SOLVE OPTIMIZATION PROBLEM

To solve the trajectory optimization problem, the MATLAB application DIDO was used. This technique was used because it is the most efficient way to apply Pontryagin's Principle based on the problem formulation. This resulted in a useful solution and DIDO was able to find an extremal solution to the problem. This solution found that a separation error of 50 km was reduced to 0 km which took 23,540.8 seconds, or 4.24 orbits, and resulted in an altitude drop of 4.17 km. This was accomplished using a bang-bang control which involved the satellite in the rear entering a high drag configuration for the first half of the maneuver, and switching to low drag while the second satellite simultaneously entered a high drag maneuver from low drag. By doing this, a vertical separation is created between the two satellites. The spacecraft which is initially in a high drag configuration drops below the other and thus begins to increase in speed relative to the satellite at a higher altitude. Once the change in separation is halfway complete the satellites reverse their configurations and therefore end at the same altitude with the desired separation. This overall trajectory closely matches the profile described in Figure 3 but does not include a coasting phase as this is a minimum time maneuver. All figures show engineering units for increased clarity.

Figure 21 shows that the DIDO solution is able to accurately meet the desired boundary conditions. The satellites both begin at an orbital period of 5,553.58 seconds and end at 5,548.45 seconds, which means they start and end at the same altitude as desired. The initial gap in their orbital position is 0.001174 orbits, or a 50 km separation, and they both end the maneuver at 4.241 orbits meaning the resulting separation is zero.

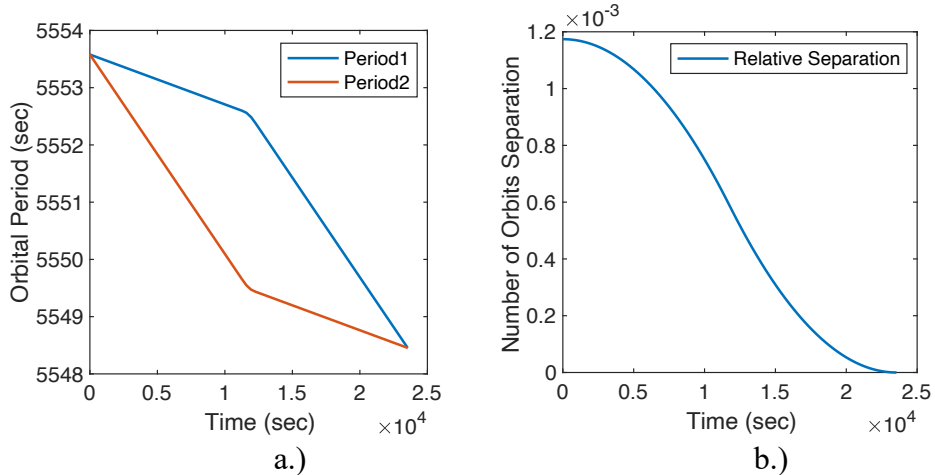


Figure 21. Graph of states from DIDO solution: a.) Periods of each satellite; b.) Difference between the distances travelled by each satellite

This solution shows that this is the case and therefore the solution accomplishes the desired result described by Equations 51 and 52.

$$P_1(tf) - P_2(tf) = 0 \text{ seconds} \quad (51)$$

$$X_1(tf) - X_2(tf) = 0 \text{ orbits} \quad (52)$$

Next, it is important to understand the orientations of each spacecraft through the optimal differential drag maneuver. To do this, their drag areas were plotted, as shown in Figure 22.

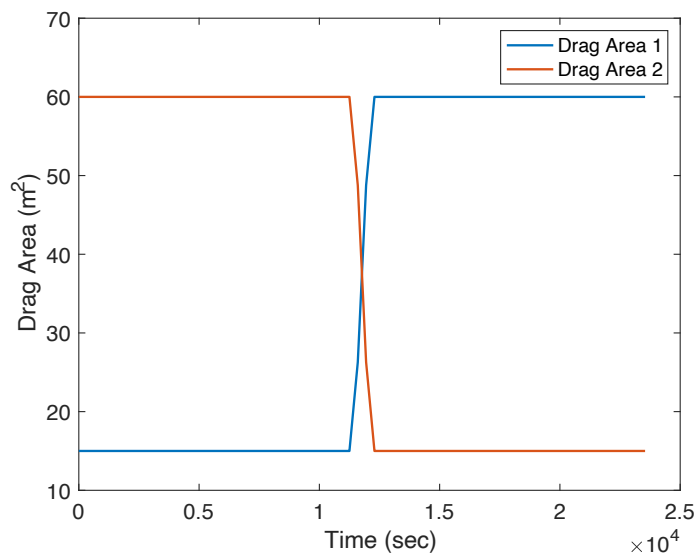


Figure 22. Satellite's drag areas from DIDO solution

From this depiction it is clear that the fastest means to close the desired distance is to use a bang-bang control between the highest and lowest drag areas for the two satellites. The resulting relative trajectories are calculated from the data shown in Figure 20 and are shown in Figure 23.

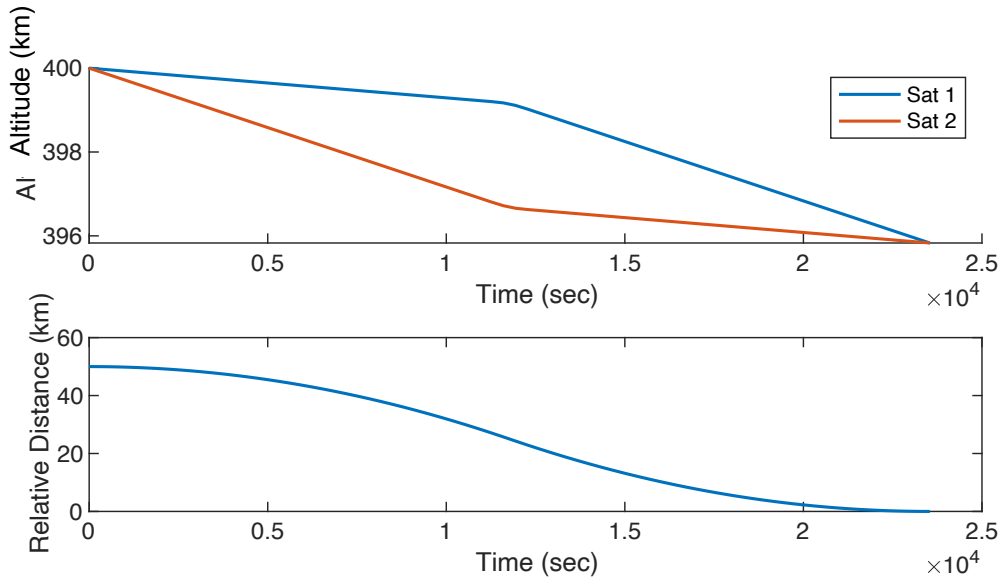


Figure 23. Trajectories of satellites during maneuver from DIDO solution

## D. FEASIBILITY AND OPTIMALITY OF SOLUTION

### 1. Feasibility Assessment

To measure the feasibility of the solution the dynamics and initial states of the problem were propagated using MATLAB's ode45 solver. The control histories from DIDO were then interpolated with the time of the solver and added into the dynamics to assess if the controls produced by DIDO would create the desired results in an independent propagation.

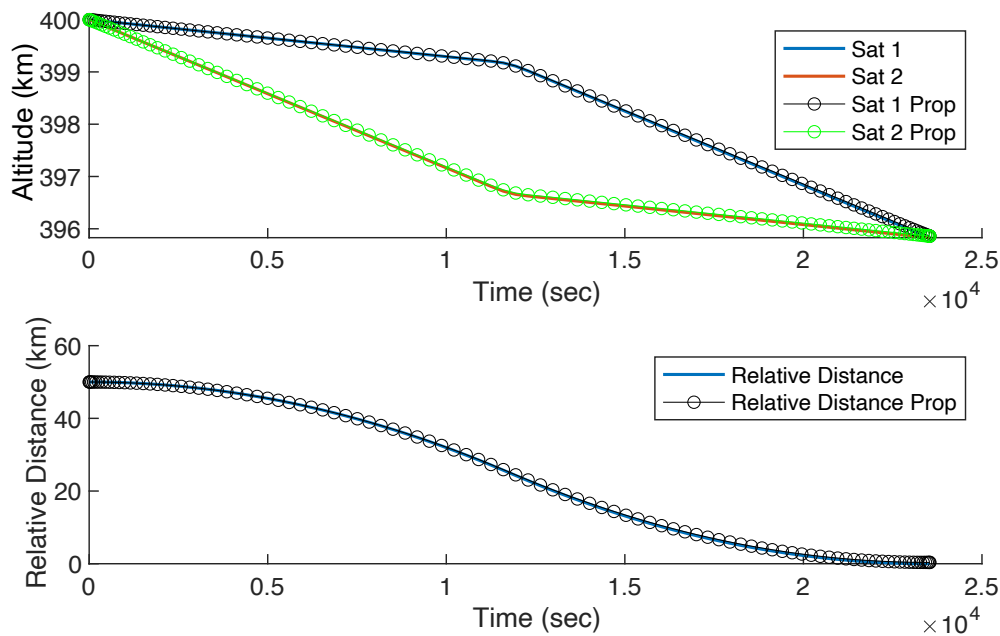


Figure 24. Propagation test for feasibility of DIDO solution

As shown in Figure 24 this test matched up very closely with the DIDO results. This shows that the orientations produced by the DIDO control histories are feasible.

## 2. Optimality Assessment

### a. Stationarity and Complementarity Conditions

To evaluate the stationarity conditions, the DIDO outputs for each term of Equations 66 and 67 ( $U_1^*$  and  $U_1^*$ ) were used to entered into the equations. In order for the stationary condition to be satisfied, these equations should equal zero throughout the entire trajectory. This was checked and the resulting values for  $U_1^*$  and  $U_1^*$  were within  $\pm 0.0003$ , or very nearly zero, for the duration of the maneuver. This shows that the solution meets the stationarity condition for optimality.

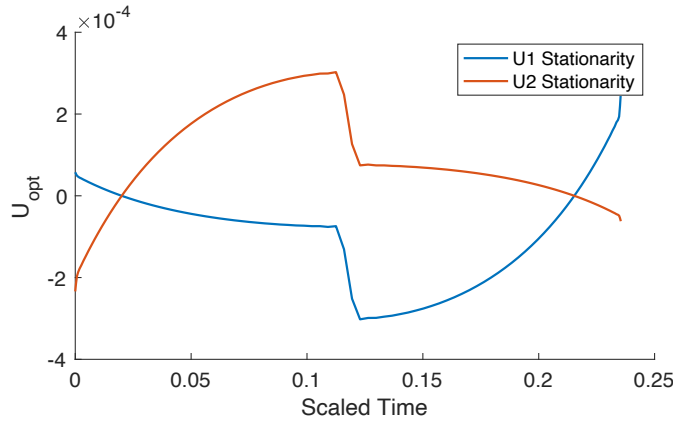


Figure 25. Stationary condition plots demonstrating the control optimality

To evaluate the complementarity condition, the relationship between the values of  $\mu_1$  and  $\mu_2$  and the control histories must be examined. Equations 68 and 69 dictate that when the values of  $\mu_1$  and  $\mu_2$  are above or below zero they will impose maximum and minimum limits on the controls. The  $\mu_1$  and  $\mu_2$  values are shown with the control histories in Figure 26.

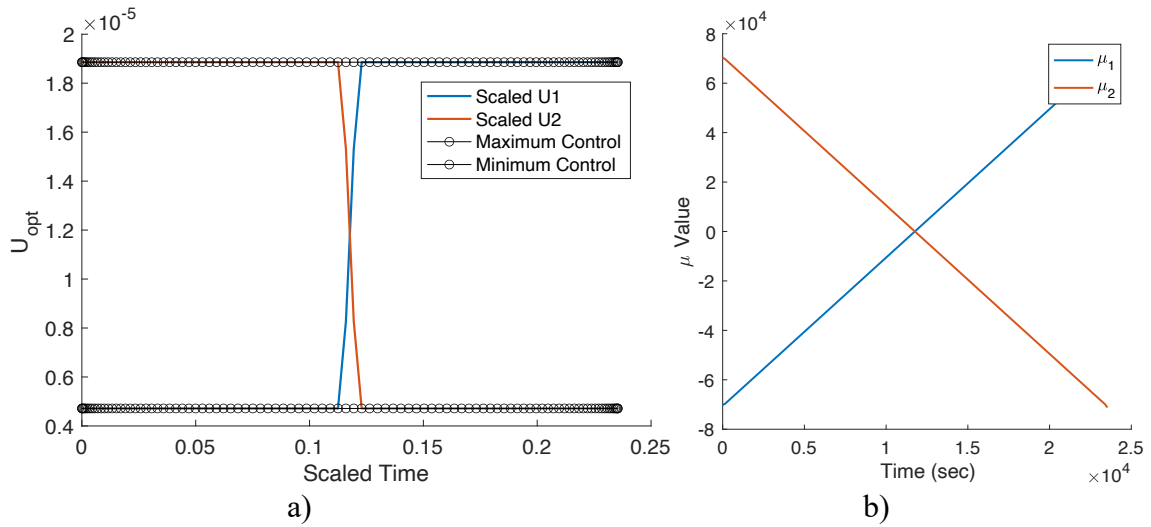


Figure 26. a) Control histories which are bounded due to the values  $\mu_1$  and  $\mu_2$   
b) Values  $\mu_1$  and  $\mu_2$

As Figure 26 a) shows the controls do not exceed their bounds and once again behave in a bang-bang manner. The physical interpretation of this is that Satellite 2, which starts out too far away from Satellite 1, enters a high drag configuration where its face with the largest surface area faces toward the direction of travel while Satellite 1 faces its smallest area into the wind. Halfway through the maneuver they switch configurations, a situation which allows them to end up with the same altitude at the end.

Figure 26 b), displays that the values of  $\mu_1$  and  $\mu_2$  are either greater than or less than zero for the duration of the maneuver, and therefore the values of  $U_1$  and  $U_2$  must be their maximum or minimum values. This is the origin of the bang-bang control that was discussed previously, and it corroborates the resulting trajectories of the two spacecraft.

Figures 25 and 26 demonstrate that the stationarity and complementary conditions of optimality are satisfied, or in other words the control histories produced by DIDO are able to solve the boundary value problem described in the problem formulation, and they are properly restricted by the maximum and minimum drag area values.

#### ***b. Hamiltonian Value and Evolution Equations***

The last conditions for optimality can be assessed by evaluating the graph of the value of the Lagrangian of the Hamiltonian over time. This is shown in Figure 27.

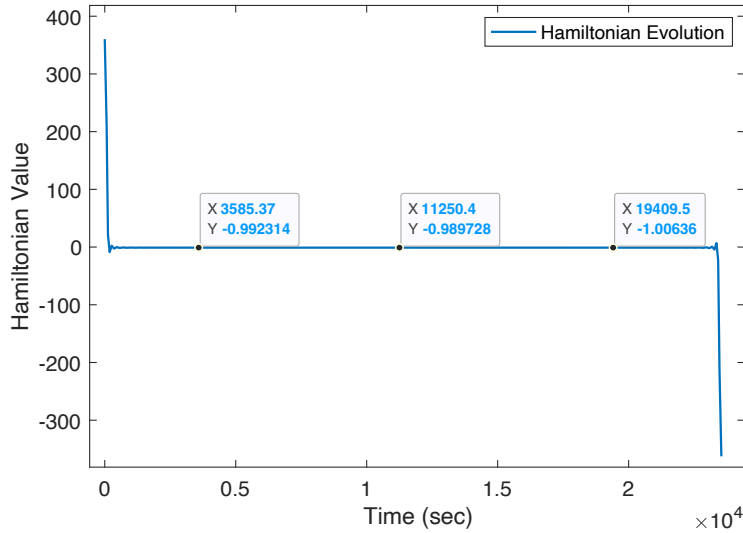


Figure 27. Hamiltonian value over time

Based on the hand calculations the Hamiltonian should be a constant value of -1 for the duration of the maneuver. This is the case for the vast majority of the solution, with the exception of the beginning and end of the simulation. The extreme values are a numerical artifact. Aside from the defects at the time boundaries, Hamiltonian's value is very nearly -1 for the entire maneuver. This shows that the bang-bang control method is the optimal minimum time method to conduct differential drag maneuvers for maintaining desired spacings in formations.

By using Pontryagin's Principle, an optimal trajectory was found for differential drag maneuvers which can adjust the separation between two satellites. Despite this being a simplified model, it still shows that the feasible and minimum time solution is a bang-bang control in which the satellites use alternate high and low drag configurations to adjust their separation. This trajectory can then be applied to a simulation which uses the full atmospheric model and rotational dynamics to determine the exact orientations the spacecraft must assume to turn their rotation motion into translations of their orbital positions. Chapter V will discuss how that simulation is developed, and how it can achieve a more general solution to this problem that allows for a much wider range of satellite types and orbital regimes to be modeled.



THIS PAGE INTENTIONALLY LEFT BLANK

## V. GENERAL SOLUTION FOR DIFFERENTIAL DRAG MANEUVERS FOR FORMATION FLYING

The insight and understanding gained from the optimization problem allows for the construction of a general tool that can help plan differential drag maneuvers and generate a set of commands for spacecraft to execute. This will allow for more rapid and automated mission operations and ultimately provide the solution to the question of how to create optimized and automated differential drag formation flying maneuvers.

### A. COMPLETE PROBLEM FORMULATION

All the models and dynamics equations can be used together to calculate the trajectories of spacecraft for the maneuver tool. These dynamics represent the full model. Optimization techniques required that the problem be scaled back by removing rotational dynamics and atmosphere modeling. This was useful in demonstrating the optimal trajectories, but a simulation with higher fidelity and greater number of steps is needed to accurately propagate and describe the maneuver. The simulation method will then apply the optimal “bang-bang” trajectory into a shooting function that will iterate to determine the maneuver duration needed to meet the desired end state. By employing this simulation method, Pontryagin’s Principle is not directly applied to this method, so the necessary conditions of optimality are not evaluated. Also, the controls are now the rates of rotation about each of the spacecraft body frame axis represented by  $\omega_{11}$  in which the first number represents the axis, and the second number represents the spacecraft. For example,  $\omega_{32}$  is the rate of rotation about the body frame z-axis of spacecraft number two. The orientations of the spacecraft are shown by  $q_{01} - q_{31}$  and  $q_{02} - q_{32}$  showing each of the four quaternion values for each spacecraft starting with the scalar value of  $q_0$ .

$$\text{Orbital States: } \overrightarrow{X_{orbit}}^T = [P_1, X_1, P_2, X_2] \quad (73)$$

$$\text{Rotational States } \overrightarrow{X_{rotation}}^T = [q_{01}, q_{11}, q_{21}, q_{31}, q_{02}, q_{12}, q_{22}, q_{32}] \quad (74)$$

$$\text{Control Inputs: } \vec{U}^T = [\omega_{11}, \omega_{21}, \omega_{31}, \omega_{12}, \omega_{21}, \omega_{32}] \quad (75)$$

$$\text{Minimize } J[x(\cdot), u(\cdot), t_f] = t_f \quad (76)$$

Orbital Dynamics:

$$\dot{P}_1 = -3\pi \sqrt{\frac{\left( \left( \frac{\sqrt[3]{2} \sqrt[3]{\pi} \sqrt[3]{\mu}}{\sqrt[3]{P_1}} \right) - \cos(\sin(X_1 * 2\pi) * i) * \cos(i) * \left( \frac{P_1 \sqrt{\mu}}{2\pi} \right)^{\frac{2}{3}} * \omega \right)^2}{4\pi^2}} P_1^2$$

$$* \rho * (1.1 * \cos(i * |\sin(X_1 * (2\pi))|) + 0.4) * DragArea1 * Cd/m \quad (77)$$

$$\dot{P}_2 = -3\pi \sqrt{\frac{\left( \left( \frac{\sqrt[3]{2} \sqrt[3]{\pi} \sqrt[3]{\mu}}{\sqrt[3]{P_2}} \right) - \cos(\sin(X_2 * 2\pi) * i) * \cos(i) * \left( \frac{P_2 \sqrt{\mu}}{2\pi} \right)^{\frac{2}{3}} * \omega \right)^2}{4\pi^2}} P_2^2$$

$$* \rho * (1.1 * \cos(i * |\sin(X_2 * (2\pi))|) + 0.4) * DragArea2 * Cd/m \quad (78)$$

$$DragArea = 1 / \left( 1 + e^{-200 * ([1 \ 0 \ 0] * (C_{BO} * \begin{bmatrix} A_{face1} \\ 0 \\ 0 \end{bmatrix})) / \|C_{BO} * \begin{bmatrix} A_{face1} \\ 0 \\ 0 \end{bmatrix}\|} \right) * [1 \ 0 \ 0] \left( C_{BO} \begin{bmatrix} A_{face1} \\ 0 \\ 0 \end{bmatrix} \right)$$

$$+ DragArea_{Face2} + DragArea_{Face3} + \dots \quad (79)$$

$$A_{face1,2} = ydim * zdim \quad (80)$$

$$A_{face3,4} = xdim * zdim \quad (81)$$

$$A_{face5,6} = ydim * zdim \quad (82)$$

$$C_{BO} = \begin{bmatrix} 1 - 2(q_2^2 + q_3^2) & 2(q_1 q_2 + q_3 q_0) & 2(q_1 q_3 - q_2 q_0) \\ 2(q_2 q_1 - q_3 q_0) & 1 - 2(q_1^2 + q_3^2) & 2(q_2 q_3 + q_1 q_0) \\ 2(q_3 q_1 + q_2 q_0) & 2(q_3 q_2 - q_1 q_0) & 1 - 2(q_1^2 + q_2^2) \end{bmatrix} \quad (83)$$

$$\rho = 6x10^{-10} * e^{\left( \left( \left( \frac{P\sqrt{m\mu}}{2\pi} \right)^{\frac{2}{3}} - Re \right) - 175 \right)} / \frac{900+2.5(F10.7-70)+1.5Ap}{27-0.012 \left( \left( \frac{P\sqrt{\mu}}{2\pi} \right)^{\frac{2}{3}} - Re \right) - 200} \quad (84)$$

$$\dot{X}_1 = \operatorname{atan} \frac{\left( \frac{\sqrt[3]{2} \sqrt[3]{\pi} \sqrt[3]{\mu}}{\sqrt[3]{P_1}} \right)^{\frac{2}{3}}}{\left( \frac{P_1 \sqrt{\mu}}{2\pi} \right)^{\frac{2}{3}}} / 2\pi \quad (85)$$

$$\dot{X}_2 = \operatorname{atan} \frac{\left( \frac{\sqrt[3]{2} \sqrt[3]{\pi} \sqrt[3]{\mu}}{\sqrt[3]{P_2}} \right)^{\frac{2}{3}}}{\left( \frac{P_2 \sqrt{\mu}}{2\pi} \right)^{\frac{2}{3}}} / 2\pi \quad (86)$$

Rotational Dynamics:

$$\dot{q}_{01} = \frac{1}{2} (-\omega_{11}q_{11} - \omega_{21}q_{21} - \omega_{31}q_{31}) \quad (87)$$

$$\dot{q}_{11} = \frac{1}{2} (\omega_{11}q_{01} - \omega_{21}q_{31} + \omega_{31}q_{21}) \quad (88)$$

$$\dot{q}_{21} = \frac{1}{2} (\omega_{11}q_{31} + \omega_{21}q_{01} - \omega_{31}q_{11}) \quad (89)$$

$$\dot{q}_{31} = \frac{1}{2} (-\omega_{11}q_{21} + \omega_{21}q_{11} + \omega_{31}q_{01}) \quad (90)$$

$$\dot{q}_{02} = \frac{1}{2} (-\omega_{12}q_{12} - \omega_{22}q_{22} - \omega_{32}q_{32}) \quad (91)$$

$$\dot{q}_{12} = \frac{1}{2} (\omega_{12}q_{02} - \omega_{22}q_{32} + \omega_{32}q_{22}) \quad (92)$$

$$\dot{q}_{22} = \frac{1}{2} (\omega_{12}q_{32} + \omega_{22}q_{02} - \omega_{32}q_{12}) \quad (93)$$

$$\dot{q}_{32} = \frac{1}{2} (-\omega_{12}q_{22} + \omega_{22}q_{12} + \omega_{32}q_{02}) \quad (94)$$

Boundary Values

$$P_1 o = \frac{2\pi}{\sqrt{\mu}} (a)^{\frac{3}{2}} \quad ; \quad P_2 o = \frac{2\pi}{\sqrt{\mu}} (a)^{\frac{3}{2}} \quad (95)$$

$$X_1 o = \frac{\arctan\left(\frac{\text{Initial Separation}}{a}\right)}{2\pi} \text{ orbits} ; \quad X_2 o = 0 \quad (96)$$

$$P_1f - P_2f = 0 \quad (97)$$

$$\tan(X_1f - X_2f) * (\textit{AltitudeFinal} + Re) = \textit{Desired Separation} \quad (98)$$

### Parameters

$$Re = 6378.1 \textit{ km} = \textit{Earth Radius} \quad (99)$$

$$\mu_{\textit{Earth}} = 3.986004418 \times 10^5 \frac{\textit{s}^2}{\textit{km}^3} = \textit{Earth's Gravitational Parameter} \quad (100)$$

$$Cd = 2.2 = \textit{Standard Coefficient of Drag for Spacecraft} \quad (101)$$

$$i = \textit{Spacecraft Inclination (deg)} \quad (102)$$

## **B. DIFFERENTIAL DRAG MANEUVER PLANNING TOOL**

The goal of this thesis was to produce a general solver which could generate the commands needed for any satellites to conduct a differential drag maneuver that could maintain the desired spacing while flying in a formation. To do this, the solver would need to intake any spacecraft's mass and dimensions, orbital parameters, the current and desired spacing, environmental data, and the current date and time and then use these values to calculate the orientations needed for the spacecraft to correct the error in their formation. It will require using higher fidelity models and different methods than the DIDO optimal control solver, but the insights gained from the previous solution are critical to producing a minimum time solution.

The differential drag maneuver tool employs all the orbital and rotational dynamics previously described and uses all the atmosphere modeling previously described in order to create the highest fidelity possible while planning maneuvers. It uses these equations in MATLAB's ode45 integration solver to propagate the orbits with the reorientation maneuvers calculated based on the spacecrafts' orbits and the bang-bang minimum time solution previously found by the DIDO solver. The reorientation maneuvers are interpolated at the appropriate times to create the desired results. All the orientations are

expressed as quaternions in the Earth Centered Inertial (ECI) reference frame to make them more generally applicable, and easier to input as commands for flight software.

Several assumptions and compromises must also be made so that the maneuver tool is user friendly, operates at all altitudes, inclinations, and spacecraft masses. First, it will assume a circular orbit; this is reasonable because drag forces will force orbiting satellites into very nearly circular orbits since they have a greater impact on the satellite when it is at its periapsis, or lowest point in the orbit, and less effect on the apoapsis or highest point. Over time this will mean that the apoapsis decays faster than the periapsis until they are roughly equal. Also, it is relatively uncommon that highly elliptical orbits are used to operate in regions where differential drag is effective (lower than 600 km) especially for CubeSats which lack propulsion systems for station keeping.

Next, all maneuvers will begin and end at the ascending node, or the point when the satellite passes over the equator from south to north, which means they will last for a whole number of orbits. This is done to ensure reliable results at all altitudes and inclinations and reduce the computation time for the maneuver tool. Without this, the rotations of the spacecraft could result in undesirable orientations depending on altitude and inclination. Fixing this problem creates other issues that resulted in instances when the solver created sub-optimal maneuvers. By using whole numbers of orbits, reliability is greatly increased and the resulting error in desired separation is very small. The resulting error is a function of altitude, inclination, solar activity, and the spacecraft mass and shape and generally will increase over longer distances. This error should be acceptable for the majority of formation flying applications, but if finer corrections are needed, they can be made in additional maneuvers. Also, the uncertainty associated with all atmospheric models, generally 10–15%, means that any open loop guidance will result in some error either way. Also, the tool prioritized the final altitude error between the spacecraft over the in-track distance. This is done to ensure there is no remaining relative drift between the spacecraft at the end of the maneuver.

Finally, the maneuver tool only focuses on a minimum time maneuver to reduce the operational impact of the maneuver, and it does not fix an axis to point at the Earth or

sun based on mission requirements. This means that it does not specifically meet the goal of completely eliminating the impact of formation-keeping maneuvers from the spacecraft's operations. There are several reasons for this. First, this is meant to be a general maneuver planning tool that can assist in the planning of spacecraft operations and is applicable to a wide range of possible scenarios. There is a sizeable amount of variation in the physical characteristics of spacecraft, their missions, sensors, pointing requirements, etc., so creating a tool that could meet all of those requirements is very difficult. As a result, the minimum time approach was used to try to reduce the overall impact by decreasing the length of time needed to conduct the operation. Also, this can be easily implemented multiple times so that many short duration maneuvers can be used to reduce the impact. Finally, options for slower maneuvers were developed that would break up the impact and give time back to the operators during the coast phases of the maneuver to reduce the impact to operations. This remains an area for future work but would likely be more appropriate as a bespoke solution to each individual spacecraft formation.

Overall, the differential drag maneuver solver can be used for most CubeSat with attitude control systems, or even small satellite applications, and can generate quaternion commands to adjust the separation between any two satellites in the same orbital plane and for any set of generally circular orbital parameters. Modifications for making it more applicable for specific use cases would be relatively straight forward. The code for the tool is available upon request.

### **1. User Inputs for Maneuver Planning Tool**

To use the differential drag tool a user must input a number of specifications that define the spacecraft, orbits, environment, date and time, and desired maneuver that needs to be performed. The tool uses these to calculate all the necessary data and generate a set of commands that can be uploaded to the satellite in the form of quaternions in the ECI reference frame over time. The user inputs are shown in Table 5.

Table 5. User inputs for maneuver planning tool

	Input	Notes
<b>Date &amp; Time</b>	Month	Month
	Day	Day
	Hour	Start time hour (0-23)
	Minute	Start time minute (0-60)
<b>Environmental Conditions</b>	F10.7	Solar Flux Units 10e-22 W/m2/Hz
	Ap	Geomagnetic Index
<b>Spacecraft Specifications</b>	Spacecraft Mass	Kilograms
	X-Axis Dimension	Shortest dimension (meters)
	Y-Axis Dimension	Medium dimension (meters)
	Z-Axis Dimension	Longest dimension (meters)
	Solar Panel Coverage Face 1	% (0-1) Face 1 is body frame [1 0 0]
	Solar Panel Coverage Face 2	% (0-1) Face 2 is body frame [-1 0 0]
	Solar Panel Coverage Face 3	% (0-1) Face 3 is body frame [0 1 0]
	Solar Panel Coverage Face 4	% (0-1) Face 4 is body frame [0 -1 0]
	Solar Panel Coverage Face 5	% (0-1) Face 5 is body frame [0 0 1]
	Solar Panel Coverage Face 6	% (0-1) Face 6 is body frame [0 0 -1]
Solar Panel Efficiency	% efficiency (0-1)	
<b>Orbital Parameters</b>	Altitude	Starting altitude (km)
	Inclination	Spacecraft Inclination (deg)
	RAAN	Right Ascension of Ascending Node (deg)
<b>Maneuver Preferences</b>	Speed	1-3; 1 is fast and 3 is slowest
	Current Separation	Current separation between spacecraft (km)
	Desired Separation	Desired final separation between spacecraft (km)

## 2. Defining Initial Conditions

The user inputs are used in calculations to define a number of different variables which are in turn used throughout the tool. These values are used to drive the simulation itself, as well as to conduct additional useful calculations such as the expected power production of the satellite during the maneuver.



The date and time data are used to calculate the current longitude of the ecliptic of the Earth. This is the angle of the Earth's current position in its orbit around the sun as measured from its position at the Vernal Equinox, or March 21, each year as shown in Figure 28. These data will be needed to determine the amount of sunlight the spacecraft receive during their orbit so that power levels onboard can be properly managed during the operation.

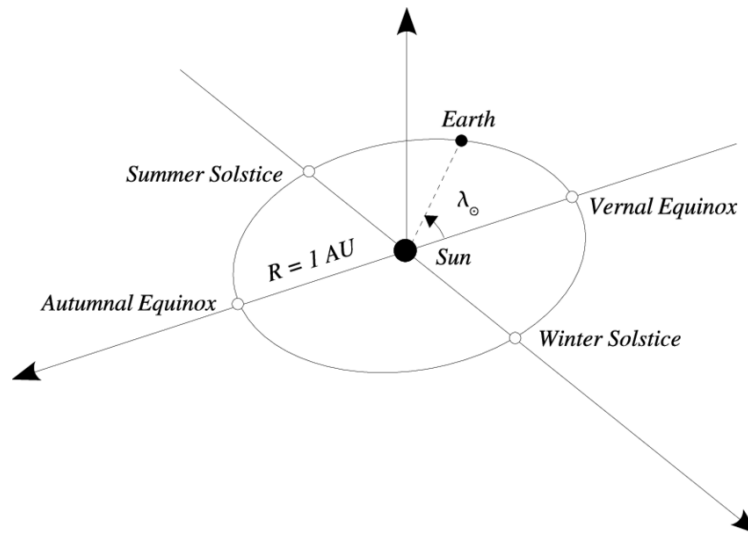


Figure 28. Depiction of the earth's orbit with longitude of the ecliptic represented by  $\lambda_{\odot}$ . Source: [30]

The environmental data of the current sun and Earth geomagnetic activity is used to calculate the air density in space. These values are critical and have significant impacts on the propagation of the orbits, and since they change daily, they must be pulled from the National Oceanic and Atmospheric Association, or a number of other sources, before any maneuver [26]. The environmental values are static throughout the maneuver, but it is possible that they could change if the maneuver duration is more than several days, and this could impact the accuracy of the maneuver in a real-world scenario. Forecasts for space weather anomalies, such as solar storms or coronal mass ejections, should be monitored when planning for differential drag maneuvers since they could impact the mission.

The spacecraft's physical characteristics are used to calculate the external forces due to drag as well as the power produced during the maneuver. The mass is used as a parameter in the orbital dynamics equations, and the dimensions are used to calculate the drag area according to the equations shown in the problem formulation. The solar panel data is used to determine the power production during the maneuver.

The altitude and inclination of the orbit are critical values for the simulator and are arguably the most important values that impact the duration of the maneuver and the orientations of the spacecraft. The altitude is used to calculate the initial orbital period for each satellite, which is then used in the dynamics equations to define the initial density, velocity, and combined with the inclination to define the in-track atmospheric speed due to the Earth's rotation. The Right Ascension of the Ascending Node (RAAN) is used after the simulation to convert the quaternion outputs to useful commands that can be uploaded to a satellite. This value is used to rotate all orientations about the z-axis so that they represent the true orientation of the satellites based on the orbital plane defined by the RAAN in the ECI reference frame.

The maneuver preferences are also important factors to describe what the maneuver must accomplish and how. The current and desired separations are used to determine if the satellites must get closer or further away, which impacts the order of the high and low drag orientations taken by the two satellites, and the overall duration. These initial orientations are used to define the initial quaternion states for each of the satellites, and this orientation is also a function of the inclination of the orbit. All orientations are initially set as facing the vector  $[1\ 0\ 0]$  in the ECI frame, which is the equivalent of a RAAN of 270 degrees. This is done for increased reliability of the calculations. Again, the RAAN is used to adjust all the quaternions after the simulation to ensure that the commands output by the maneuver tool are accurate. Also, the current and desired separations are used to define the initial "X" state for each satellite, or the separation in terms of the percentage of an orbit between the satellites. Longer distances will intuitively take longer to complete, take longer for the solver to calculate, increase the altitude lost due to the maneuver, and possibly increase the final error.

The speed input determines how the maneuver is to be conducted. A value of “1” means that a minimum time maneuver is to be conducted with no coast phase in which both satellites are in a low drag, or other, configuration. Values of “2” and “3” are slower and do incorporate coast phases, which could be opportunities for the spacecraft to return to normal operations while waiting for the next orientation change, and they will trade maneuver time to retain altitude and thus preserve mission life. Conceptually, slower maneuvers are more suited for longer adjustments, such as those over 10 km, but increase the error and may need additional fine adjustments.

### **3. Orbit Propagation**

The initial conditions created by the user inputs are used as starting locations for the propagator. The simulation is run using MATLAB’s ode45 integration solver. This particular differential equation solver was chosen because it offered the best solve time and most reliably accurate results. Several other solvers were explored, most notably ode15s which is more suitable for stiff problems such as the dynamics equations used by this thesis. Using ode15s allowed for a smaller number of nodes and thus faster computation times, but this had negative impacts for longer duration maneuvers due to the way the orientation switches between high and low drag maneuvers. For a higher number of time steps, ode15s was actually slower than ode45 and delivered very similar results. Therefore, ode45 was chosen because the problem requires a high number of nodes regardless of the solver and ode45 was the fastest choice. Also, an absolute tolerance and relative tolerance of  $1 \times 10^{-9}$  was used as an input option for the ode45 solver to ensure that the results were accurate. These are the same tolerances used to validate the dynamics equations.

When the spacecraft switches from one orientation to the other it must do so within a certain range of speeds to produce predictable results. If it moves too slowly from one orientation to another it will have moved too far in its orbit and a rotation about a single axis will mean that it does not meet the desired final orientation. By increasing the nodes, in this case to 10,000, there is more fidelity to control the rate of rotation. The rates of rotation about each axis of the spacecraft are the control inputs of  $\omega_1$ ,  $\omega_2$ , and  $\omega_3$  for each satellite. It is imperative to ensure that the rates are not too fast or too slow for the length

of the maneuver. Over short maneuvers each of the 10,000 nodes could represent less than a second, and for very long maneuvers each node could represent as long as 30 seconds or more so the rate of rotation must be adjusted based on the number of orbits it takes to complete the maneuver. This is done using a number of logic gates in the MATLAB code. Ideally the rate of rotation for the reorientation should be roughly 0.5 degrees/second of rotation. This rotation is inserted to the dynamics equations as  $\omega_2$  using a time interpolated array and it represents a 90-degree rotation about the spacecraft body frame's y-axis. This flips the spacecraft between the largest to smallest drag areas.

The time at which the rotations occur in the overall maneuver depends on the speed chosen by the user. If a speed of "1" is used, the maneuver occurs in the minimum time which means it will follow the trajectory determined using optimization techniques in Chapter IV. This means the rotation occurs at the exact middle point of the maneuver. For a speed of "2" the rotation occurs for the first spacecraft a third of the way into the maneuver and two thirds for the second. This means that they are both in a low drag coast phase for the middle third of the overall maneuver. Speed "3" means these rotations occur at one quarter and three quarters of the maneuver, meaning the middle 50% is a coast. Again, these coast phases could theoretically be used by the spacecraft operators to perform other mission related tasks. The orientations could be anything the operators need as long as they are both the same for each spacecraft so that their drag forces are equal. This could reduce the impact of the drag maneuver on the operation of the spacecraft.

The ode45 solver then runs using the initial inputs and the interpolated controls. The values of  $\omega_1$  and  $\omega_3$  are calculated as part of the dynamics equations to match the orbital rate of rotation to ensure that the same face of the spacecraft remains pointed towards the direction of travel. This is done using Equations 103 and 104:

$$\omega_1 = \frac{2\pi \sin(\textit{inclination})}{\textit{Orbital Period}} \quad (103)$$

$$\omega_3 = \frac{-2\pi \cos(\textit{inclination})}{\textit{Orbital Period}} \quad (104)$$

The drag area of the satellite is calculated in a separate function which intakes the spacecraft dimensions, orientation quaternions, and the current number of orbits to use as the true anomaly. It used these values to calculate the drag area relative to the direction of travel in the ECI frame, which changes based on the position of the spacecraft in its orbit and the inclination. This is necessary while using the ECI reference frame as opposed to the orbital frame in which the direction of travel would always be in the positive x-axis direction. This direction of travel vector is calculated using Equation 105 which uses  $X$  to define the number of orbits completed by the satellites and  $i$  to represent the orbital inclination:

$$Direction\ of\ Travel\ in\ ECI = \begin{bmatrix} \cos(i) * \cos(X * 2\pi) \\ \sin(X * 2\pi) \\ \sin(i) * \cos(X * 2\pi) \end{bmatrix} \quad (105)$$

After the simulation runs, the state histories are captured and used to calculate the relative positions of the two satellites during the maneuver. Both the final error in their altitude and their separations are calculated using Equations 106 and 107:

$$Final\ Altitude\ Error = \left( \frac{[P1(tf)]\sqrt{\mu}}{2\pi} \right)^{\frac{2}{3}} - \left( \frac{[P2(tf)]\sqrt{\mu}}{2\pi} \right)^{\frac{2}{3}} \quad (106)$$

$$Final\ Separation\ Error = \tan(X1f - X2F) * \left( \frac{[P(tf)]\sqrt{\mu}}{2\pi} \right)^{\frac{2}{3}} - Desired\ Separation \quad (107)$$

The entire simulation is then encompassed within a “while” loop which will repeat the simulation again and again until certain conditions are met. In this case, the final separation error must be driven as low as possible before the stop condition is met. The loop starts at a small number of orbits, depending on the length of the maneuver, and increases the number of orbits each time until the error is driven as close as possible to zero. At this point the loop is broken, and the final state histories are used as the outputs for the maneuver planning tool. This loop is the reason why longer maneuvers will take longer to calculate as the number of orbits required increases the number of times it must

rerun the entire simulation. To reduce this computation time, more orbits are added in each loop while the separation is still large, and they reduce as the spacecraft get closer to the desired gap. The slower maneuver speeds also calculate faster for longer maneuvers because they inherently add more runs per loop to ensure that the reorientation maneuvers occur at the ascending or descending nodes of the orbit. As a result, they are less accurate and result in greater final errors, since they do not add single orbits per loop, but instead three orbits per loop for speed “2” and two orbits for speed “3.”

Finally, it is imperative to ensure that the final altitudes match, even at the expense of meeting the desired gap. If there is any remaining altitude difference the satellites will drift relative to each other at the end of the maneuver and this would be much harder to correct. If there is a small error in the spacing between them this can be easily corrected by another maneuver, and in most cases the error should not be significant to impact the mission of the satellites. An altitude error threshold of one meter was set for this, and any maneuver generated by this planning tool will meet this requirement. For speed “1” maneuvers, it was found that no errors were naturally produced. However, for the maneuvers with a coasting phase there was a small altitude error that would develop in longer separation adjustments. This is because the satellite at the lower altitude is moving faster which is good for changing the relative positions, but also increases the drag force and causes it to fall faster even at the same low drag orientation. To fix this, the second high drag maneuver actually begins two orbits early and ends as soon as the altitudes are equal to each other. This can result in errors when the slow speed maneuvers are used for very small separation changes, however this is a necessary exchange to ensure effective maneuvers in a wider range of cases.

#### **4. Solar Power Production Calculations**

Another capability of the maneuver planning tool is that it is also able to provide analysis for the amount of power the satellites will produce while they conduct the maneuver. Given that small satellite operations are heavily influenced by their ability to produce power, and their ability to produce power depends on their orientations, these differential drag maneuvers could greatly impact the satellite’s operations. By providing

data on solar power generation, the maneuver tool will help satellite operators forecast and assess the level of impact on the satellite's mission and how the maneuver should be conducted. For example, they could choose a large number of short duration maneuvers to slowly adjust the positions and thus be able to work around the power impacts more easily. Also, the tool will show operators how the different times of year will impact maneuvers based on the orientation of the sun to the Earth from current longitude of the ecliptic.

First, the effective area of solar panels pointing toward the sun must be calculated. This is done using the same area calculations done for the drag area, but each face also includes a term for the amount of that face covered in solar panels. This is shown the Equations 108, 109, 110, and 111. In these equations the percentage of solar panel coverage for a particular face of the spacecraft is represented by %SP, and the sun vector, of the direction of the sun from the spacecraft, is represented by SV.

$$SolarArea = \frac{\% \text{ Solar Panel Coverage for face } x}{1 + e^{-200 * ([SV] * (C_{BO} * \begin{bmatrix} A_{face} \\ 0 \\ 0 \end{bmatrix})) / \|C_{BO} * \begin{bmatrix} A_{face} \\ 0 \\ 0 \end{bmatrix}\|}} * \left( [SV] * \left( C_{BO} * \begin{bmatrix} A_{face} \\ 0 \\ 0 \end{bmatrix} \right) \right) \quad (108)$$

$$A_{face1,2} = ydim * zdim ; A_{face3,4} = xdim * zdim ; A_{face5,6} = ydim * zdim \quad (109)$$

$$SolarPanelArea (q0, q1, q2, q3) = A_{face1} + A_{face2} + A_{face3} + A_{face4} + A_{face5} + A_{face6} \quad (110)$$

$$C_{BO} = \begin{bmatrix} 1 - 2(q2^2 + q3^2) & 2(q1q2 + q3q0) & 2(q1q3 - q2q0) \\ 2(q2q1 - q3q0) & 1 - 2(q1^2 + q3^2) & 2(q2q3 + q1q0) \\ 2(q3q1 + q2q0) & 2(q3q2 - q1q0) & 1 - 2(q1^2 + q2^2) \end{bmatrix} \quad (111)$$

The sun vector will change based on the time of year and is affected by the inclination of the Earth's orbit around the sun which is 23.45 degrees [31]. It is calculated using Equation 112:

$$Sun\ Vector = \begin{bmatrix} \cos(23.45) * \cos(\lambda_{\odot}) \\ \sin(\lambda_{\odot}) \\ \sin(23.45) * \cos(\lambda_{\odot}) \end{bmatrix} \quad (112)$$

Second, it must be determined whether or not the satellite is in sunlight. During certain parts of the orbit the satellite will be behind the Earth, and thus not illuminated, based on the relative positions of the Earth, sun, and spacecraft at different parts of the year. The geometry associated with this phenomenon is shown in Figure 29.

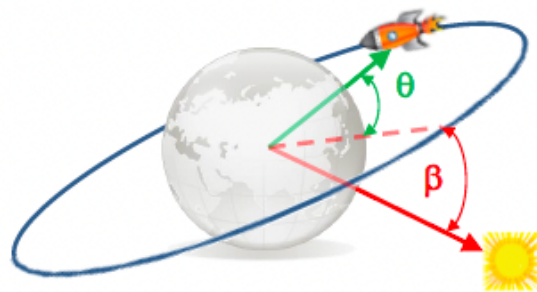


Figure 29. Earth, Sun, Spacecraft Geometry. Source: [31]

Figure 28 shows two angles represented by  $\theta$  and by  $\beta$ . The  $\theta$  is the true anomaly of the spacecraft in its orbit. The  $\beta$  represents the beta angle of the spacecraft's orbit. The beta angle is a value between -90 degrees and +90 degrees that describes the percentage of the total orbital time that the spacecraft is in view of the sun [31]. The beta angle is a function of the longitude of the ecliptic, the inclination of the spacecraft's orbit, the inclination of the Earth's orbit, and the RAAN of the spacecraft's orbit. It is described by Equation 113 [31].

$$\beta = \arcsin (\cos(\lambda_{\odot}) \sin (RAAN) \sin (i) - \sin (\lambda_{\odot}) \cos (23.45) \cos (RAAN) \sin (i) + \sin (\lambda_{\odot}) \sin (23.45) \cos (i)) \quad (113)$$



The beta angle and the true anomaly can then be used together to determine which parts of the orbit are in view of the sun. This relationship is described by Equation 114 and depicted in Figure 30.

$$\sin(\theta) = \sqrt{\frac{1}{\cos^2(\beta)} \left( \left( \frac{R_e}{R_e + \text{Altitude}} \right)^2 - \sin^2(\beta) \right)} \quad (114)$$

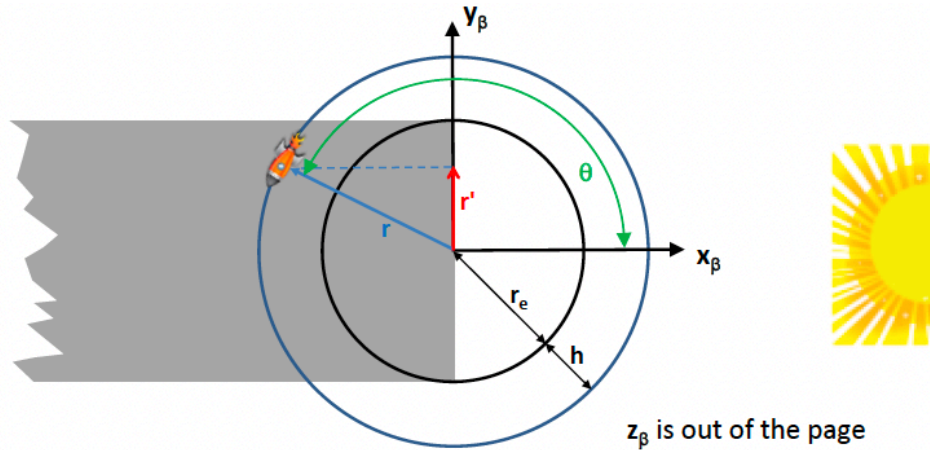


Figure 30. Geometry of the spacecraft relative to the Earth's umbra. Source: [31]

This information is then used to determine in which time steps of the simulation the spacecraft are in view of the sun, which is captured as either a 0 or 1 and used to turn on the power production or off depending on the true anomaly of the satellites.

Next, the amount of power generated must be calculated for each node of the simulation. This is a function of the solar panel area pointing at the sun, whether or not the sun is visible, the solar panel efficiency, and the power emanating from the sun. At the distance of Earth's orbit this power flux is approximately  $1350 \frac{\text{Watts}}{\text{meter}^2}$  [32].

$$\text{Solar Panel Power Output} = \text{SolarArea} * \text{Visibility} * \text{Efficiency} * 1350 \quad (115)$$

Equation 115 is used for both satellites to show how much electrical power the satellites can produce during the differential drag maneuver.

## **VI. RESULTS OF MANEUVER PLANNING TOOL**

The maneuver planning tool was then tested in a wide range of scenarios to determine the limits and usefulness of this method of generating commands for differential drag maneuvers. The tool was tested against many different orbital scenarios involving different altitudes and inclinations, as well as different spacecraft parameters. From this, it is clear that the tool is very useful for planning maneuvers, and for exploring different design choices for spacecraft during mission planning. The size and shape of the spacecraft can make it more or less effective at these maneuvers, as well as the specific orbits.

To examine the outputs of the tool, the following scenario was developed. This is a generic baseline example which can be used as a point of comparison when extreme cases are tested, and it will show what the outputs of the tool are. This case used two 6U CubeSats, as previously described, which are orbiting at 400 km without any adverse environmental conditions from space weather. The satellites are currently separated by 10 km and must maneuver to extend the gap to 15 km. The inputs to the maneuver tool are shown in Table 6.

Table 6. Example maneuver inputs

	<b>Input</b>	<b>Value</b>
<b>Date &amp; Time</b>	Month	June
	Day	16
	Hour	10
	Minute	00
<b>Environmental Conditions</b>	F10.7	100
	Ap	0
<b>Spacecraft Specifications</b>	Spacecraft Mass	12 kg
	X-Axis Dimension	0.1 m
	Y-Axis Dimension	0.2263 m
	Z-Axis Dimension	0.3405
	Solar Panel Coverage Face 1	0.9
	Solar Panel Coverage Face 2	0.9
	Solar Panel Coverage Face 3	0.9
	Solar Panel Coverage Face 4	0.9
	Solar Panel Coverage Face 5	0.9
	Solar Panel Coverage Face 6	0.9
	Solar Panel Efficiency	0.25
<b>Orbital Parameters</b>	Altitude	400 km
	Inclination	45 deg
	RAAN	0 deg
<b>Maneuver Preferences</b>	Speed	1
	Current Separation	10 km
	Desired Separation	15 km

The first major figure produced by the tool shows the trajectories of the spacecraft and their relative motions and positions to each other as displayed in Figure 31.

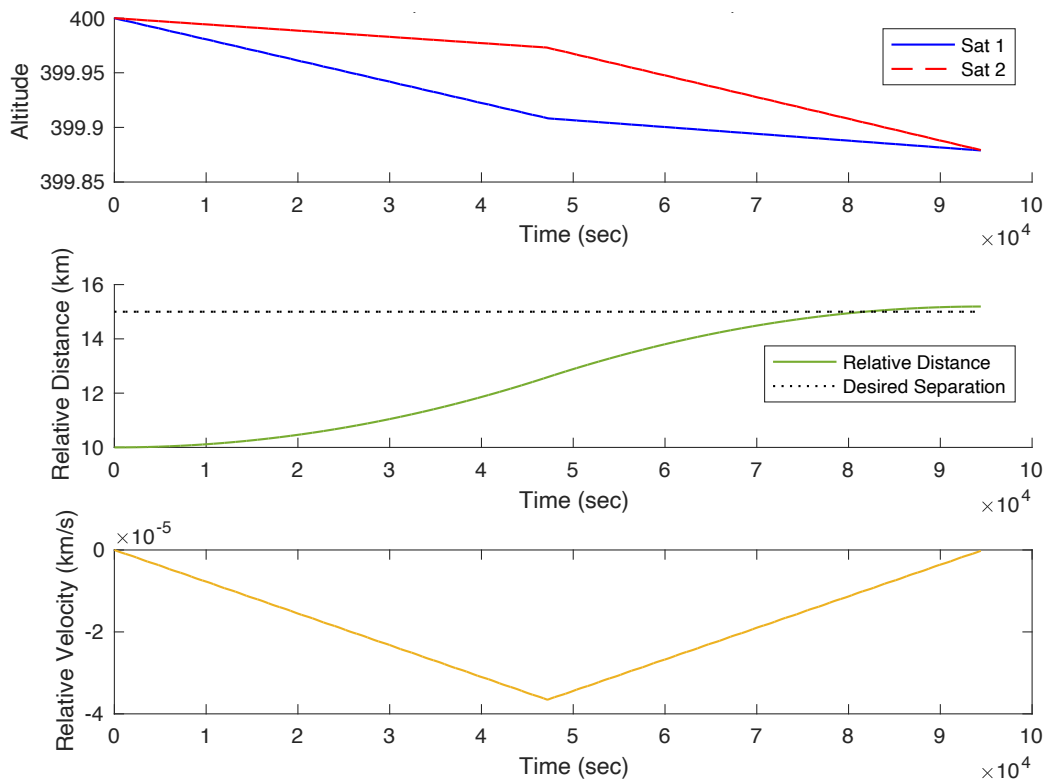


Figure 31. Example maneuver’s relative orbital motion

From Figure 31, the results of the bang-bang maneuver can be clearly seen. Satellite 1 enters the high drag orientation first while Satellite 2 is in a low drag configuration, and then they switch halfway through. In the first sub-plot, the altitudes of each spacecraft are shown, revealing that for this maneuver the maximum vertical distance between the satellites was 65 meters. If they were increasing the distance between them the order would be reversed. The second sub-plot in Figure 30 shows how their relative distances change during the maneuver; shown in the third sub-plot are the relative velocities which are quite small at a maximum of less than 0.04 meters per second. Finally, the performance metrics of the maneuver are displayed at the top of the figure. In this case the maneuver lasted 26.23 hours, resulted in 120 meters of lost altitude total, and had a resulting separation error of 192 meters. The separation error will increase or decrease depending on many factors but is generally small enough that it will not impact the mission. In cases where the

separation error remains large at the end of the maneuver, a second maneuver may be needed if the remaining gap is still impacting the mission of the satellites. The final altitude error is  $3.4 \times 10^{-4}$  km or 0.34 meters. This is very small, roughly the size of the spacecraft, and thus will result in a negligible drift rate of a millimeter or less per second. Over a long period of time this drift combined with orbital perturbations will mean that another maneuver will have to be conducted at some point based on the mission requirements of the spacecraft.

Next, the orientations of each spacecraft will be examined. The rotations and timing of rotations is critical to maintaining the desired orientations throughout the maneuver. Figure 32 shows the drag areas of each spacecraft that resulted from the orientations. From this figure it is clear that the rotations were effective at maintaining the high and low drag configurations that contributed to the trajectories shown in Figure 31.

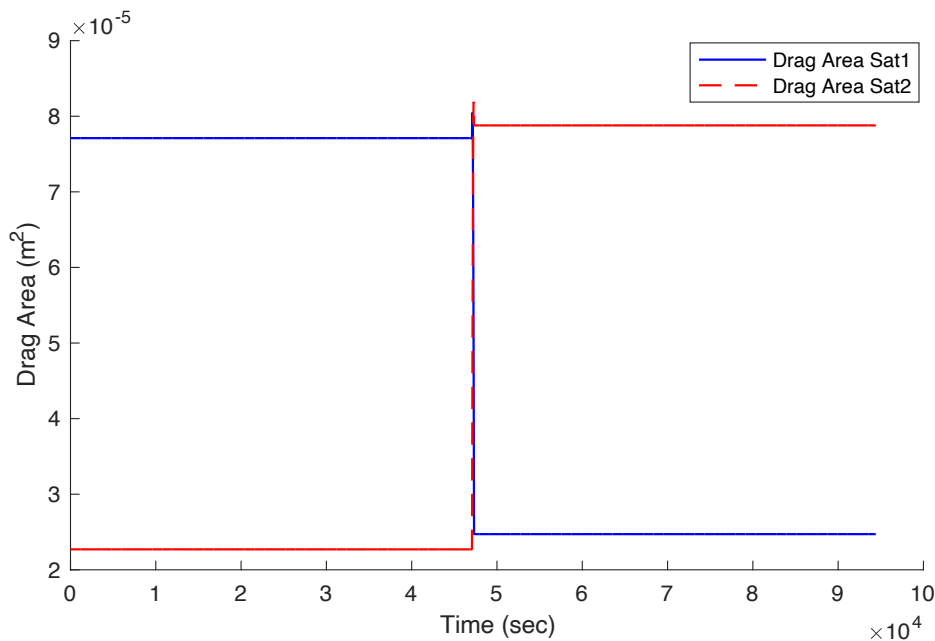


Figure 32. Drag areas of each satellite in the example maneuver

As was discussed in an earlier section, these drag areas are a result of the different rates of rotation about each of the spacecraft body axis. The x and z axis rates of rotation

are set to match the orbital motion of the spacecraft so that the same face of the spacecraft continues to point directly towards the direction of motion. The change in the drag area results from a 90-degree rotation about the y axis. These rotations are shown in Figure 32. The axes in the figure are in the ECI frame and the plots represent the x, y, and z axis of the spacecraft body frame. The spacecraft rotates with every orbit which creates the circular shape in Figure 33, and then when the flip about the y axis occurs halfway through the maneuver the x and z axes of the spacecraft effectively switch places. The x axis corresponds to the largest face of the spacecraft and the z axis to the smallest face of the spacecraft. Also, the plots are canted 45 degrees due to the inclination of the orbit.

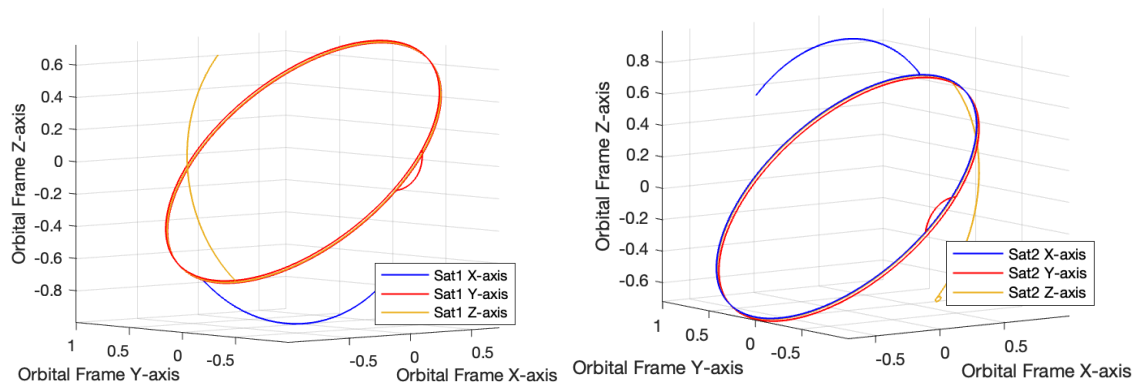


Figure 33. Depiction of the spacecraft orientations

Another view of this is shown in Figure 34. This figure is looking down onto the spacecraft along the body frame z axis. From this angle it is clear that the y axis rotates continuously and then the x and z axes flip between pointing forward. The 0.5 degree per second rate of rotation results in the curved arc that the x and z axis take during the movement.

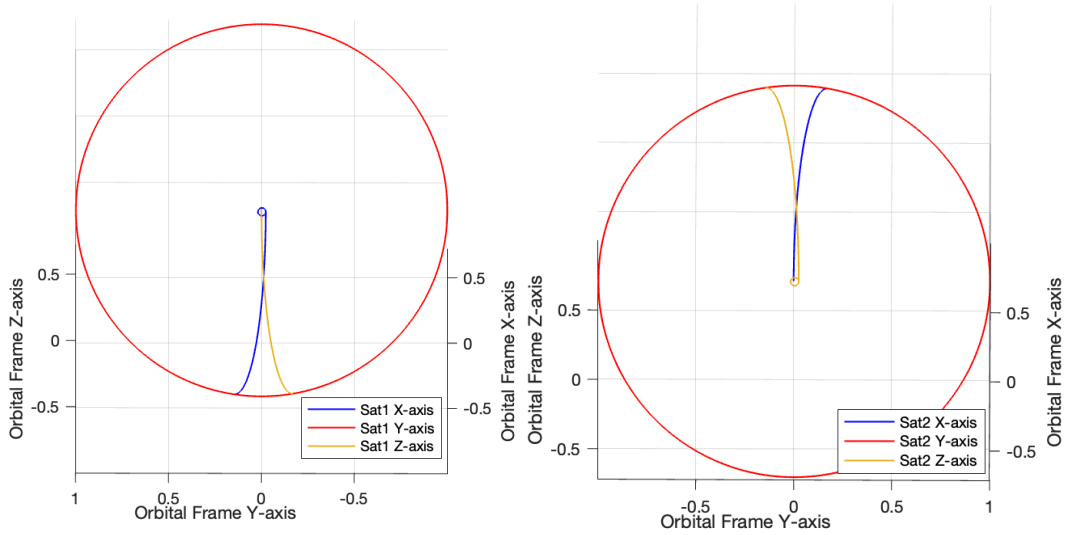


Figure 34. Top-down view of the rotation

The rotation of the spacecraft is also displayed in quaternions. These quaternions are initially calculated during the maneuver as if the RAAN were 270 degrees and then processed after the simulation runs to change them into true spacecraft orientations based on the actual RAAN of the spacecraft. The simulation quaternions for Satellite 1 are shown in Figure 35 and the RAAN adjusted quaternions are shown in Figure 36.

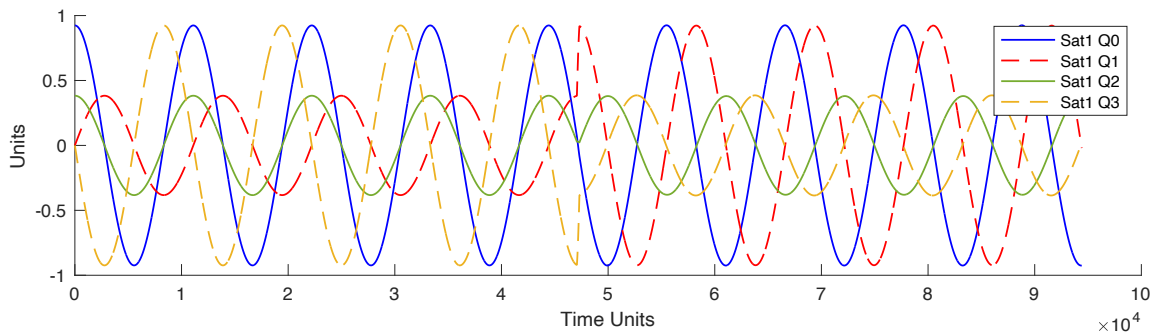


Figure 35. Simulation quaternions for Satellite 1

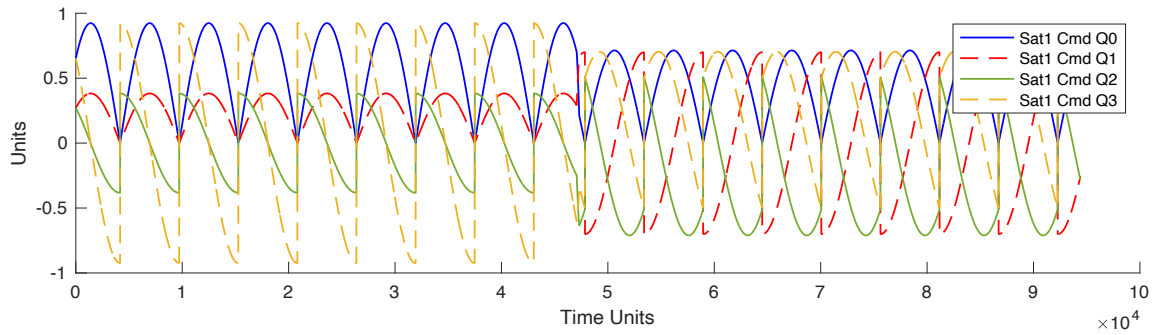


Figure 36. RAAN adjusted quaternions for Satellite 1

One feature of the command quaternions to note is that they jump each orbit. This is because the algorithm used to recalculate them changes the signs of them to maintain a positive value for the scalar  $q_0$ . The end result represents the same orientation but presents as a non-smooth curve when plotted. To double check this process, the rotations of each of the body frame axis were replotted using the command quaternions and then compared to the original values. They should show a rotation about the z-axis which represents the impact of the RAAN input on the quaternions. This comparison is shown in Figure 37 and confirms that this process works as desired and did rotate the orientations about the z-axis by 90 degrees. This reflects the shift from a RAAN of 270 degrees to a RAAN of 0 degrees.

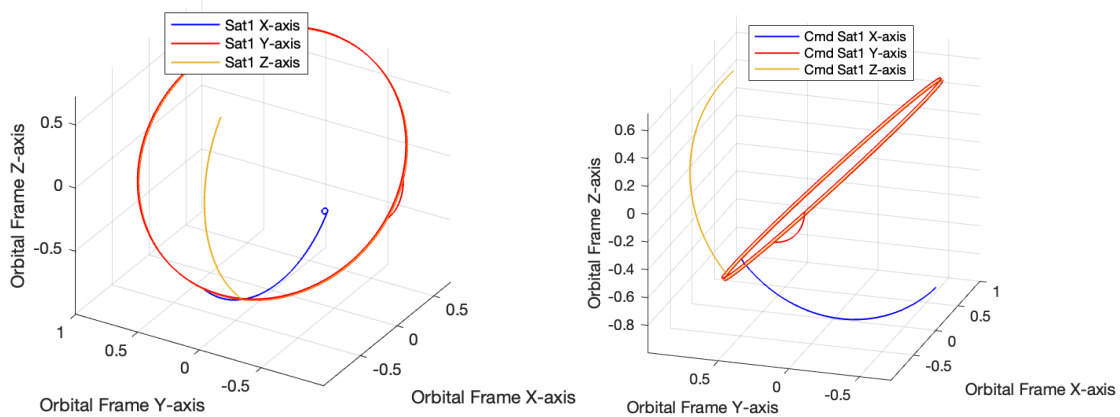


Figure 37. Left: Original quaternions; Right: RAAN adjusted quaternions



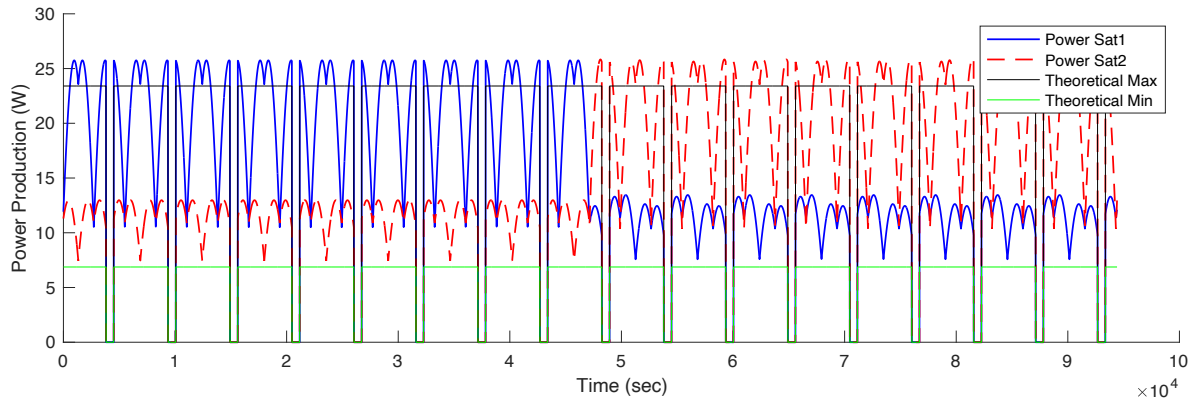


Figure 38. Graph of power production of each satellite during the maneuver

Lastly, the power production of satellites during the maneuver is plotted. Figure 38 shows how each satellite's power levels change throughout their orbits. The theoretical maximum shows what the power production would be if the highest surface area face pointed at the sun for the entire maneuver and vice versa for the theoretical minimum. The graph shows that at times the power goes above the theoretical maximum because the geometry of the orientation of the satellite actually means that the surface area pointed at the sun is higher than it would be if just the largest face was pointed at the sun. Also, there are narrow gaps where no power is produced, and these represent the areas where the spacecraft is behind the Earth relative to the sun. The duration of this occultation is dependent on the inclination and altitude of the satellite and the time of year. The same maneuver could result in very different power production levels at different times of year.

## A. IMPACT OF ORBIT SELECTION ON MANEUVERS

### 1. Altitude Effects

To better understand the effects of spacecraft altitude on differential drag maneuvers, the same maneuver as the previous example was repeated at different altitudes. These altitude effects are shown in Table 7 which shows the figures of merit for the maneuvers at a range of altitudes.

Table 7. Figures of merit for differential drag maneuvers performed at different altitudes

Altitude (km)	Separation Error (m)	Number of Orbits	Time Elapsed (hr)	Altitude Lost (m)
200	2501	1	1.48	980
300	1725	6	9.05	439
400	192	17	26.23	120
500	100	48	75.69	42
600	1.6	120	193.37	16

From Table 7 several important conclusions can be drawn. First, maneuvers at higher altitudes will take much longer to perform. The air is less dense at high altitudes so the difference in altitude between the two satellites accumulates more slowly and thus increases the maneuver duration. Also, with a greater number of orbits, there is more ability to fine tune how close the final separation is to the desired state. Finally, the amount of altitude lost is greatly affected by the starting altitude. At the lower altitudes, entering a high drag configuration greatly impacts the total mission life lost. Overall, these differential drag maneuvers are valuable between 500 and 300 km of altitude; above this level they take a very long time which could be detrimental for the mission, and below this they begin to impact the remaining lifetime of the mission.

## 2. Inclination Effects

Next is the examination of the effects of the inclination of the spacecraft’s orbit on these formation flying maneuvers. The same maneuver as the initial example was repeated at different inclinations. The inclination effects are shown in Table 8 which shows the figures of merit for the maneuvers in different inclinations.

Table 8. Figures of merit for maneuver performed at different inclinations

Inclination (deg)	Separation Error (m)	Number of Orbits	Time Elapsed (hr)	Altitude Lost (m)
0	23	16	24.68	124
45	192	17	26.23	121
90	129	20	30.85	101
135	616	17	26.23	131
180	22	15	23.14	132

One major conclusion from Table 8 is that the closer the orbit is to being polar (closer to an inclination of 90 degrees), the more it behaves like a maneuver happening at a higher altitude. This is because the average density over the orbit decreases the more time the spacecraft spend over the poles versus the equator. Next, the effect of the in-track atmospheric speed is shown by the iterations conducted in retrograde orbits. When the altitude loss is compared between 45 and 135 degrees and 0 and 180 degrees, there is a larger drop for the orbits which are greater than 90. This is also reflected by the duration of the maneuver in the retrograde orbits. In these orbits, the in-track atmospheric speed is impacting the spacecraft from ahead, acting like a headwind for an airplane, as opposed to the tailwind effect for prograde orbits. This results in a greater drag force and thus more control authority, shorter durations, and greater altitude loss for the maneuver.

The impacts of different inclinations are also shown in Figures 39 and 40. These figures show a maneuver conducted at a 350 km and changing an 11 km orbit to 10 km at 90 and 0 degrees inclination respectively.

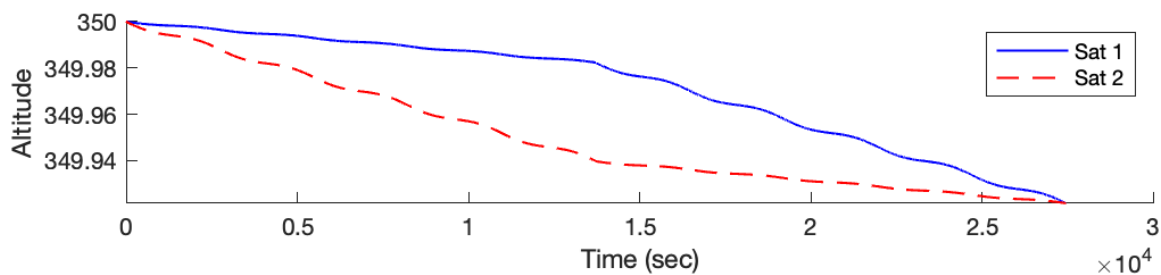


Figure 39. Maneuver at 90 degrees inclination

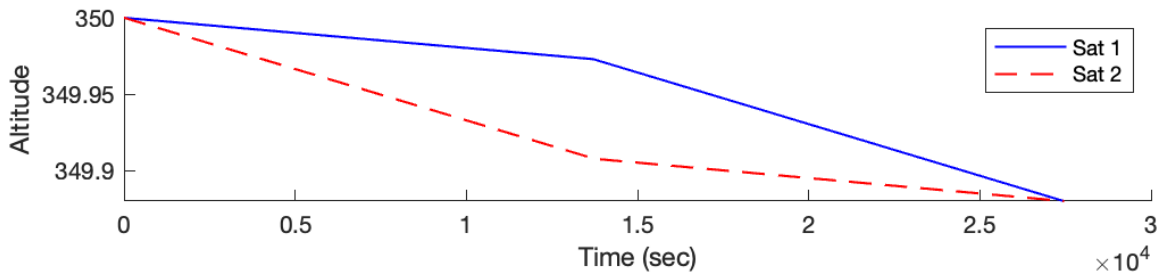


Figure 40. Maneuver at 0 degrees inclination

As shown by these two plots, the polar orbit has a characteristic wobble in the trajectories of the two spacecraft. This is a result of the spacecraft flying through regions of high density, the equator, and low density, the poles. This means that each orbit will have two peaks and two troughs of density, and this results in variable drag forces which appear on the chart as wobbles. This could have impacts on the maneuver if the spacecraft are separated by a great distance in the case of constellation management versus a tighter swarm formation. This is also a benefit of using a whole number of orbits for the maneuver, as this effect is largely averaged out over the duration of the maneuver and thus does not impact the final altitudes. Without using this technique, a final altitude error between the spacecraft could result. These density differences are shown in Figure 41, which depicts the densities experienced by the spacecraft through the orbit. There were five orbits in the maneuver which resulted in ten peaks and troughs in the plot. Also, the final density is slightly higher,  $9.88 \times 10^{-12} \text{ kg/m}^3$ , than the start,  $9.77 \times 10^{-12} \text{ kg/m}^3$ , due to the reduction in altitude.

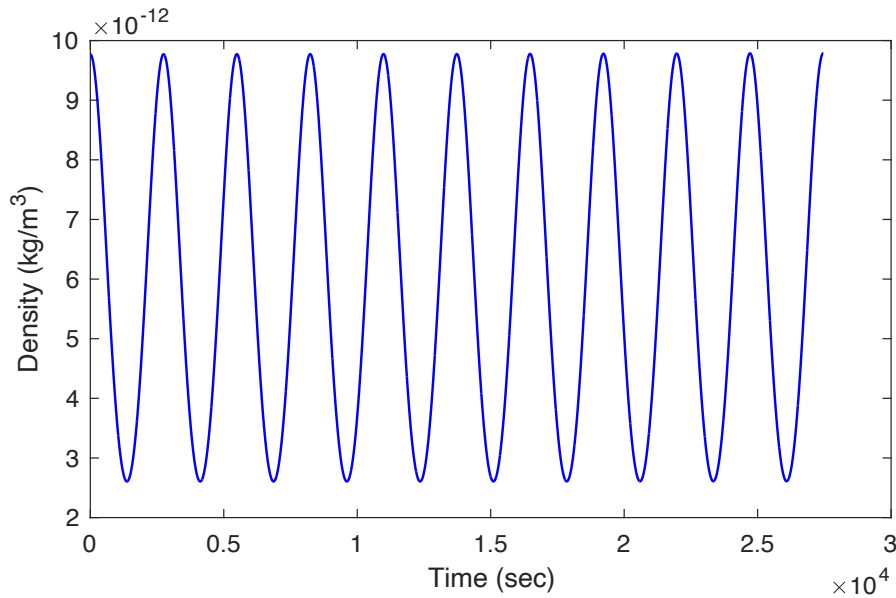


Figure 41. Atmospheric density experienced by spacecraft during maneuver

Finally, the inclination has a very large impact on the power production of the spacecraft. Generally, higher inclination and altitudes will provide a greater period of time in direct sunlight. Also, the orientations of the spacecraft are very different in high versus low inclinations, which results in a different amount of surface area facing towards the sun. This difference is shown in Figures 42, high inclination, and 43, low inclination. The theoretical maximum power level shows the power production when the largest face points directly at the sun. As the spacecraft rotates, it can achieve a larger surface area than this which is why the power produced is higher than the maximum amount at times.

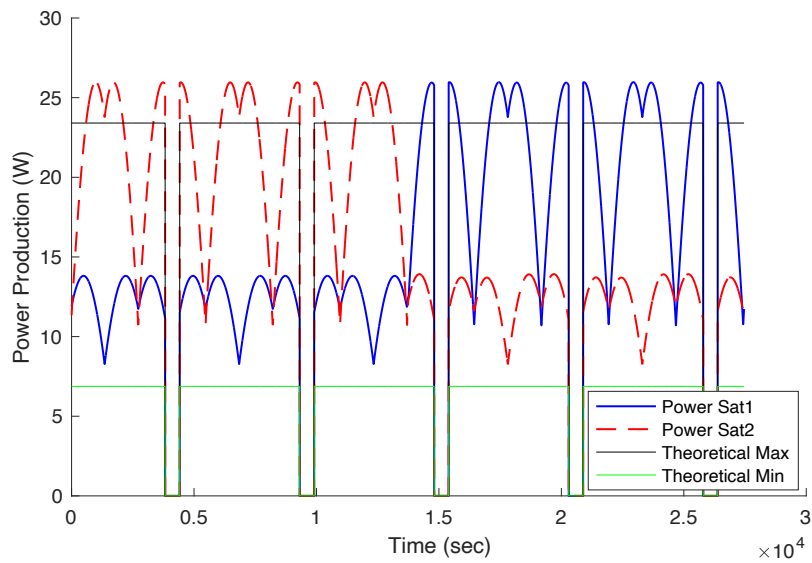


Figure 42. Impact of high inclination on solar power production

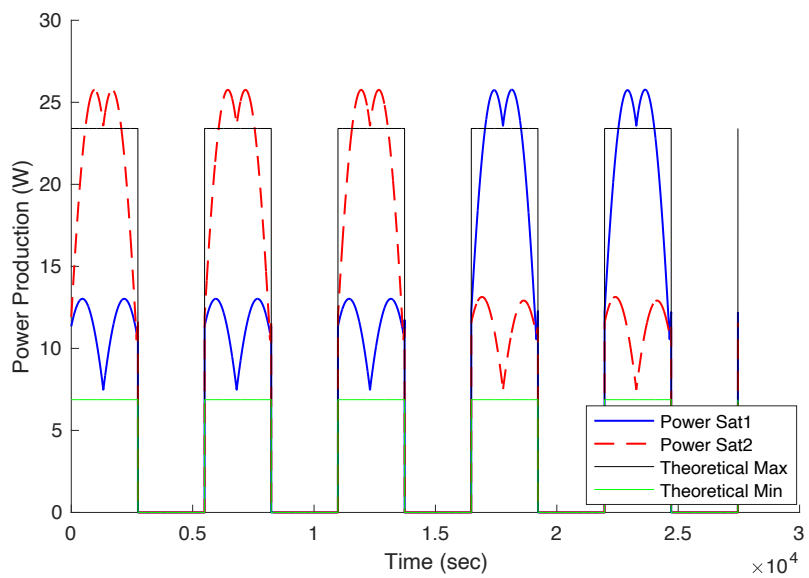


Figure 43. Impact of low inclination on solar power production

Overall, inclination of the spacecraft's orbits is a very important factor to consider when planning for a maneuver or for engineering and system designers for any mission architecture which calls for differential drag maneuvers to be used.

## B. IMPACT OF SPACECRAFT DESIGN ON MANEUVERS

### 1. High vs. Low Drag Configuration Ratio

Another critical factor that affects the performance of spacecraft in differential drag maneuvers is the ratio between the surface areas of the high and low drag configurations. The difference between these means the maneuver will happen more or less quickly, since this allows the vertical distance, thus relative velocity, to accumulate more quickly. This concept was tested using the same maneuver at 400 km changing a gap from 10 to 15 km just as before, but this this time with different spacecraft dimensions. The results of this are shown in Table 9.

Table 9. Effect of high to low drag ratios on maneuvers

High-Low Ratio	X-Dim (m)	Y-Dim (m)	Z-Dim (m)	Separation Error (m)	Number of Orbits	Time Elapsed (hr)	Altitude Lost (m)
2:1	0.1	0.2	0.2	166	28	43.19	119
3:1	0.1	0.2	0.3	269	20	30.85	113
4:1	0.1	0.2	0.4	68	16	24.68	114
5:1	0.1	0.2	0.5	170	14	21.60	120
6:1	0.1	0.2	0.6	571	13	20.05	130
7:1	0.1	0.2	0.7	696	12	18.51	136
8:1	0.1	0.2	0.8	582	11	16.97	140

From the results of this test, it is clear that the area ratio of the spacecraft has a significant impact on the figures of merit for the maneuver. A higher ratio will significantly decrease the amount of time needed to complete a maneuver. However, there are diminishing returns for how much of an impact this will make. After a ratio of 5:1 the time reductions become very small, and the loss of altitude begins to increase. This is consistent with the analysis conducted by Planet when designing their satellites, as they also found that a ratio of 5:1 is optimal for differential drag operations [12]. This is a key piece of information for any engineers working to design spacecraft for a mission which will use differential drag maneuvers.

## 2. Size and Mass

The next important factor of the spacecraft's design is the density of the spacecraft, or in other words how the mass of the spacecraft versus its total size will impact the mission. Given that the rate of change in the period is proportional to the mass and drag area, the same should be true for maneuver durations. This was again evaluated using the example maneuver as the baseline with different spacecraft densities. This was done simply by adjusting the spacecraft's mass and shown in Table 10.

Table 10. Effect of spacecraft mass with fixed 6U volume on maneuver

Spacecraft Mass (kg)	Separation Error (m)	Number of Orbits	Time Elapsed (hr)	Altitude Lost (m)
1	392	5	7.71	422
5	211	11	16.97	186
10	517	16	24.68	136
15	191	19	29.31	108
20	205	22	33.94	93

As shown by Table 10, the relationship between the spacecraft's mass for a given size and the length of the maneuver is roughly linear. The lighter the spacecraft is, the faster it will fall in altitude and vice versa. Also, this greatly impacts the overall mission life as a lighter spacecraft will deorbit faster regardless of orientations.

## 3. Solar Power Considerations

It is critical to evaluate the impact of different factors on the satellites' ability to produce solar power during the maneuvers. The maneuvers tend to last for a relatively long time, and they can have major impacts on the ability of the satellite to maintain all of its functions if the power is not properly managed.

First, the case is considered where a satellite has a deployable solar panel such as the one pictured in Figure 43. In this example the 6U CubeSat has one face with a very large solar panel area but much smaller or even no coverage on other faces.



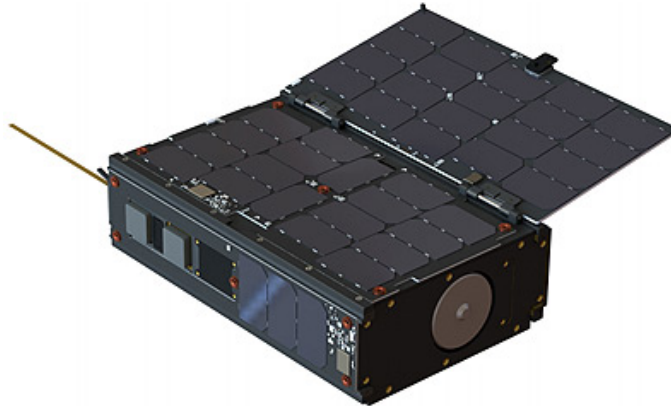


Figure 44. 6U CubeSat with deployable solar panel. Source: [33]

This satellite will be compared to the baseline satellite for a maneuver at 400 km altitude and changing the separation from 11 km to 10 km. The shorter duration will result in clearer graphics. The inputs for the new spacecraft are estimates based on the spacecraft pictured in Figure 44 and are shown in Table 11.

Table 11. Solar power evaluation space craft parameters

	Input	Value
<b>Spacecraft Specifications</b>	Spacecraft Mass	12 kg
	X-Axis Dimension	0.1 m
	Y-Axis Dimension	0.3405 m
	Z-Axis Dimension	0.4526 m (2x the previous y-dimension)
	Solar Panel Coverage Face 1	0.9
	Solar Panel Coverage Face 2	0.4
	Solar Panel Coverage Face 3	0.5
	Solar Panel Coverage Face 4	0.5
	Solar Panel Coverage Face 5	0
	Solar Panel Coverage Face 6	0.25
Solar Panel Efficiency	0.25	

The maneuver performed by the new spacecraft took less time due to the higher drag area from the solar panel at only 9.26 hours. The resulting solar power from this is shown in Figure 45. From this graphic it is clear that the power distribution is heavily impacted by the maneuver, and it is very uneven throughout the maneuver. During the low drag area times the power is very low, and the main solar panel is never able to directly

view the sun. In high drag orientations the spacecraft produced more, but there are still large variations in the levels.

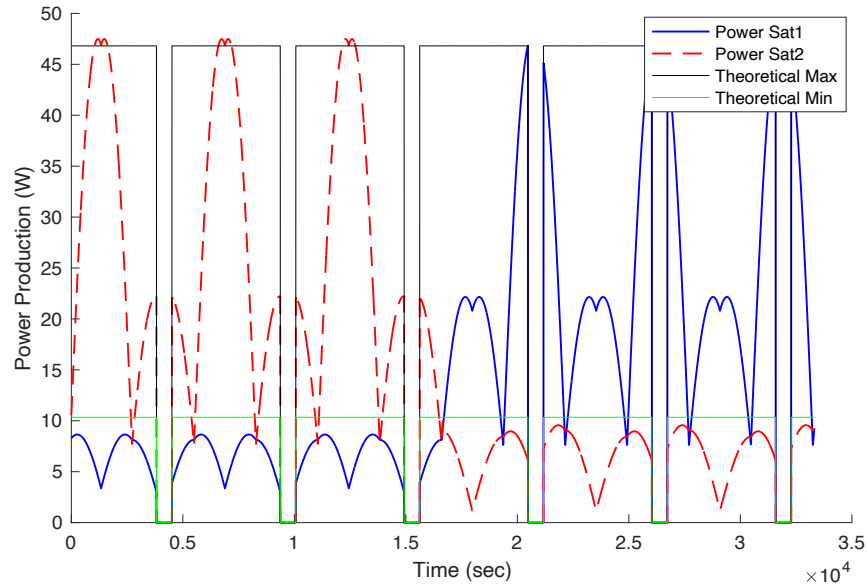


Figure 45. Solar power evaluation spacecraft power levels

The power produced by this spacecraft is an average of 14.96 Watts over the entire maneuver. This is compared to the baseline spacecraft whose solar power production is shown in Figure 46. These satellites' maneuver lasted 12.34 hours and produced an average of 14.43 Watts over the maneuver. This is an important consideration for spacecraft operators as the addition of the panel allows for faster maneuvers, but it is unlikely that all of its payloads will function fully during the maneuver. Despite having the larger deployable solar panel, the spacecraft still does not product significantly more power on average during the maneuver. Also, its production is highly variable and inconsistent during the maneuver.

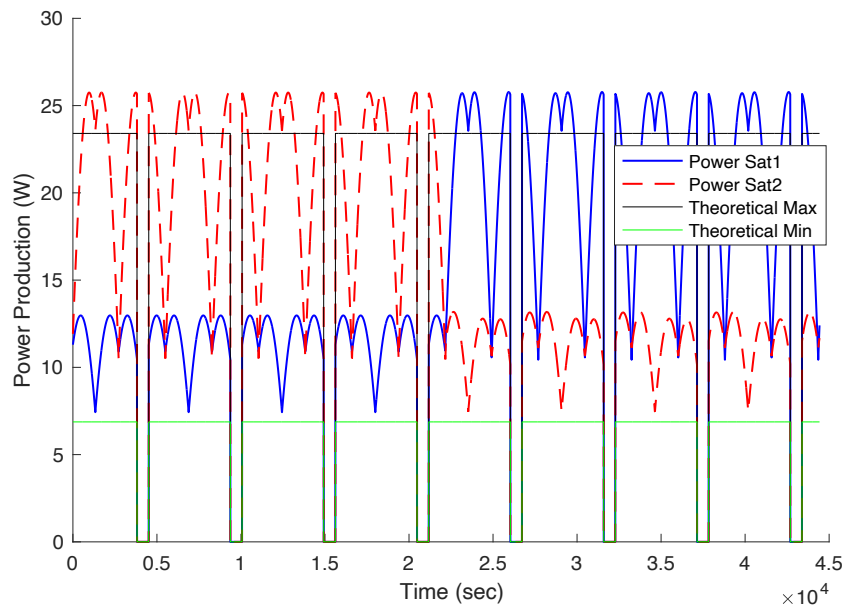


Figure 46. Baseline spacecraft power levels

Another factor to consider is the time of year as this impacts the direction of the sun in relation to the spacecraft, and the amount of time the spacecraft is occulted by the Earth. To evaluate this the maneuver was repeated at different times through the year as shown in Table 12.

Table 12. Average power produced at different times of year

Date	Average Power (W)
21 March	18.73
21 June	14.23
21 September	18.35
21 December	14.25

From Table 12, there are clearly large differences in the amount of power generated by the same maneuver during the year. For this particular case March provides the highest levels; the graph of this is shown in Figure 47 for comparison against the baseline case from June 16 as shown in Figure 46. This difference should be appreciated by spacecraft

operators as they plan maneuvers and missions that rely on differential drag. They could consider waiting until a different time of year to reduce the impacts.

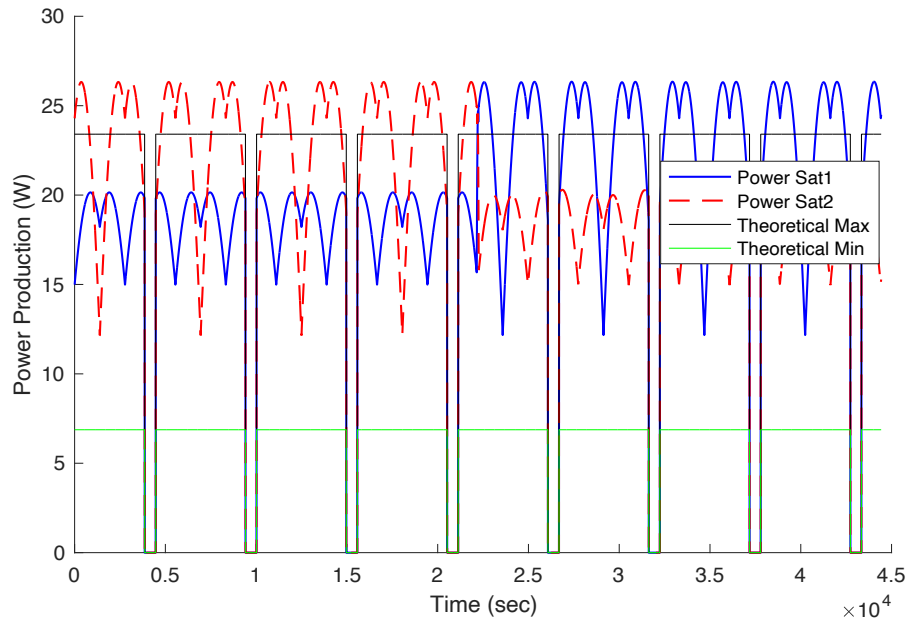


Figure 47. Power production for baseline maneuver performed in March

### C. MANEUVER SPEED

Finally, the maneuver speeds were examined. These are options for satellite operators to increase the duration of a maneuver for the option of creating usable time within the maneuver to perform other tasks or to preserve mission life. Given that the benefits of the different speeds are more pronounced at longer distances, a maneuver at 400 km to close a 25 km separation to 10 km was performed at each of the three speed options. Speed 1 is the minimum time maneuver, Speed 2 is broken up into thirds, and Speed 3 is split into quarters with the middle 50% of the duration being a coast phase. Each of these three options are shown in Figures 48, 49, and 50.

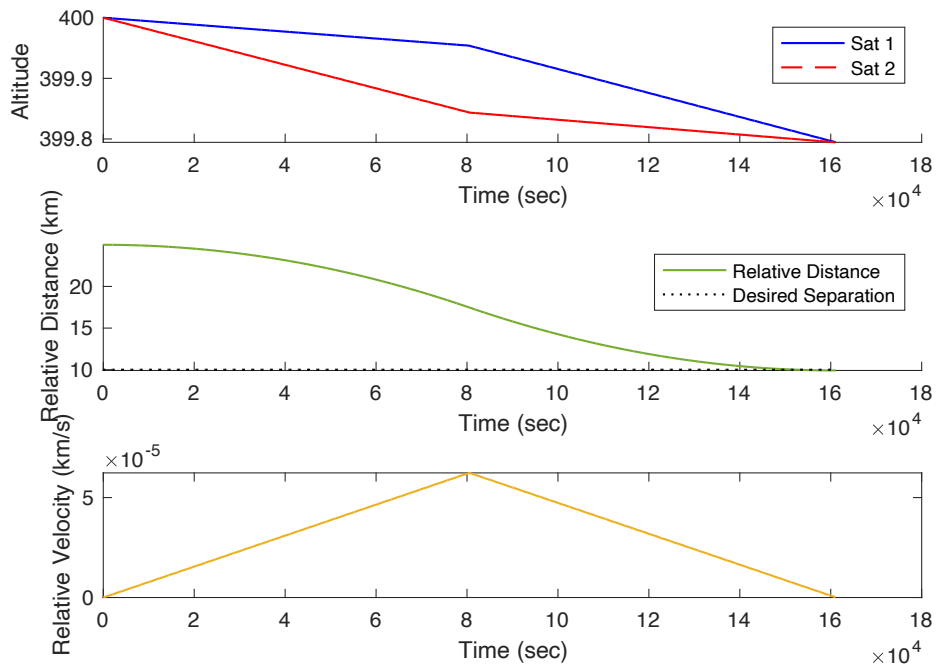


Figure 48. Maneuver performed at Speed 1

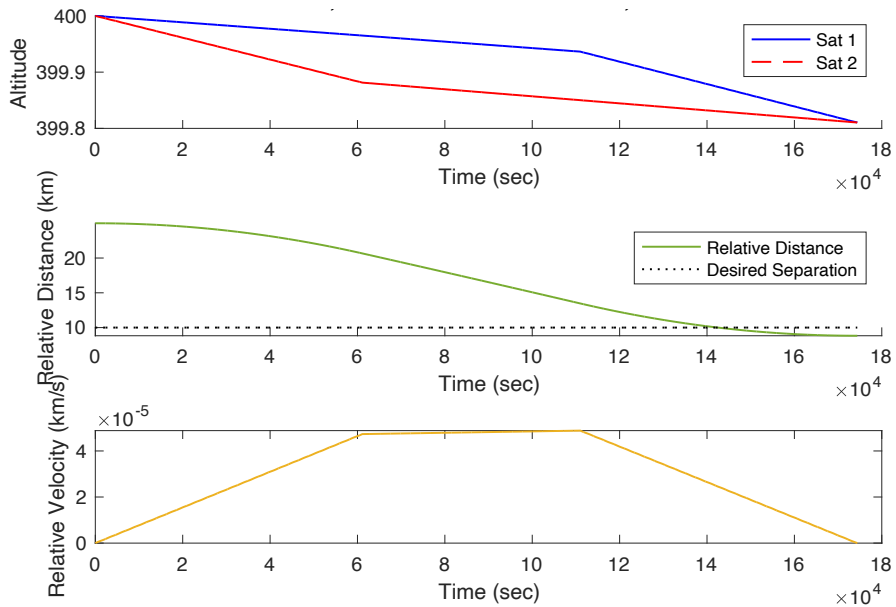


Figure 49. Maneuver performed at Speed 2

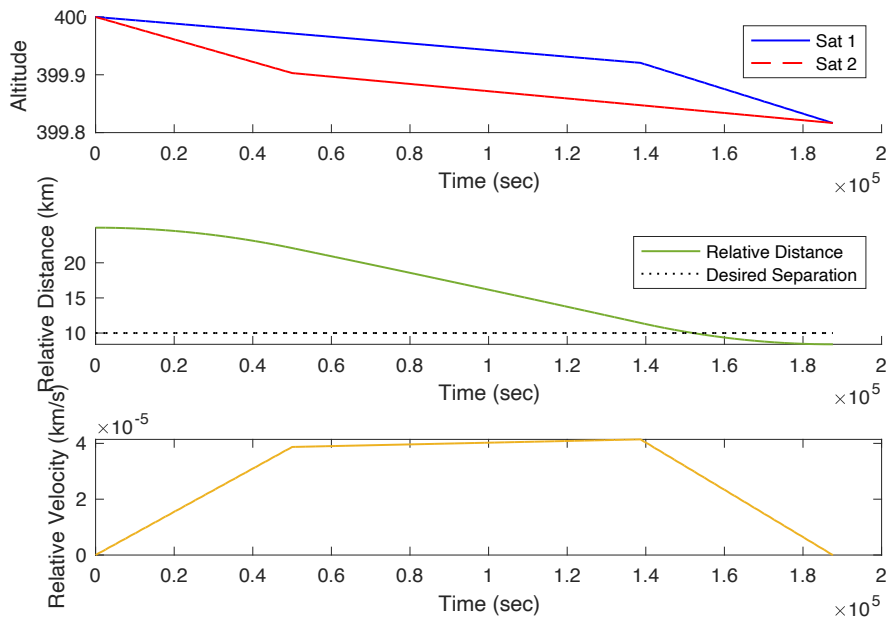


Figure 50. Maneuver performed at Speed 3

As shown by these three figures, the trajectory profiles at each speed are quite different as are the durations. The minimum time maneuver lasted 44.74 hours as opposed to the slowest speed which lasted 52.11 hours. The main advantage is that, as long as the spacecraft are maintaining the same drag area as each other, they could be in whatever orientation they need to be. If they did reorient away from the low drag configuration, their vertical separation would not change if their drag forces were the same and therefore their relative velocities would not change meaning it would have no impact on the overall maneuver. In this case, that would mean that spacecraft would be restricted in orientation during only half of the 52.11 hours, or 26.06 hours, which is much less than the minimum time maneuver. This gives satellite operators many more options on how to employ the spacecraft. They could maintain a sun pointing orientation for power production, point at places at the ground, or whatever else they need to do as part of everyday operations.

Also, it is worth noting that this maneuver adjusts the separations three times further than the baseline but lasts less than twice as long at Speed 1. This highlights the nonlinear relationship between maneuver duration and the distance covered by the satellites. This is

because their relative velocities are a function of the altitude separation and the longer the maneuver the greater the vertical distance between the satellites, thus the greater their relative velocity and shorter the duration needs to be. This makes predicting the duration of a maneuver difficult without a tool like this and increases the value of having more than one option for the trajectory profile through multiple speeds.

## VII. CONCLUSIONS AND FUTURE RESEARCH

Formation flying using differential drag is a challenging and complicated problem set, which requires many engineering design choices regarding the spacecraft and its orbit. This investigation provides an in depth look at the factors which impact differential drag maneuvers, but more research must still be done.

### A. KEY TAKEAWAYS

This thesis provides a deeper understanding to the use of differential drag maneuvers for satellites flying in formation. Likely, the most significant takeaway is that any spacecraft operators who wish to use these techniques will be faced with difficult choices as there are many tradeoffs and compromises that must be made. Decisions to make maneuvers occur more quickly will also shorten the lifetime of the mission, and decisions to slow maneuvers will have greater impacts on the mission of the spacecraft if timeliness is a factor. However, some of these disadvantages can be mitigated by changing the design of the spacecraft itself, but this could come with a high price tag for the mission. These difficult choices must be weighed against the mission requirements and what services or capabilities the spacecraft and its mission architecture provide to the end users.

One very versatile and useful output of this thesis was the development of analytic models for the atmosphere based on a statistical survey of several other models and for the calculation of drag surface areas. This allows for the atmosphere's density at any location around the Earth to be quickly and continuously calculated as part of more complex dynamics equations for the purposes of optimization or other mathematical analysis. This is a critical aspect of spacecraft operations in LEO, and thus it could be applied to many other applications. This is also true for calculating the surface area of a spacecraft. In this thesis the area calculations were done to find the drag area and the area facing the sun for power production, but the area calculation equations could be applied to many other potential uses as well.



The use of optimization techniques proved very valuable in finding a minimum time trajectory to accomplish the maneuver. This minimum time solution allows for the smallest impact to the mission of the spacecraft, and it has implications for reducing the amount of time needed to begin a mission after launch by allowing for satellite swarms to be established more quickly.

Finally, it is also very important to note that the formation flying methods discussed in this thesis allow for any spacecraft to perform these maneuvers. They would not require specialized hardware such as a deployable drag device to perform the maneuvers, nor would there be a need for computationally intensive software, specialized sensors, inter-satellite communications; it could even be used by any spacecraft regardless of size or mass. Adjusting the drag area calculations to account for a larger variety of shapes and sizes would be a relatively straightforward process, and thus even larger spacecraft could use this method to precisely adjust formations while saving fuel for other purposes. This is a unique aspect of this thesis that makes it more generally applicable for a wider range of spacecraft types, more appropriate for integration into autonomous systems, and reduces cost for constellation deployment and management.

## **B. FUTURE RESEARCH**

### **1. Improvements and Potential Additional Capabilities for the Maneuver Planning Tool**

There are several areas where the maneuver tool created as part of this thesis could be improved to increase its capabilities. This includes improvements to not only the existing model, but also the addition of new functions that will allow it to complete more complex operations.

First, the restriction to conduct maneuvers in whole numbers of orbits could be changed to allow for more accurate maneuvers. This would carry some drawbacks, including a much longer run time and it would require many of the supporting code which controls the simulation to be rewritten.

Second, the code could be expanded to include additional satellites. This would likely require some additional analysis to determine the optimal trajectory for accomplishing this. The model with three or more satellites could be tested in the DIDO optimal control solver to produce a new trajectory which could then be replicated in the maneuver tool. This could make the system more suitable for larger scale constellation management or the management of a much larger satellite swarm. Something like this would likely need to be built to support a specific constellation with a defined architecture, in order for it to meet the requirements of the specific mission architecture.

Lastly, the same dynamics equations and problem boundary values could be used in a bespoke, purpose built, optimized solver. This would allow for many new constraints to be modeled on the satellites' operations to create truly unique trajectories for each individual maneuver and mission set.

## **2. Using the Maneuver Planning Tool for Satellite Operations, Architecture Design, and Mission Development**

Another area for future study would be to apply the maneuver planning tool to a specific use case. This would test the tool's validity and usefulness, and it would show how it could be integrated into spacecraft operations most effectively. This could be done using a software-based approach and then be tested on actual spacecraft in orbit. The satellites in question would need to be modeled in a software platform, such as the Systems Tool Kit (STK) with the SOLIS plug in, and then the commands from the planning tool would be uploaded. STK could then propagate the orbit using a traditional atmospheric model and spacecraft dynamics, and then observe how closely the results of the tool match the final relative positions of the satellites in STK. If there are large discrepancies, adjustments could be made to the maneuver tool to correct them and then it could be re-tested until the two simulations match. This may require changes to the spacecraft model, a rectangular shape may not be appropriate for that particular satellite, or the atmosphere model which largely drives the amount of drag experienced by the spacecraft. If possible, the same maneuver could then be tested on spacecraft in orbit, which would ultimately validate the tool, especially if it was done in a large number of orbits and environmental conditions. As

of this writing, the Naval Postgraduate School may be granted access to two satellites which use differential drag to fly in formation and this tool could be used to operate them.

The maneuver planning tool could also be used as a method to evaluate and test a series of different mission designs and system architectures. This could include testing spacecraft designs for their effectiveness at performing differential drag maneuvers, and thus helping to drive certain design choices of the spacecraft. It could also be used to compare and contrast certain orbital regimes for a particular mission and evaluate the mission life of a particular mission. In this way, the maneuver planning tool could be especially useful as part of a trade study that evaluated different designs and costs of the mission. Some applications which traditionally have required a larger, more expensive spacecraft, could be cheaper and more effective using a swarm of small satellite which use differential drag to stay in formation. The planning tool could help in evaluating the impact to the mission if this option were chosen and provide insight to mission architects.

### **3. Applications Beyond Formation Flying**

The sets of equations and the underlying physics of the models developed for this thesis could be used for other investigations and applications aside from differential drag maneuvers. The ability to calculate the precise drag forces and densities at different portions of the orbit could be useful in evaluating the operations of different spacecraft.

The model could be used to determine the operating orientations of a single satellite operating in LEO. If orbital lifetime is an important factor, the operators could evaluate the spacecraft's maneuvers' impact on mission life by testing its orientations against the drag area equations and propagating the orbit through a certain orbit. It is possible that small changes in the orientation could increase the lifespan of the mission by preserving its altitude or saving valuable fuel.

Another interesting use of the models would be for a single CubeSat to use differential drag to conduct rendezvous or proximity operations (RPO) on another object. This other object could be cooperative or non-cooperative. RPO using differential drag could be useful by allowing for a small CubeSat to dock with a larger spacecraft to provide

on-orbit services such as refueling, providing additional communications capabilities, offering an alternative propulsion system, or replacing attitude control authority for damaged systems. It could also be useful for a low-cost system designed to remove orbital debris. A small CubeSat could use differential drag to maneuver close to debris such as a rocket body or other object and then attach itself using magnets or hooks. The CubeSat could then deploy a drag device, such a thin sheet of mylar, which would act as a sail to catch the wind and help deorbit the debris more quickly.

### **C. FINAL CONCLUSIONS**

Space plays a critical role in global commercial activities and national defense. To maintain a competitive edge in this domain, the United States must actively pursue innovative theories and policies for conducting operations in space [34]. To translate these policies into practice, the Department of Defense (DOD) has a responsibility to continuously develop advanced technical solutions that lower costs, enhance capabilities, and increase accessibility to space-enabled services for the Warfighter on the ground, in the air, and at sea. One promising approach is the deployment of large numbers of small, cost-effective satellites operating in formation. Differential drag maneuvers hold significant potential in enabling these spacecraft to deliver essential capabilities to the Warfighter. This thesis has developed the necessary tools to effectively integrate differential drag maneuvers into satellite formation flying operations, thereby enhancing the overall space capability and capacity of the United States.

THIS PAGE INTENTIONALLY LEFT BLANK

## LIST OF REFERENCES

- [1] Harrison et al., “Defense Against the Dark Arts in Space,” Center for Strategic & International Studies, New York, NY, USA, 978–1-5381-4031-4, 2021 [Online]. Available: <https://www.csis.org/analysis/defense-against-dark-arts-space-protecting-space-systems-counterspace-weapons>
- [2] T. Taverney, “The Evolution of Space-Based ISR,” *The Air Force Magazine*, Aug. 10, 2022 [Online]. Available: <https://www.airforcemag.com/article/the-evolution-of-space-based-isr/>
- [3] M. Easley, “JUST IN: NRO, Air Force Boosting Collaboration on Space-Based ISR,” *National Defense*, Aug. 4, 2022 [Online]. Available: <https://www.nationaldefensemagazine.org/articles/2022/8/4/nro-air-force-want-tighter-collaboration-for-space-based-isr>
- [4] S. Erwin, “BlackSky, Maxar, Planet win 10-year NRO contracts for satellite imagery.” *SpaceNews*, May 25, 2022 [Online]. Available: <https://spacenews.com/blacksky-maxar-planet-win-10-year-nro-contracts-for-satellite-imagery/>
- [5] G. Allen, “Across Drones, AI, and Space, Commercial Tech Is Flexing Military Muscle in Ukraine.” *Center for Strategic & International Studies*, May 13, 2022 [Online]. Available: <https://www.csis.org/analysis/across-drones-ai-and-space-commercial-tech-flexing-military-muscle-ukraine>
- [6] Euroconsult, “Prospectus for the small satellite market 2022: One ton of smallsats to be launched per day on average over the next decade, yet challenges remain,” Euroconsult, Washington, DC, USA, 2022 [Online]. Available: <https://www.euroconsult-ec.com/press-release/one-ton-of-smallsats-to-be-launched-per-day-on-average-over-the-next-decade-yet-challenges-remain/>
- [7] D. Chow, “To cheaply go: How falling launch costs fueled a thriving economy in orbit.” NBC News, Apr. 8, 2022 [Online]. Available: <https://www.nbcnews.com/science/space/space-launch-costs-growing-business-industry-rcna23488>
- [8] Spaceflight rideshare provider, “Rideshare Pricing,” 2022 [Online]. Available: <https://spaceflight.com/pricing/>
- [9] J. Heyman, “Focus: CubeSat – A Costing + Pricing Challenge,” *Satellite Magazine*, Oct. 2009 [Online]. Available: <http://www.satmagazine.com/story.php?number=602922274>

- [10] Ames Spaceflight Division. “Formation Flying.” NASA, Aug. 10, 2021 [Online]. Available: [https://www.nasa.gov/\\_centers/ames/engineering/divisions/spaceflight/flight-dynamics/formation-flying](https://www.nasa.gov/_centers/ames/engineering/divisions/spaceflight/flight-dynamics/formation-flying)
- [11] GA Sundaram and R Reshma, “Influence of orbital perturbations due to non-spherical Earth shape on the Landsat multispectral imaging platform,” *Journal of intelligent & fuzzy systems*, vol. 34, no. 3, p. 1723–, 2018 [Online], Available: DOI: 10.3233/JIFS-169465.
- [12] C. Foster *et al.*, “Orbit determination and differential-drag control of Planet Labs CubeSat constellations,” *arXiv preprint arXiv:1509.03270*, 2015 [Online]. Available: <https://arxiv.org/abs/1509.03270>
- [13] C. Gentgen *et al.* “A Path to Flight for Reconfigurable Satellite Constellations: Mission Design and Systems Architecture.” *Ascend*, AIAA 2021–4146, Nov. 3, 2021 [Online]. Available: <https://doi.org/10.2514/6.2021-4146>
- [14] H. Loomis. “Geolocation of Electromagnetic Emitters.” Naval Postgraduate School, 2014. NPS-EC-00-03 version GEOLOChhlreve.doc. unpublished.
- [15] C. Duan and N. Xiao, “Parallax-Based Spatial and Channel Attention for Stereo Image Super-Resolution,” *IEEE access*, vol. 7, pp. 183672–183679, 2019 [Online]. Available: DOI: 10.1109/ACCESS.2019.2960561
- [16] G. Krieger, “Advanced Bistatic and Multistatic SAR Concepts and Applications.” *Microwaves and Radar Institute*, DLR, Germany, 2006 [Online]. Available: [https://elib.dlr.de/43805/1/eusar06tutorial\\_advanced\\_bistatic\\_sar\\_final\\_reduced.pdf](https://elib.dlr.de/43805/1/eusar06tutorial_advanced_bistatic_sar_final_reduced.pdf)
- [17] C. Mireault-Lecourt *et al.*, “Study of a SAR Mission Onboard a 12U CubeSat using the Reflectarray Technology,” *2021 IEEE 19th International Symposium on Antenna Technology and Applied Electromagnetics (ANTEM)*, 2021 [Online], pp. 1–2, Available: DOI: 10.1109/ANTEM51107.2021.9518994.
- [18] Kumar *et al.*, “Differential Drag as Means of Spacecraft Formation Control.” *IEEE Transactions on Aerospace and Electronic Systems* Vol. 47, NO. 2, Apr. 2011 [Online]. Available: <https://sdac.blog.torontomu.ca/files/2016/02/diffdragpaper.pdf>
- [19] C. Riano-Rios *et al.*, “Adaptive Control For Differential Drag-Based Rendezvous Maneuvers with an Unknown Target.” *Acta Astronautica* Volume 181, Pages 733–740, Apr. 2021 [Online]. Available: <https://www.sciencedirect.com/science/article/pii/S0094576520301399>

- [20] R. Panwar, "Satellite Orbital Decay Calculations," *The Australian Space Weather Agency, Australian Government Bureau of Meteorology*, Haymarket, Australia, 2023 [Online]. Available: <https://www.sws.bom.gov.au/Category/Educational/Space%20Weather/Space%20Weather%20Effects/SatelliteOrbitalDecayCalculations.pdf>
- [21] F. Vallado, "A Critical Assessment of Satellite Drag and Atmospheric Density Modeling," *Center for Space Standards and Innovation*, Colorado Springs, CO, USA, 2007 [Online]. Available: <https://www.agi.com/getmedia/280be1f7-7d1a-49f3-8d78-3492ce527d8c/A-Critical-Assessment-of-Satellite-Drag-and-Atmospheric-Density-Modeling.pdf?ext=.pdf>
- [22] NatGeo, "Atmosphere," *National Geographic Encyclopedia*, 2023 [Online]. Available: <https://education.nationalgeographic.org/resource/atmosphere>
- [23] A. Harris, "Over What Part of the Earth Is the Atmosphere the Deepest & Thickest?" *Seattle Pi*, 2022 [Online]. Available: <https://education.seattlepi.com/rate-diffusion-vary-molecular-weight-temperature-6379.html>
- [24] G. Dinis, "Sun-Synchronous Satellite Simulator," *Turku University of Applied Sciences*, 2017 [Online]. Available: [https://www.theseus.fi/bitstream/handle/10024/129244/Dinis\\_Gustavo.pdf;jsessionid=9A851915D81BD00DDB34988BDEC63916?sequence=1](https://www.theseus.fi/bitstream/handle/10024/129244/Dinis_Gustavo.pdf;jsessionid=9A851915D81BD00DDB34988BDEC63916?sequence=1)
- [25] MathWorks, "High Precision Orbit Propagation of the International Space Station," *MathWorks Help Center*, 2022 [Online]. Available: <https://www.mathworks.com/help/aeroblks/high-precision-orbit-propagation-of-the-international-space-station.html>
- [26] NOAA, "Current Space Weather Conditions: Solar Cycle Progression," *National Oceanic and Atmospheric Administration*, Products and Data, 2023 [Online]. Available: <https://www.swpc.noaa.gov/products/solar-cycle-progression>
- [27] V. Nwankwo and S. Chakrabarti, "Theoretical Model of Drag Force on a Model International Space Station Satellite due to Solar Activity," *Japanese Society of Aeronautical and Space Sciences*, 2014 [Online]. Available: DOI: 10.2322/tastj.12.47.
- [28] I. Ross, *A Primer on Pontryagin's Principle in Optimal Control*, Second Edition, Collegiate Publishers, San Francisco, CA, 2015.
- [29] I. Ross, "Enhancements to the DIDO Optimal Control Toolbox." *Naval Postgraduate School*, 2022 [Online]. Available: [https://cle.nps.edu/access/content/group/2e832bb9-d5ea-48bc-8f30bc195e042378/DIDO/DIDO\\_TechPaper.pdf](https://cle.nps.edu/access/content/group/2e832bb9-d5ea-48bc-8f30bc195e042378/DIDO/DIDO_TechPaper.pdf)



- [30] P. Gondolo and M. Alenazi, “Phase-space distribution of unbound dark matter near the Sun,” *Physical Review, Astrophysics*, Aug. 18, 2006 [Online]. Available: <https://doi.org/10.1103/PhysRevD.74.083518>
- [31] S. Rickman, “Introduction to On-Orbit Thermal Environments.” *NASA Engineering & Safety Center and the NASA Thermal and Fluids Analysis Workshop*, Cleveland, OH, USA, 2014 [Online]. Available: [https://tfaws.nasa.gov/wp-content/uploads/OnOrbit\\_Thermal\\_Environments\\_TFAWS\\_2014.pdf](https://tfaws.nasa.gov/wp-content/uploads/OnOrbit_Thermal_Environments_TFAWS_2014.pdf)
- [32] M. Sherif. “Space Power and Radiation Effects.” *Course materials for EC3230*, Naval Postgraduate School, Monterey, CA, USA, summer 2022.
- [33] “Ignis AstroDigital 6U,” Gunter’s Space Page, 2023 [Online]. Available: [https://space.skyrocket.de/doc\\_sdat/ignis.htm](https://space.skyrocket.de/doc_sdat/ignis.htm)
- [34] Klein. “Space Warfare,” *Space Warfare: Strategy, Principles, and Policy* Routledge Taylor and Francis Group, New York, NY, USA, 2006. Page 3.

## INITIAL DISTRIBUTION LIST

1. Defense Technical Information Center  
Ft. Belvoir, Virginia
2. Dudley Knox Library  
Naval Postgraduate School  
Monterey, California



## DUDLEY KNOX LIBRARY

NAVAL POSTGRADUATE SCHOOL

[WWW.NPS.EDU](http://WWW.NPS.EDU)

---

WHERE SCIENCE MEETS THE ART OF WARFARE